26793

National Library of Canada | Bibliothèque nationale du Canada

CANADIAN THESES ON MICROFICHE | THÈSES CANADIENNES SUR MICROFICHE

NAME OF AUTHOR/*NOM DE L'AUTEUR* DOMINIQUE Wen KAO

TITLE OF THESIS/*TITRE DE LA THÈSE* The ENHENCEMENT of Signal to Noise in Magnetotelluric Data

UNIVERSITY/*UNIVERSITÉ* The University of ALBerta

DEGREE FOR WHICH THESIS WAS PRESENTED/*GRADE POUR LEQUEL CETTE THÈSE FUT PRÉSENTÉE* Ph. D.

YEAR THIS DEGREE CONFERRED/*ANNÉE D'OBTENTION DE CE GRADE* 1975

NAME OF SUPERVISOR/*NOM DU DIRECTEUR DE THÈSE* Dr. D. Rankin

Permission is hereby granted to the NATIONAL LIBRARY OF CANADA to microfilm this thesis and to lend or sell copies of the film.

The author reserves other publication rights, and neither the thesis nor extensive extracts from it may be printed or otherwise reproduced without the author's written permission.

L'autorisation est, par la présente, accordée à la BIBLIOTHÈQUE NATIONALE DU CANADA de microfilmer cette thèse et de prêter ou de vendre des exemplaires du film.

L'auteur se réserve les autres droits de publication; ni la thèse ni de longs extraits de celle-ci ne doivent être imprimés ou autrement reproduits sans l'autorisation écrite de l'auteur.

DATED/*DATÉ* 9/9/75 SIGNED/*SIGNÉ* Dominic W. Kao

PERMANENT ADDRESS/*RÉSIDENCE FIXÉ*

NL-91 (3-74)

THE UNIVERSITY OF ALBERTA

THE ENHANCEMENT OF SIGNAL TO NOISE IN MAGNETOTELLURIC DATA

by

© DOMINIQUE WEN KAO

A THESIS

SUBMITTED TO THE FACULTY OF GRADUATE STUDIES AND RESEARCH

IN PARTIAL FULFILLMENT OF THE REQUIREMENTS FOR THE DEGREE

OF DOCTOR OF PHILOSOPHY

IN

GEOPHYSICS

DEPARTMENT OF PHYSICS

EDMONTON, ALBERTA

FALL, 1975

THE UNIVERSITY OF ALBERTA

FACULTY OF GRADUATE STUDIES AND RESEARCH

The undersigned certify that they have read, and recommend to the Faculty of Graduate Studies and Research, for acceptance, a thesis entitled THE ENHANCEMENT OF SIGNAL TO NOISE IN MAGNETOTELLURIC DATA submitted by Dominique Wen Kao in partial fulfillment of the requirements for the degree of Doctor of Philosophy in Geophysics.

D. Rankin
Supervisor

D. B. Jones

E. R. Kanasewich

R. E. Johnson

E. R. Niblett
External Examiner

Date: July 24, 1975

W. J. Kroeger

ABSTRACT

The magnetotelluric (MT) method of sounding is reviewed and the interpretative techniques including both numerical modelling and tensor impedance concepts are presented in a formulation suitable for the study of the problem of noise in magnetotelluric signals.

A statistical treatment of the noise problem has resulted in the development of a cyclical process which produces a pronounced enhancement of the signal to noise ratio over the complete spectral range in the majority of processed data samples. In those cases where the data was not so improved a definite confidence limit could be placed on that portion of the spectral range which was acceptable.

This technique was applied to magnetotelluric soundings made at 14 sites around the Black Hills of South Dakota in the frequency band 10^{-3} to 10 Hz. The soundings cover an area of approximately 30,000 square Km and correspond to a depth range of 0.1 to 50 Km.

A three dimensional earth model of the estimated resistivity distribution is derived from the sounding results, using the generalized impedance concepts. An anomaly of high conductivity at depths of 3 to 10 Km is found in the central region of the Hills, under the cover of highly resistive granitic material.

ACKNOWLEDGEMENTS

I am indebted first and foremost to Dr. D. Rankin, my thesis supervisor, for his guidance and encouragement during this project; the stimulation and friendship which he has given me are greatly valued. Thanks are due to Dr. I.K. Reddy who supplied programs employed in this work and whose knowledge of these techniques saved many long hours of work; to Dr. A. Rogers for very helpful preliminary editing of this work; and to Dr. R. Sigal for final editing and many invaluable criticisms. As well, I would like to acknowledge the assistance of Mr. N. Ouellette for the field work, and the excellent typing of this thesis by Mrs. M. Yiu. Finally, I wish to express my sincere gratitude to Mrs. Helen Hawkes for her kindness and enthusiastic help with many aspects of the production of this work during the course of studies in the Physics Department. Throughout the course of this research financial support was provided by a Graduate Teaching Assistantship from the Department of Physics, University of Alberta.

TABLE OF CONTENTS

		Page
CHAPTER I	INTRODUCTION	1
A.	Historical Review	1
B.	Outline of the Thesis	3
CHAPTER II	THEORETICAL DISCUSSION	5
A.	Maxwell's Equations for Plane Waves in a Uniform Medium	5
B.	Consideration of Skin Depth Effect	7
C.	Plane Wave Incident on an Uniform Earth	8
D.	Apparent Resistivity of Layered Earth	9
	1) Single-layer earth	9
	2) n-layer earth	11
E.	Tensor Impedance Analysis	14
F.	Examples of Impedance Functions	18
	1) Uniform earth	18
	2) Layered earth	19
	3) Vertical fault - two-dimensional model	21
G.	Reduction of a Three-Dimensional Problem to a Two-Dimensional Formulation	23
H.	Orientational Behavior	28

Page

CHAPTER II (cont'd)

I. Special Cases and the Indication of Dimensionality 33

1) One-dimensional case 33

2) Two-dimensional case 34

3) Three-dimensional case 37

CHAPTER III INSTRUMENTATION AND DATA ANALYSIS 42

A. Instrumentation 42

1) Magnetic system 42

2) Electric system 45

3) Digital recording 45

B. Data Analysis 45

1) Power spectrum computation 45

a) Truncation 46

b) Removing mean and trend 46

c) Tapering 46

d) Fourier transform 47

e) Hamming window 48

f) System response correction 48

g) Power spectrum computation 48

2) Polarization Discussion 50

a) Degree of Polarization 50

b) Polarization Angle 51

c) Ellipticity 51

Page

CHAPTER III (cont'd)

B. 3) Impedance computation 52

4) Criteria of data reliability 55

a) Phasor Coherency (CP) 55

b) Predicted Coherency (PCH) 56

CHAPTER IV NOISE DISCUSSION 58

A. General Discussion 59

1) Covariance and coherence 59

2) Power spectrum of signal and noise 62

a) Power spectrum of random noise 62

b) Power spectrum of signal 64

c) Spectral densities with mixed signal and noise 65

3) Power estimates and averaging effect 68

4) Experiment 71

B. Investigation of Noise Effect in Impedance Elements 72

1) General solution 72

2) Impedance solutions for noise-free cross-power estimates 78

3) Impedance solutions as noise in both auto- and cross-power estimates 83

		Page
CHAPTER V	MT SOUNDING	90
A.	Geological Background	90
B.	Data Analysis and Result	98
C.	Interpretation and Discussion	112
	1) General discussion	112
	2) Earth model	113
	3) Summary and comment	115
APPENDIX A	MODELLING CONSIDERATION	130
I.	One-Dimensional Model	130
II.	Two-Dimensional Model	131
APPENDIX B	TABULATED ANALYSIS RESULTS	141
BIBLIOGRAPHY		125

CHAPTER I

INTRODUCTION

1-A. Historical Review

The process of determining the subsurface resistivity structure of the earth, by measurements made at the surface, using the naturally occurring electromagnetic fields as a source, was originally proposed by Tikhonov (1950). Measurements were carried out both by Tikhonov (1950), Kato and Kikuchi (1950), and Rikitake (1950, 1951). In a definitive work Cagniard (1953) presented a graphical method for the interpretation of results in the case of a horizontally layered earth and introduced the expression "Magnetotelluric Method" to designate the technique.

As originally envisaged by Cagniard, the source was infinitely extended and thus a plane wave impinged on the horizontally stratified earth. Wait (1954), and later Price (1964), investigated the effect of finite source dimension on the measured impedances, and argued that if the source is finite in extent or possesses horizontal gradients, complex angles of incidence must be considered. However, Madden and Nelson (1964) showed that for reasonable earth conductivity models, the plane wave assumption appears to

be valid in the frequency range of interest for the MT method.

A more important consideration than that of source dimensions, may be that a one-dimensional model is inadequate for a real earth where lateral inhomogeneity and anisotropy in the conductivity are present, and the electric and magnetic fields may, in general, no longer be orthogonal. d'Erceville and Kunetz (1962) and Rankin (1962) gave analytic solutions for a vertical fault and vertical dyke respectively. Chetaev (1960), Cantwell (1960), Bostick and Smith (1962), Mann (1965), O'Brien and Morrison (1967), Praus and Petr (1969), Rankin and Reddy (1969, 1970), and others have studied various types of anisotropy in conductivity by means of impedance tensor technique, and have proposed methods to find the principal directions of conductivity anisotropy. Madden and Nelson (1964), Swift (1967), Morrison et al. (1968), Sims and Bostick (1969), Word et al. (1970), Vozoff (1972), and others have presented technique to compute tensor impedance elements; this tensor matrix relates the electro-magnetic fields for two and three dimensional structures. Analog model studies have been carried out by Rankin et al. (1965), Dosso (1966), Takaes (1969), and others.

A considerable number of experimental results have been reported from various locations in North America, Europe, and Russia (Srivastava et al. 1963, Whitham and Anderson 1966, Berdichevsky 1966, Vozoff 1969, 1972, Peeples and Rankin 1973, and others). While the results have been significant, many of the questions and problems involved, particularly with respect to interpretive techniques, still remain.

I-B. Outline of the Thesis

Chapter two will present the theory of the MT methods.

Chapter three will describe the recording system and the techniques of data analysis.

Chapter four will discuss the noise effect, and present a technique for improving the signal to noise ratio.

Chapter five will present the sounding results, geological background, and model interpretation for the Black Hills in South Dakota.

CHAPTER II

THEORETICAL DISCUSSION

II-A. Maxwell's Equation for Plane Waves in a Uniform (homogeneous and isotropic) Medium

Consider the model in the cartesian coordinate system represented by xyz-axes as shown in Fig. (2-1). The z-axis is vertically downward and the earth of conductivity $\sigma(x,y,z)$ occupies the half space $z \geq 0$ with the surface at $z = 0$. The source is in free space $z < 0$. Maxwell's Equations in the MKS system for $e^{j\omega t}$ time dependence are

$$\nabla \times \vec{E} = -\frac{\partial \vec{B}}{\partial t} = -j\omega\mu\vec{H} \qquad (2\text{-}1a)$$

$$\nabla \times \vec{H} = \vec{J} = (\sigma + j\omega\varepsilon)\vec{E} \qquad (2\text{-}1b)$$

$$\nabla \cdot \vec{E} = q/\varepsilon \qquad (2\text{-}1c)$$

$$\nabla \cdot \vec{H} = 0$$

where $\omega = 2\pi f$ is the angular frequency; q is free charge density; and σ,μ,ε are the conductivity, permeability, and dielectric constant respectively, of the media. Except for anomalies which will not be discussed in this thesis, $\mu = \mu_o$, and $\varepsilon = \varepsilon_o$. For a uniform half space, the wave equation can be obtained from (2-1a,b) by taking the Curl.

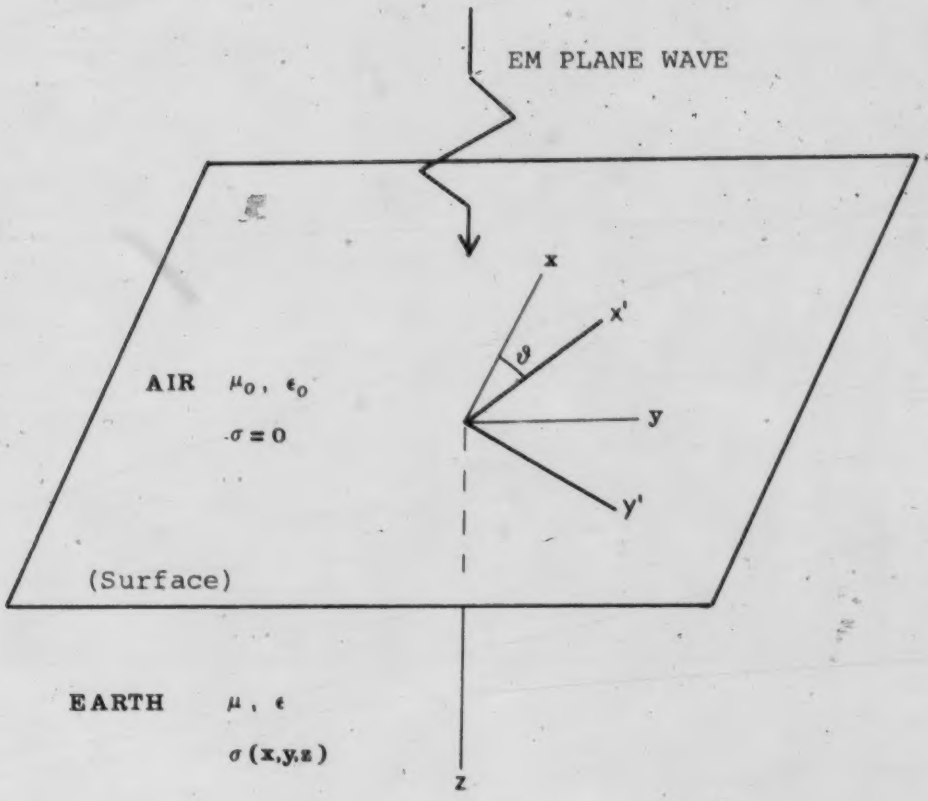

Fig.(2-1). Coordinate system and earth model.

$$\nabla \times \nabla \times \vec{A} = -j\omega\mu(\sigma + j\omega\varepsilon)\vec{A} \qquad (2\text{-}2)$$

where $\vec{A}$ represents a field vector $\vec{E}$ or $\vec{H}$. Eqn. (2-2) describes the field for all regions.

Except at discontinuities or in the source region, the free charge density is zero and hence within the medium $\nabla \cdot E = 0$ and Eq. (2-2) becomes the Helmholtz Equation

$$\nabla^2\vec{A} = j\omega\mu(\sigma + j\omega\varepsilon)\vec{A} \; . \qquad (2\text{-}3)$$

In a homogeneous region where σ is constant, Eqn. (2-3) is satisfied by a plane wave solution of the form

$$\vec{A} = A_o e^{\pm\vec{k}\cdot\vec{r}}$$

where

$\vec{r} = \hat{i}x + \hat{j}y + \hat{k}z$ is the position vector, and

$\vec{k} = \hat{i}k_x + \hat{j}k_y + \hat{k}k_z$ is the propagation vector, and

$$K = |\vec{k}| = \sqrt{j\omega\mu(\sigma + j\omega\varepsilon)} \; . \qquad (2\text{-}4)$$

The frequency of interest in this work will range from 10^{-3} — 10 Hz, and the conductivity of the earth from 10^{-4} — 1 mhos. Thus $\sigma >> \omega\varepsilon$ within the earth, and henceforth the propagation constant in the earth becomes approximately

$$K_1 = \sqrt{j\omega\mu\sigma} = (1+j)\sqrt{\omega\mu\sigma/2} \quad . \qquad (2\text{-}5a)$$

In the air where $\sigma = 0$, the propagation constant is

$$K_o = j\omega\sqrt{\mu\varepsilon} \quad . \qquad (2\text{-}5b)$$

It is obvious that $K_o << K_1$.

II-B. Consideration of Skin Depth Effect

When the field propagates in the earth, the real component of K_1 produces an attenuation effect on the field. The attenuation factor for a given wave in a medium with conductivity σ is

$$Re[K_1] = \sqrt{\omega\mu\sigma/2} \qquad \text{or} \qquad \sqrt{\pi\mu_o/\rho T} \quad .$$

The propagation distance or penetration depth δ, within which the strength of the field is attenuated by a factor of e^{-1}, is defined as the skin depth, where

$$\delta = 1/Re[K_1] = \sqrt{2/\omega\mu\sigma} \quad . \qquad (2\text{-}6)$$

The wave length of the field in this conductive medium is related to the skin depth by

$$\lambda = 2\pi\delta \quad .$$

The field measured at the surface due to reflecting surfaces at a depth equivalent to approximately one half-wave length for example, will be attenuated by a

factor $e^{-6.28}$. In addition the secondary fields are reduced by the finite reflective coefficient of the anomaly and possibly out of phase relations.

The velocity of phase propagation of the wave within a medium of conductivity σ, is $f\lambda$. Thus for a conductivity $\sigma = 10^{-1}$ mhos and $f = 10^{-1}$ Hz, the velocity is

$$v = \sqrt{\frac{4\,f}{\mu_o \sigma}} \cong 3 \times 10^3 \text{ m/sec} .$$

As a consequence a plane wave incident at an oblique angle will propagate perpendicular to the surface as though it were at normal incidence.

II-C. Plane Wave Incident on a Uniform Earth

In the case of a uniform earth where σ is constant, the E and H-fields are related in Eqn. (2-1a)

$$\nabla \times \vec{E} = -j\omega\mu\vec{H} .$$

Considering the E-field polarized in the x-direction and the H-field in the y-direction, the above relation can be rewritten as

$$j\omega\mu H_y = -\frac{\partial E_x}{\partial z} = K_1 E_x$$

and

$$E_x = \sqrt{j\omega\mu\rho}\, H_y \qquad (2\text{-}7)$$

where $\rho = 1/\sigma$ is the resistivity of the medium.

The impedance Z is defined

$$Z \equiv \frac{E_x}{H_y} = \sqrt{j\omega\mu\rho} = \sqrt{\omega\mu\rho}\, e^{j\pi/4} \quad . \qquad (2\text{-}8)$$

Thus the phase angle between the E and H-fields for a uniform half space is $\phi = \pi/4$. The resistivity in this case of the uniform earth obtained from Eqn. (2-7) or (2-8) is

$$\rho = \frac{1}{\omega\mu} |Z|^2 = \frac{1}{\omega\mu} \left|\frac{E_x}{H_y}\right|^2 \quad . \qquad (2\text{-}9)$$

II-D. Apparent Resistivity of Layered Earth

For a uniform earth as discussed in the previous section, the true resistivity of the medium can be directly deduced from the measured fields. For a more general case, however, the true resistivity of the medium is a more complex function of the measured fields.

(1) Single layered earth: This model consists of a uniform layer of thickness h and resistivity ρ_1, overlying a half space with resistivity ρ_2, as shown in Fig. (2-2a). Choosing the source E-field polarized in the x-direction, the plane wave equation can be written (from Eqn. (2-3)) as

$$\frac{\partial^2 H_y}{\partial z^2} = K_i^2 H_y \quad .$$

A solution has the form

$$H_y(z) = A_i e^{-K_i(z-z_{i-1})} + B_i e^{K_i(z-z_{i-1})}$$

$$E_x(z) = K_i \rho_i (A_i e^{-K_i(z-z_{i-1})} - B_i e^{K_i(z-z_{i-1})})$$

in each layer. The coefficient A_i is associated with a positive going (downward) transmitted wave, and B_i with the upward reflected wave. z_{i-1} is the depth to the upper surface of the i-th layer. Thus in medium 1, where $z_{i-1} = z_o = 0$

$$H_y(z) = A_1 e^{-K_1 z} + B_1 e^{+K_1 z}$$

$$E_x(z) = K_1 \rho_1 [A_1 e^{-K_1 z} - B_1 e^{+K_1 z}]$$

while in medium 2 where $z_{i-1} = z_1 = h$ (the thickness of the first layer)

$$H_y(z) = A_2 e^{-K_2(z-h)}$$

$$E_x(z) = K_2 \rho_2 A_2 e^{-K_2(z-h)}$$

where $B_2 = 0$ since there is no upward reflected wave. From the boundary condition that the tangential components of the field are equal at $z = h$,

$$A_1 = \frac{1}{2}\left(1 + \frac{K_2\rho_2}{K_1\rho_1}\right)A_2 e^{K_1 h}$$

$$B_1 = \frac{1}{2}\left(1 - \frac{K_2\rho_2}{K_1\rho_1}\right)A_2 e^{-K_1 h} .$$

Thus, the surface impedance is obtained

$$Z_o \equiv \frac{E_x(0)}{H_y(0)} = \rho_1 K_1 \left(\frac{A_1 - B_1}{A_1 + B_1}\right)$$

$$= \rho_1 K_1 \left(\frac{\sqrt{\rho_2}(1+\alpha) + \sqrt{\rho_1}(1-\alpha)}{\sqrt{\rho_2}(1-\alpha) + \sqrt{\rho_1}(1+\alpha)}\right) \qquad (2\text{-}10)$$

where $\alpha = e^{-2K_1 h}$.

The apparent resistivity is defined by

$$\rho_a \equiv \frac{1}{\omega\mu}[Z_o]^2 = \rho_1 \left(\frac{A_1 - B_1}{A_1 + B_1}\right)^2 . \qquad (2\text{-}11)$$

This is the apparent resistivity of a single-layer earth, which differs from the true resistivity ρ_1 by a factor $[(A_1-B_1)/(A_1+B_1)]^2$. This factor is a function of the earth parameters, i.e., the resistivities of the two differently conductive regions and the thickness of the overlying layer.

(2) n-layered earth: A typical n-layered earth model is as shown in Fig. (2-2b). The solutions for the m-th layer have the form

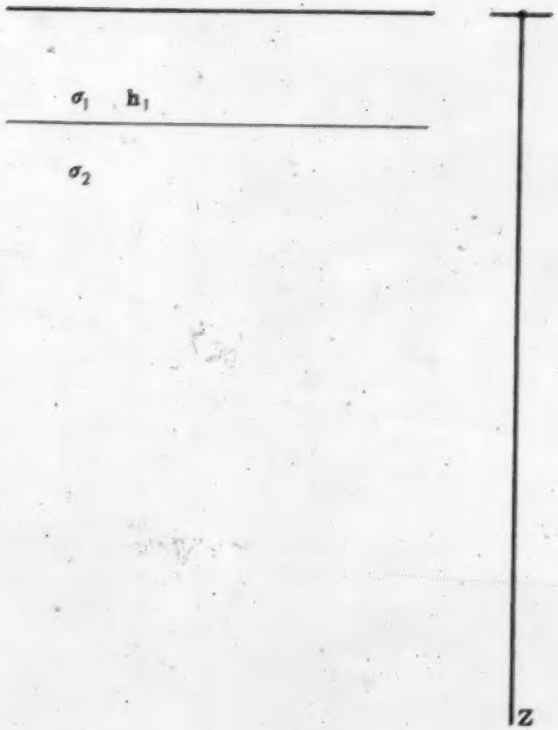

Fig.(2-2a). Single-layer model.

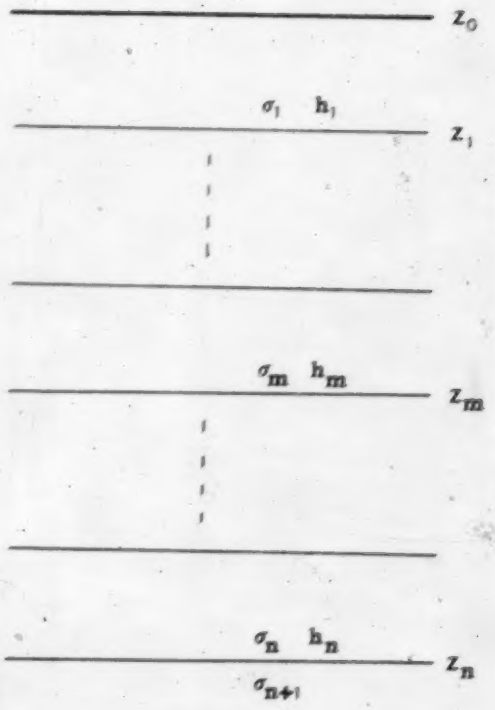

Fig.(2-2b). n-layer model.

$$H_{y,m}(z) = A_m e^{-K_m(z-z_{m-1})} + B_m e^{K_m(z-z_{m-1})}$$

$$E_{x,m}(z) = K_m \rho_m [A_m e^{-K_m(z-z_{m-1})} - B_m e^{K_m(z-z_{m-1})}] .$$

Applying the boundary conditions at $z = z_m$, the transmission and reflection coefficients can be expressed by

$$A_m = \frac{1}{2}[(1+\gamma)A_{m+1} + (1-\gamma)B_{m+1}]e^{K_m h_m}$$

$$B_m = \frac{1}{2}[(1-\gamma)A_{m+1} + (1-\gamma)B_{m+1}]e^{-K_m h_m}$$

where $\gamma = (K_{m+1}\rho_{m+1})/(K_m\rho_m)$, and $h_m = z_m - z_{m-1}$ is the thickness of the m-th layer. The impedance of this m-th layer is defined

$$Z_m = \frac{E_{x,m}}{H_{y,m}} = K_m \rho_m \frac{K_m\rho_m \tanh(K_m\rho_m) + Z_{m+1}}{K_m\rho_m + Z_{m+1}\tanh(K_m\rho_m)} . \qquad (2\text{-}12)$$

The surface impedance is

$$Z_o = \frac{E_x(0)}{H_y(0)} = K_1\rho_1 \frac{A_1 - B_1}{A_1 + B_1} = K_1\rho_1 \frac{K_1\rho_1 \tanh(K_1\rho_1) + Z_2}{K_1\rho_1 + Z_2 \tanh(K_1\rho_1)} \qquad (2\text{-}13a)$$

and the apparent resistivity is

$$\rho_a = \frac{1}{\omega\mu}|Z_o|^2 = \rho_1\left(\frac{A_1 - B_1}{A_1 + B_1}\right)^2 \qquad (2\text{-}13b)$$

where A_1, B_1, and in turn $[A_1-B_1/A_1+B_1]^2$ are functions of the resistivities and thickness of all the layers.

II-E. Tensor Impedance Analysis

In the previous section, the case of a uniform or piecewise uniform medium was discussed in which the field component variations were a function of one variable only and the resistivity was a scalar. In a more general case both the components of the fields and the resistivity are functions of 3 spatial variables. In this case one defines an impedance tensor [Z] such that

$$[\vec{E}] = [Z]\ [\vec{H}] \qquad (2\text{-}14)$$

where $[\vec{E}]$ and $[\vec{H}]$ are the electric and magnetic field vectors written as column matrices and [Z] is in general a 3×3 impedance matrix relating each of the components of E to 3 components of H. The components of [Z] are point functions of earth parameters together with the appropriate frequency dependence. While analytic solutions are possible only in very special cases, it is of interest to develop general expressions for the electromagnetic fields in terms of the earth parameters.

Assuming the earth behaves like a linear system, the secondary field and in turn the total field is linearly related to the primary magnetic field, $H_p(r)$. At the surface, $x,y,z = 0$

$$[\vec{H}_p(0)] = (H_{px}(0),\ H_{py}(0),\ 0) \qquad (2\text{-}15)$$

Thus, the total H-field within the earth can then be related to the primary field at the surface

$$[\vec{H}(r)] = [\phi(r)]\ [\vec{H}_p(0)] \qquad (2\text{-}16)$$

where $[\phi(r)]$ is generally a 3×3 matrix. However, since $H_{pz}(0) = 0$, only the 3×2 part is present. The elements of $[\phi(r)]$ are functions of the transmission and reflection coefficients, which are in turn, of the position r and other earth parameters.

The E-field at position r can be obtained from a generalized form of Ohms law, appropriate to an anisotropic earth, and Maxwell's equations,

$$[\vec{E}(r)] = [\rho(r)][\vec{J}(r)] = [\rho(r)][\nabla \times \vec{H}(r)] \qquad (2\text{-}17)$$

where $\rho(r)$ is a 3×3 matrix, its elements representing the tensor coefficients of the resistivity of the earth; and J is the current density. At the surface, the components of J in terms of $H_p(0)$ can be obtained by substituting H(r) from Eqn. (2-16) into $J(r) = \nabla \times H(r)$ and evaluating at the surface

$$J_x(0) = (y\phi_{31} - z\phi_{21})H_{px}(0) + (y\phi_{32} - z\phi_{22})H_{py}(0) \qquad (2\text{-}18a)$$

$$J_y(0) = (z\phi_{11} - x\phi_{31})H_{px}(0) + (z\phi_{12} - x\phi_{32})H_{py}(0) \qquad (2\text{-}18b)$$

$$J_z(0) = ({}_x\phi_{21} - {}_y\phi_{11})H_{px}(0) + ({}_x\phi_{22} - {}_y\phi_{12})H_{py}(0) \quad (2\text{-}18c)$$

where ${}_q\phi_{ij} \equiv \left(\frac{\partial}{\partial q}\ \phi_{ij}(r)\right)_{r=0}$.

Since no conduction current flows in the air region, the continuity condition at the air-earth interface requires that in the earth at or near the surface, J_z vanishes. Thus the E-field at the surface can be expressed in terms of $H_p(0)$ by

$$E_x(0) = \rho_{11}J_x(0) + \rho_{12}J_y(0)$$

$$= \{\rho_{11}({}_y\phi_{31} - {}_z\phi_{21}) + \rho_{12}({}_z\phi_{11} - {}_x\phi_{31})\}H_{px}(0)$$

$$+ \{\rho_{11}({}_y\phi_{32} - {}_z\phi_{22}) + \rho_{12}({}_z\phi_{12} - {}_x\phi_{32})\}H_{py}(0) \quad (2\text{-}19a)$$

$$E_y(0) = \rho_{21}J_x(0) + \rho_{22}J_y(0)$$

$$= [\rho_{21}({}_y\phi_{31} - {}_z\phi_{21}) + \rho_{22}({}_z\phi_{11} - {}_x\phi_{31})]H_{px}(0)$$

$$+ [\rho_{21}({}_y\phi_{32} - {}_z\phi_{22}) + \rho_{22}({}_z\phi_{12} - {}_x\phi_{32})]H_{py}(0) \quad (2\text{-}19b)$$

$$E_z(0) = \rho_{31}J_x(0) + \rho_{32}J_y(0)$$

$$= [\rho_{31}({}_y\phi_{31} - {}_z\phi_{21}) + \rho_{32}({}_z\phi_{11} - {}_x\phi_{31})]H_{px}(0)$$

$$+ [\rho_{31}({}_y\phi_{32} - {}_z\phi_{22}) + \rho_{32}({}_z\phi_{12} - {}_x\phi_{32})]H_{py}(0). \quad (2\text{-}19c)$$

Eqns. (2-19) define the primary impedance relating the primary H-field to the E-field at the surface, by

$$[E(0)] = [Z_p][H_p(0)] \tag{2-20}$$

where $[Z_p]$ is a 2×3 matrix as indicated in Eqns. (2-19).

The surface impedance, which defines the relationship between the total H-field and the E-field at the surface, can be determined as follows. From Eqn. (2-16), the inverse matrix of $[\phi(0)]$ can be generated and evaluated at the surface,

$$[H_p(0)] = [\phi(0)]^{-1} [H(0)] \tag{2-21}$$

where $[\phi(0)]^{-1}$ is defined by $[\phi(0)]^{-1}[\phi(0)] = [I]$. Substituting Eqn. (2-21) to (2-20), the total H-field and the E-field at the surface are related by

$$[E(0)] = [Z_p] [\phi(0)]^{-1} [H(0)] . \tag{2-22}$$

Thus, the surface impedance function for the three dimensional earth is

$$[Z] = [Z_p] [\phi(0)]^{-1} \tag{2-23}$$

where $[Z]$ is a 3×3 matrix. An explicit form of E-H fields relation can then be expressed in terms of the elements of $[Z]$.

$$E_x = Z_{11}H_x + Z_{12}H_y + Z_{13}H_z \qquad (2\text{-}24a)$$

$$E_y = Z_{21}H_x + Z_{22}H_y + Z_{23}H_z \qquad (2\text{-}24b)$$

$$E_z = Z_{31}H_x + Z_{32}H_y + Z_{33}H_z \qquad (2\text{-}24c)$$

II-F. Examples of the Impedance Functions

(1) Uniform Earth: $(\sigma(x,y,z) = \sigma_o = 1/\rho_o)$.

In a uniform half-space the total H-field is the transmitted primary H-field. If the surface value of the field is denoted by

$$\vec{H}_p(0) = (H_{xo}, H_{yo}, 0) ,$$

then the total field at $z > 0$ is

$$\vec{H}(z) = \vec{H}_p(z) = (H_{xo}e^{-Kz}, H_{yo}e^{-Kz}, 0) ,$$

for which,

$$[\phi(r)] = \begin{pmatrix} e^{-Kz} & 0 \\ 0 & e^{-Kz} \\ 0 & 0 \end{pmatrix} \qquad (2\text{-}25)$$

where $K=\sqrt{j\omega\mu\sigma_o}$.

Thus, at the surface, the inverse of $[\phi(0)]$ is

$$[\phi(0)]^{-1} = \begin{pmatrix} 1 & 0 & 0 \\ 0 & 1 & 0 \end{pmatrix} .$$

The resistivity of a uniform earth can be denoted by

$$[\rho] = \begin{bmatrix} \rho & 0 & 0 \\ 0 & \rho & 0 \\ 0 & 0 & \rho \end{bmatrix}$$

and so that

$$[Z_p] = \begin{bmatrix} 0 & \rho K \\ -\rho K & 0 \\ 0 & 0 \end{bmatrix} .$$

Therefore, the surface impedance tensor is,

$$[Z] = [Z_p][\phi(0)^{-1}] = \begin{bmatrix} 0 & \rho K & 0 \\ -\rho K & 0 & 0 \\ 0 & 0 & 0 \end{bmatrix} . \qquad (2\text{-}26)$$

Eqn. (2-26) indicates that

$$Z_{12} = -Z_{21} = \sqrt{j\omega\mu\rho} \qquad (2\text{-}27a)$$

$$Z_{ij} = 0 \qquad i,j \neq 1,2 \qquad (2\text{-}27b)$$

$$i = j \quad .$$

The result given in Eqn. (2-27) is consistent with that given in Eqn. (2-8), for a uniform earth.

(2) Layered earth:

Referring the model to (II-D) and letting the primary H-field at the surface be denoted by

$$\vec{H}_p(0) = (A_x, A_y, 0)$$

the total H-field below the surface can then be written as

$$H_x(r) = A_x e^{-K_1 z} + B_x e^{K_1 z}$$

$$H_y(r) = A_y e^{-K_1 z} + B_y e^{K_1 z} \quad .$$

Comparing the above expressions with Eqn. (2-16), it is clearly seen that $[\phi(r)]$ has the form

$$[\phi(r)] = \begin{pmatrix} e^{-K_1 z} + \frac{B_x}{A_x} e^{K_1 z} & 0 & 0 \\ 0 & e^{-K_1 z} + \frac{B_y}{A_y} e^{K_1 z} & 0 \\ 0 & 0 & 0 \end{pmatrix} \qquad (2\text{-}28)$$

where $K_1 = \sqrt{j\omega\mu/\rho_1}$ and ρ_1 is the resistivity of the first layer, and B_x, B_y represent the effective reflection coefficients from all discontinuities. Since the parameters for each layer are constant within the layer

$$\frac{B_x}{A_x} = \frac{B_y}{A_y} = \frac{B}{A} \quad .$$

By following the procedure in the last paragraph, one can obtain

$$[\phi(0)]^{-1} = \begin{bmatrix} \dfrac{1}{1 + \dfrac{B}{A}} & 0 & 0 \\ 0 & \dfrac{1}{1 + \dfrac{B}{A}} & 0 \end{bmatrix}$$

$$[Z_p] = \begin{bmatrix} 0 & \rho_1 K_1 (1 - \dfrac{B}{A}) \\ -\rho_1 K_1 (1 - \dfrac{B}{A}) & 0 \\ 0 & 0 \end{bmatrix}$$

and the surface impedance tensor

$$[Z] = [Z_p][\phi(0)]^{-1} = \begin{bmatrix} 0 & \rho_1 K_1 (\dfrac{A - B}{A + B}) & 0 \\ -\rho_1 K_1 (\dfrac{A - B}{A + B}) & 0 & 0 \\ 0 & 0 & 0 \end{bmatrix} \qquad (2\text{-}29)$$

which is consistent with the result given in Eqn. (2-13a) or (2-10).

$$Z_{12} = -Z_{21} = \rho_1 K_1 \frac{A - B}{A + B} \qquad (2\text{-}30)$$

(3) Vertical fault - two dimensional model:

A vertical fault is shown schematically in Fig. (2-3), the x-axis is along the interface of the fault, or the strike direction. ρ_i (i = 1,2) is the resistivity

of the region i.

Let the primary H-field at the surface be

$$\vec{H}_p(0) = (A_x, A_y, 0) .$$

The total H-field can then be written

$$H_x(r) = A_x(e^{-K_i z} + R_{xx}(y,z))$$

$$H_y(r) = A_y(e^{-K_i z} + R_{yy}(y,z))$$

$$H_z(r) = A_y R_{zy}(y,z)$$

where R's represent the normalized reflection coefficients and depend upon y and z in this case. The associated functions are

$$[\phi(r)] = \begin{pmatrix} e^{-K_i z} + R_{xx} & 0 \\ 0 & e^{-K_i z} + R_{yy} \\ 0 & R_{zy} \end{pmatrix} \qquad (2\text{-}31)$$

$$[\phi(0)]^{-1} = \begin{pmatrix} \frac{1}{1 + R_{xx}} & 0 & 0 \\ 0 & \frac{1}{1 + R_{yy}} & 0 \end{pmatrix}_{z=0}$$

$$[Z_p] = \begin{pmatrix} 0 & \rho_i(K_i - zR_{yy} + yR_{zy}) \\ -\rho_i(K_i - zR_{xx}) & 0 \\ 0 & 0 \end{pmatrix}$$

where ${}_{q}R_{uv} \equiv \frac{\partial}{\partial q} [R_{uv}(r)]_{z=0}$

and the surface impedance tensor

$$[Z] = \begin{bmatrix} 0 & \frac{\rho_i (K_i - {}_{z}R_{yy} + {}_{y}R_{zy})}{1 + R_{yy}(0)} & 0 \\ \frac{-\rho_i (K_i - {}_{z}R_{xx})}{1 + R_{xx}(0)} & 0 & 0 \\ 0 & 0 & 0 \end{bmatrix} \qquad (2\text{-}32)$$

$$Z_{12} = \frac{\rho_i (K_i - {}_{z}R_{yy} + {}_{y}R_{zy})}{1 + R_{yy}(0)} \qquad (2\text{-}33a)$$

$$Z_{21} = - \frac{\rho_i (K_i - {}_{z}R_{xx})}{1 + R_{xx}(0)} \qquad (2\text{-}33b)$$

$$Z_{ij} = \begin{cases} 0 & i,j \neq 1,2 \\ & i = j \, . \end{cases} \qquad (2\text{-}33c)$$

The result $Z_{12} \neq Z_{21}$ shows the anisotropic behavior of the impedance tensor elements in the two dimensional case.

II-G. Reduction of a Three-Dimensional Problem to a Formal Two-Dimensional Formulation

The following analysis only applies for the case where the principle directions of resistivity are mutually orthogonal and thus a cartesian coordinate

system is applicable. The 9 impedance coefficients shown in Eqn. (2-24), are reduced to 4, generally non-independent, coefficients. Amongst all the components of the fields, only H_{px} and H_{py} are independent, while the others, H_x, H_y, H_z, E_x, E_y are linearly related to the two independent components. The mathematical proof can be carried out by rewriting Eqn. (2-16)

$$H_x = \phi_{11}H_{px} + \phi_{12}H_{py} \tag{2-34a}$$

$$H_y = \phi_{21}H_{px} + \phi_{22}H_{py} \tag{2-34b}$$

$$H_z = \phi_{31}H_{px} + \phi_{32}H_{py} \tag{2-34c}$$

It is obvious that H_x, H_y, and H_z are not independent; and each one of the three components are dependent on the other two. To put H_z in terms of H_x and H_y for instance, H_{px} and H_{py} can first be obtained in terms of H_x and H_y from Eqn. (2-34a,b), and then substituted in the Eqn. (2-34c)

$$H_z = \alpha_x H_x + \alpha_y H_y \tag{2-35}$$

where

$$\alpha_x = \frac{\phi_{31}\phi_{22} - \phi_{32}\phi_{21}}{\phi_{11}\phi_{22} - \phi_{12}\phi_{21}}$$

$$\alpha_y = \frac{\phi_{32}\phi_{11} - \phi_{31}\phi_{12}}{\phi_{11}\phi_{22} \quad \phi_{12}\phi_{21}} \quad .$$

An alternative proof can be achieved by considering a model in which the earth resistivity $\rho(r)$ approaches some constant value in the region near the surface. At the surface, $J_z(0) = 0$, and thus $E_z(0) = 0$. Substituting $E_z(0) = 0$ into Eqn. (2-24c), an equivalent relationship to Eqn. (2-35) is obtained,

$$H_z(0) = \alpha_x H_x(0) + \alpha_y H_y(0) \quad , \qquad (2\text{-}36)$$

Substituting H_z from Eqn. (2-35) or (2-36) into (2-24),

$$E_x = Z'_{11}H_x + Z'_{12}H_y$$

$$E_y = Z'_{21}H_x + Z'_{22}H_y$$

where

$$Z'_{11} = Z_{11} + Z_{31}\alpha_x$$

$$Z'_{12} = Z_{12} + Z_{32}\alpha_y$$

$$Z'_{21} = Z_{21} + Z_{31}\alpha_x$$

$$Z'_{22} = Z_{22} + Z_{32}\alpha_y \quad .$$

For convenience, the unprimed Z_{ij} with i,j = x,y will be used in the following text for surface impedance for two-dimensional problem, unless otherwise indicated.

$$E_x = Z_{xx}H_x + Z_{xy}H_y \qquad (2\text{-}37a)$$

$$E_y = Z_{yx}H_x + Z_{yy}H_y \qquad (2\text{-}37b)$$

The vertical component of magnetic field H_z is a secondary field, and is related to the total H-field components by Eqn. (2-35) or (2-36). At the surface

$$H_z(0) = \alpha_x H_x(0) + \alpha_y H_y(0) .$$

The relation between H_z and the E-field at the surface can be written

$$H_z(0) = Y_x E_x(0) + Y_y E_y(0) \qquad (2\text{-}38)$$

which defines the surface admittances $[Y_i]$. Eqns.(2-35), (2-37), and (2-38) give the following relations

$$\alpha_x = Y_x Z_{xx} + Y_y Z_{yx} \qquad (2\text{-}39a)$$

$$\alpha_y = Y_x Z_{xy} + Y_y Z_{yy} . \qquad (2\text{-}39b)$$

As a function of frequency, the impedance and admittance are related to the field components at a given point at the surface for any polarization of the source and for any arbitrary earth conductivity distribution, and hence they contain diagnostic information for geological interpretation.

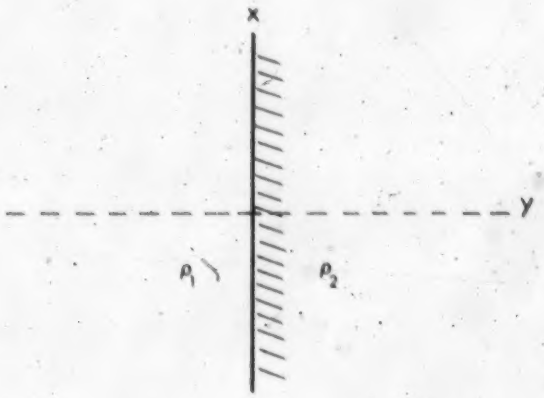

Fig.(2-3). Vertical fault.

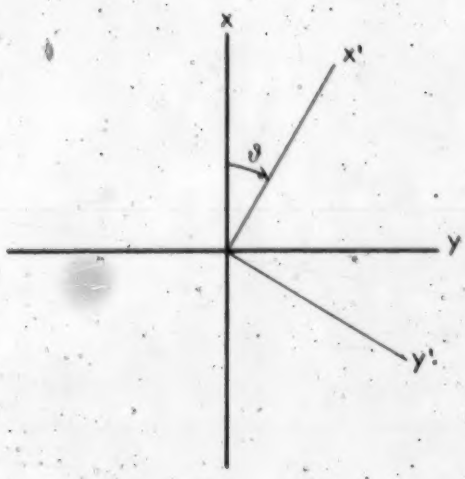

Fig.(2-4). Rotated coordinates.

II-H. Orientation Behavior

Surface impedance and admittance elements Z_{ij}, Y_i, and α_i which are functions of the earth parameters, contain the information for determination of geological substructure including their directional behavior. Taking the 2-dimensional problem as an example; as shown in Eqn. (2-33), if the axes of the coordinate system coincide with the principal directions, i.e. the strike direction and the perpendicular, Z_{xx} and Z_{yy} vanish. Physically, in either of the principal directions, a component of the E-field is correlated only with its orthogonal component of the H-field; thus the induction parameters Z_{xx} and Z_{yy} are zero. However, if the axes of the coordinates lie in any other directions, where the effective resistivity is no longer isotropic, each component of the E-field is induced by a combination of all components of the H-field, and the magnitude of each Z_{ij} is a measure of the induction effect between the corresponding E and H components.

In order to examine the directional behavior of Z_{ij}, one can rotate the fields E and H from an arbitrary direction x-y, i.e. the measuring direction, to a new direction x'-y' as shown in Fig. (2-4), where

$$E'_x = \cos\theta\, E_x + \sin\theta\, E_y$$

$$E'_y = -\sin\theta\, E_x + \cos\theta\, E_y \quad .$$

This defines the rotation matrix which is orthogonal

$$[R] = \begin{pmatrix} \cos\theta & \sin\theta \\ -\sin\theta & \cos\theta \end{pmatrix} \qquad (2\text{-}40)$$

Orhtogonality of the matrix enables one to write

$$[E'] = [R]\ [E]$$

$$[H'] = [R]\ [H]$$

$$[E'] = [Z']\ [H']$$

and the rotated impedance matrix is obtained

$$[Z'] = [R]\ [Z]\ [R]^{-1} \quad . \qquad (2\text{-}41)$$

Thus, the rotated surface impedance elements Z'_{ij} are related to those in the measuring direction

$$Z'_{xx} = \tfrac{1}{2}[(Z_{xx}+Z_{yy}) + (Z_{xx}-Z_{yy})\cos 2\theta + (Z_{xy}+Z_{yx})\sin 2\theta] \qquad (2\text{-}42a)$$

$$Z'_{yy} = \tfrac{1}{2}[(Z_{xx}+Z_{yy}) - (Z_{xx}-Z_{yy})\cos 2\theta - (Z_{xy}+Z_{yx})\sin 2\theta] \qquad (2\text{-}42b)$$

$$Z'_{xy} = \tfrac{1}{2}[(Z_{xy}-Z_{yx}) + (Z_{xy}+Z_{yx})\cos 2\theta - (Z_{xx}+Z_{yy})\sin 2\theta] \qquad (2\text{-}42c)$$

$$Z'_{yx} = \tfrac{1}{2}[-(Z_{xy}-Z_{yx}) + (Z_{xy}+Z_{yx})\cos 2\theta - (Z_{xx}+Z_{yy})\sin 2\theta] \qquad (2\text{-}42d)$$

where $Z'_{ij}(\theta)$ are functions of the rotation angle θ, and also have the following relations

$$Z'_{yy}(\theta) = Z'_{xx}(\theta+90°) \tag{2-43}$$

$$Z'_{yx}(\theta) = -Z'_{xy}(\theta+90°) \tag{2-44}$$

$$Z'_{xy}-Z'_{yx} = Z_{xy} - Z_{yx} = 2Z_1 \tag{2-45}$$

$$Z'_{xx}+Z'_{yy} = Z_{xx} + Z_{yy} = 2Z_2 \tag{2-46}$$

where Z_1 and Z_2 are new constants. As shown by Sims (1969) the loci of $Z'_{ij}(\theta)$ in the complex plane are in general elliptical as shown in Fig. (2-5). This graphical representation is very helpful in visualizing the impedance behavior as a function of rotation and in the determination of dimensionality.

For convenience all ellipses of Z'_{ij} in Fig. (2-5) are shown to the same scale and correspond to the same angle θ_o between the measuring axis and the major axis of the resistivity structure.

$$\text{major axis} = Z'_{xy}(\theta_o) + Z'_{yx}(\theta_o)$$

$$\text{minor axis} = Z'_{xx}(\theta_o) + Z'_{yy}(\theta_o) \ .$$

The angle of the major axis can be found by maximizing either

$|Z'_{xy}(\theta)-Z_1^*|$ or $|Z'_{xy}(\theta)+Z'_{yx}(\theta)|$.

$$\frac{d}{d\theta}\left|Z'_{xy}(\theta) + Z'_{yx}(\theta)\right| = 0 \ . \qquad (2\text{-}47a)$$

The 4 possible solutions of Eqn. (2-47a), corresponding to the major and minor axis intercepts, are

$$\theta_o = \frac{1}{4}\tan^{-1}\frac{2\,\mathrm{Re}[(Z_{xx}-Z_{yy})^*(Z_{xy}+Z_{yx})]}{|Z_{xx}-Z_{yy}|^2 - |Z_{xy}+Z_{yx}|^2} \ . \qquad (2\text{-}47b)$$

This result is ambiguous since either of the principle directions of resistivity is found. However, this ambiguity can be removed by apparent resistivity information.

The rotated admittance elements can also be obtained

$$Y'_x(\theta) = Y_x \cos\theta + Y_y \sin\theta \qquad (2\text{-}48a)$$

$$Y'_y(\theta) = -Y'_x \cos\theta + Y_y \cos\theta \qquad (2\text{-}48b)$$

and are related to

$$Y'_x(\theta) = Y'_y(\theta+90°) \ .$$

The locus of $Y'_i(\theta)$ is also an ellipse as shown in Fig. (2-5). The ellipse is centered on the origin and oriented at the angle θ_{ze}. The rotation period for this locus is 360° in θ, instead of 180° as for Z'_{ij}. The major and minor axes are

$$\text{major axis} = 2Y'_x(\theta_{ze}) \qquad (2\text{-}49a)$$

$$\text{minor axis} = 2Y'_y(\theta_{ze}+90°) \ . \qquad (2\text{-}49b)$$

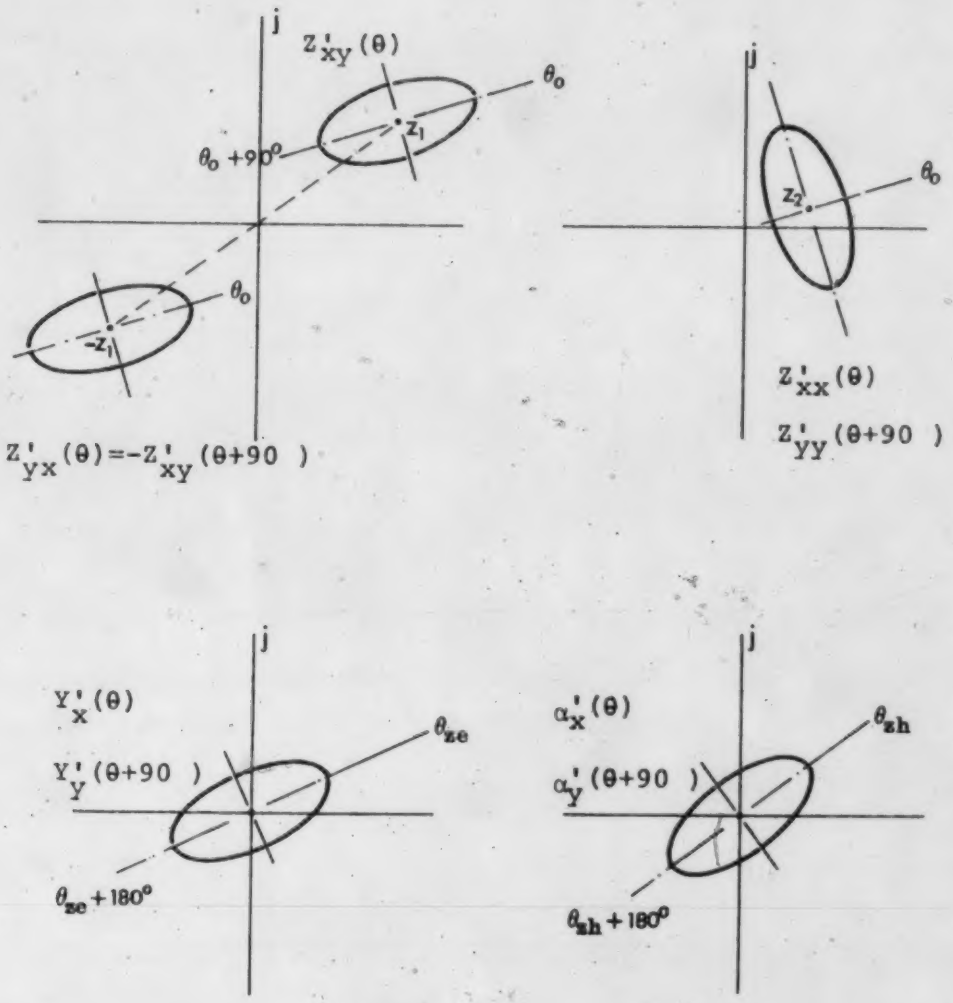

Fig.(2-5). $Z'_{ij}(\theta)$, $Y'_i(\theta)$ and $\alpha'_i(\theta)$ loci in complex plane. (θ=0 corresponding to the measuring axis not shown).

Using the procedure as used in dealing with Z'_{ij}, the angle θ_{ze} is found

$$\theta_{ze} = \frac{1}{2} \tan^{-1} \frac{2\,\mathrm{Re}(Y_x^* Y_y)}{|Y_x|^2 - |Y_y|^2} \quad . \tag{2-50}$$

The rotated α'_i behaves in a similar fashion to the Y'_i, except that $\alpha'_x \longrightarrow Y'_y$ and $\alpha'_y \longrightarrow Y'_x$.

II-I. Special Cases and the Indications of Dimensionality

(1) One-dimensional case:

When the earth conductivity is uniform or is a function of depth only, the surface impedance is invariant with rotation angle θ. Eqns. (2-27), (2-30), and (2-42) give these results

$$Z'_{xx} = Z'_{yy} = 0 \tag{2-51a}$$

$$Z'_{xy} = -Z'_{yx} = Z_1 \tag{2-51b}$$

where Z_1 is a complex scalar for all θ.

The rotation loci for Z'_{ij}, as shown in Fig.(2-6), reduce to points in the complex plane centered at $\pm Z_1$ for Z'_{xy} and Z'_{yx}, and at the origin for Z'_{xx} and Z'_{yy}.

In the one-dimensional case, no vertical magnetic field exists ($H_z = 0$), so that $Y'_x = Y'_y = 0$. The rotation loci for Y'_i and α'_i are also point ellipses

centered on the origin as shown in Fig. (2-6).

(2) Two-dimensional case:

As illustrated in Eqns. (2-33) for a two-dimensional model, Z'_{xx} and Z'_{yy} vanish along the principal axes, i.e. $\theta = \theta_o$, $\theta_o+90°$. Eqn. (2-46) also shows that the equation, $Z'_{xx}+Z'_{yy} = 2Z_2$, is invariant with rotation angle θ, so that, for a two-dimensional model $Z'_{xx}+Z'_{yy} = 2Z_2 = 0$, and thus,

$$Z'_{xx} = -Z'_{yy} \qquad \text{for all } \theta \tag{2-52a}$$

$$Z'_{xx} = Z'_{yy} = 0 \qquad \text{for } \theta = \theta_o,\ \theta_o+90° \ . \tag{2-52b}$$

The loci for Z'_{xx} and Z'_{yy} are straight line ellipses centered on the origin. The loci for Z'_{xy} and Z'_{yx} are also straight line ellipses centered at $\pm Z_1$, as shown in Fig. (2-7).

A vertical magnetic field H_z exists when the primary magnetic field has a component perpendicular to the strike. Elements of Y'_i and α'_i repeat for each 180° increment in θ. Suppose y'-axis is perpendicular to the strike (referring to Figs.(2-3) and (2-4)), Y'_i and α'_i are

$$Y'_x = \alpha'_y = 0 \qquad \theta = (\theta_{ze} + 90° \pm 180°) \tag{2-53a}$$

$$Y'_y = \alpha'_x = 0 \qquad \theta = (\theta_{ze} \pm 180°) \tag{2-53b}$$

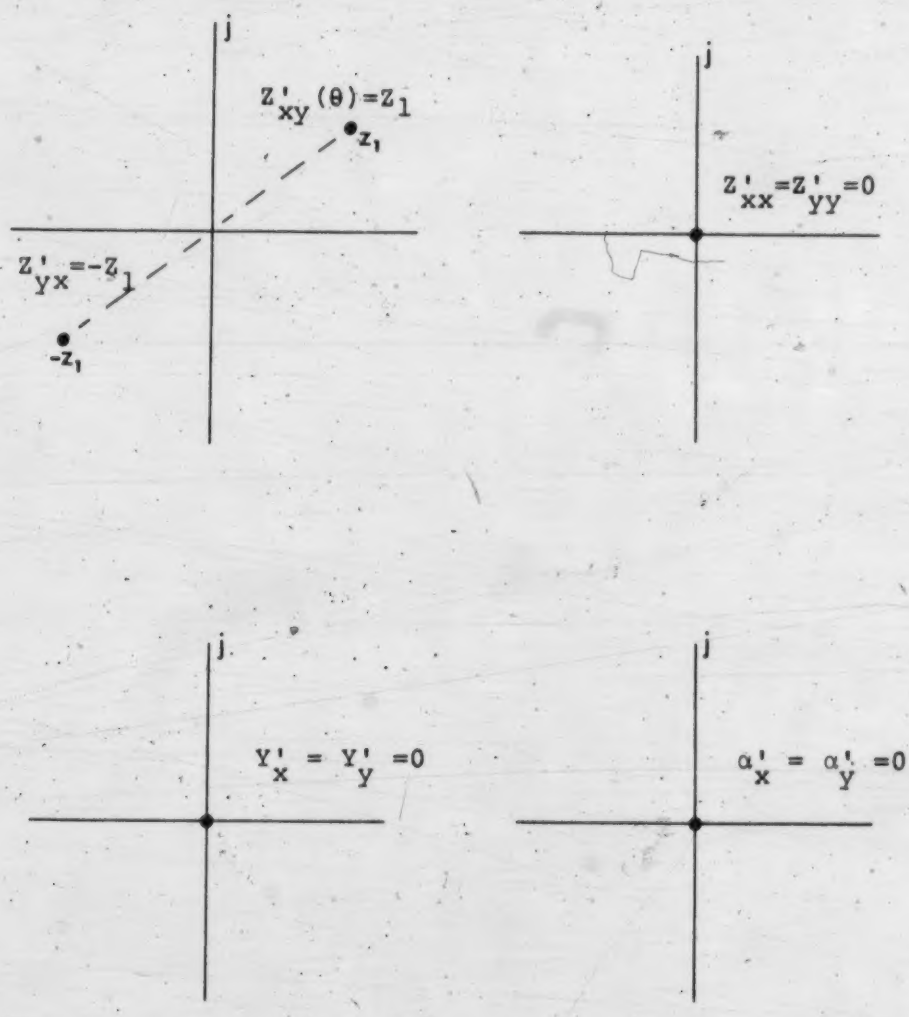

Fig.(2-6). $Z'_{ij}(\theta)$, $Y'_i(\theta)$ and $\alpha'_i(\theta)$ loci for one-dimensionality.

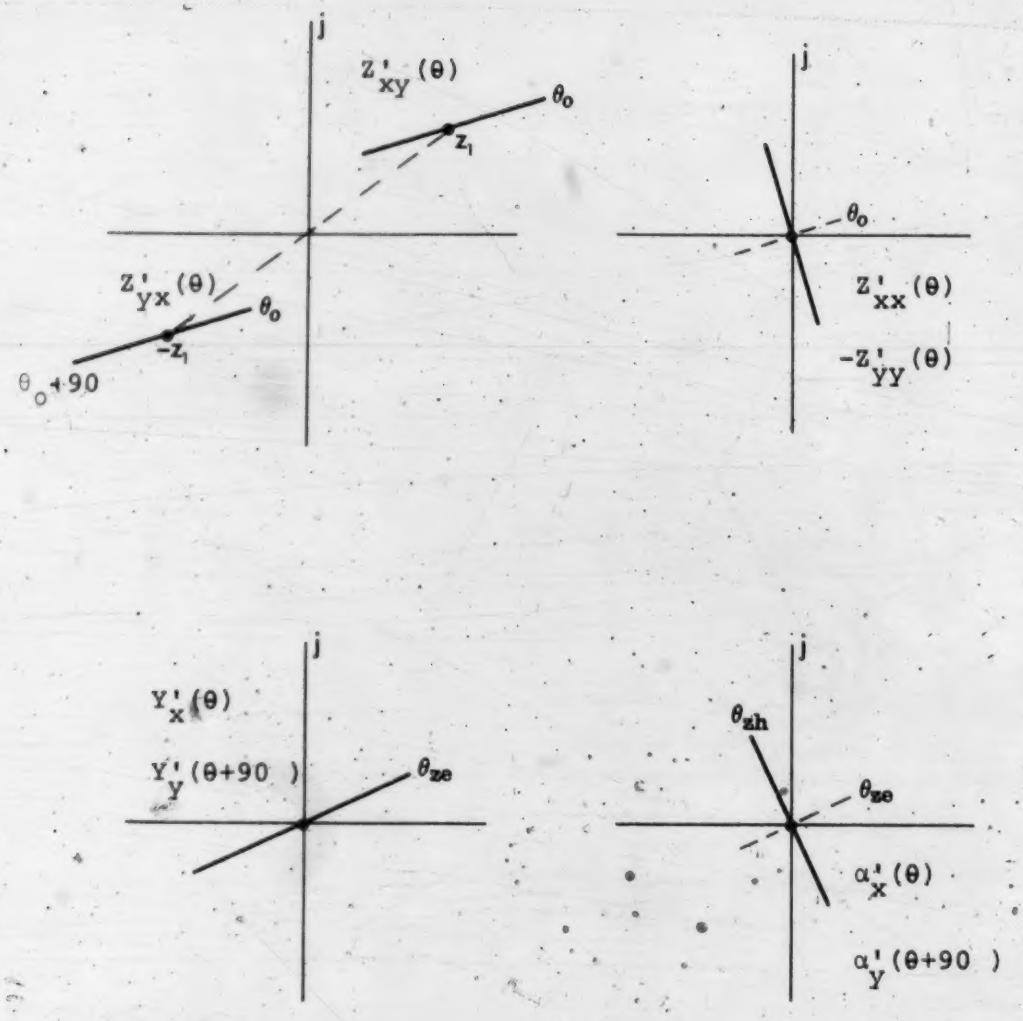

Fig.(2-7). $Z'_{ij}(\theta)$, $Y'_i(\theta)$ and $\alpha'_i(\theta)$ loci for two-dimensionality.

$$\theta_{ze} = \theta_{zh} \pm 90° \quad . \qquad (2\text{-}53c)$$

The loci of $Y_i'(\theta)$ and $\alpha_i'(\theta)$ are straight line ellipses centered on the origin as shown in Fig. (2-7).

The direction corresponding to the angle θ_o determined by Z_{ij}' can be one of the two principle directions. The angle θ_{ze}, however, determined by Y_i' (or θ_{zh} by α_i') corresponds to the direction parallel (or perpendicular) to the strike for a fault.

(3) Three-dimensional case:

Arbitrary conductivity structures could produce the elements of impedance and admittance, Z_{ij} and Y_i, having arbitrary values, and the rotation loci may in general be ellipses as given in Fig. (2-5). However, if there exists a plane of symmetry through the measuring point, the behavior of Z_{ij} and Y_i with respect to the rotation angle θ appears as those of a two-dimensional model. These special cases of three-dimensionality can be classified into the equivalent two-dimensional problems; some examples are shown in Fig. (2-8). The simplification in these cases results from the loss of information caused by making measurements at a point of symmetry. In fact the generalized two-dimensional impedance Z_{ij} and admittance Y_i can lead to unique interpretations only for two or one-dimensional models. However the more general result

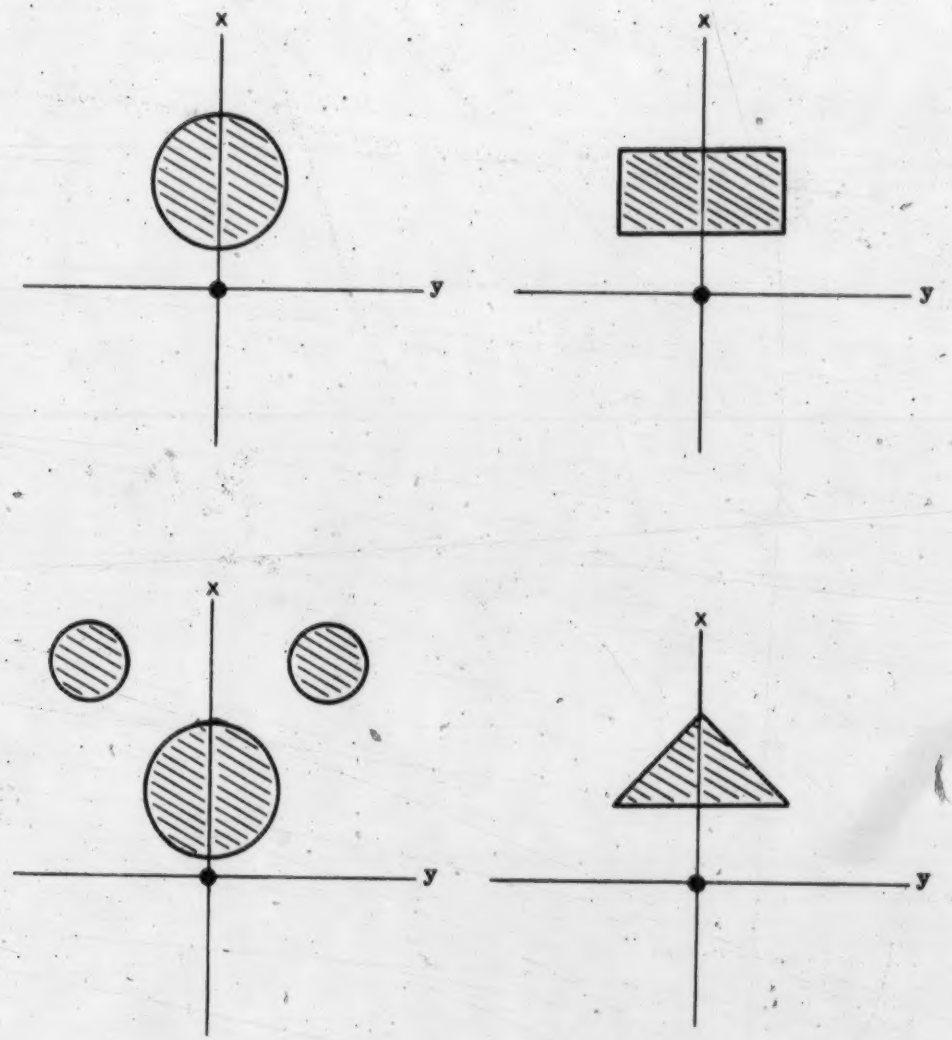

Fig.(2-8). Three-dimensional models with a plane of symmetry through the measuring point ● .

can give information on the dimensionality of the structure in terms of the dimensionality indicators

$$\bar{\alpha}(\text{skew}) \equiv \left|\frac{Z'_{xx}+Z'_{yy}}{Z'_{xy}-Z'_{yx}}\right| = \left|\frac{Z_{xx}+Z_{yy}}{Z_{xy}-Z_{yx}}\right| = \left|\frac{Z_2}{Z_1}\right| \quad \text{(Swift 1967)} \tag{2-54a}$$

$$\beta_o \equiv \left.\frac{Z'_{xx}-Z'_{yy}}{Z'_{xy}+Z'_{yx}}\right|_{\theta_o} \quad \text{(Word et al. 1970)} \tag{2-54b}$$

$$\beta_{\delta o} \equiv \left.\frac{Z'_{xx}-Z'_{yy}}{Z'_{xy}-Z'_{yx}}\right|_{\theta_o} \quad \text{(Word et al. 1970)} \tag{2-54c}$$

and

$$\beta_{ze} \equiv \left.\frac{Y'_y}{Y'_x}\right|_{\theta_{ze}} \qquad \beta_{zh} \equiv \left.\frac{\alpha'_x}{\alpha'_y}\right|_{\theta_{zh}} \quad \text{(Word et al. 1970)} \tag{2-54d}$$

Skew $\bar{\alpha}$ is invariant with rotation angle θ, and equal to the ratio between the two displacements from the origins to the centers of the corresponding ellipses as shown in Fig. (2-5). It is obvious that the condition $\bar{\alpha} = 0$ can indicate either one or two-dimensionality. Word et al. (1970) propose that $\bar{\alpha} = 0$ is a necessary but not a sufficient condition for two-dimensionality. The sufficient condition must include the condition $\beta_o = 0$. β_δ is the ratio of minor to major axes of the Z'_{ij} loci as shown in Fig. (2-5). For two-dimensional cases or equivalent, the rotation

loci are line ellipses, so that β_o is zero. However, for the one-dimensional cases, $\beta_o = (0/0)$ becomes an undetermined quantity.

For one or two-dimensional cases, $\beta_{oo} = 0$. β_{oo} has the advantage as an indicator by avoiding $\beta_o = 0/0$ for one-dimensional cases, in addition, it also has potential for judging the degree of three-dimensionality.

$\beta_{ze} = \beta_{zh} = 0$ for two-dimensionality, but is not necessarily non-zero for three-dimensionality.

The behavior of the dimensional indicators are summarized as following:

One dimensionality	$\bar{\alpha}$	$= 0$
	β_o	$= 0/0$
	β_{oo}	$= 0$
	$\beta_{ze} = \beta_{zh}$	$= 0/0$
Two dimensionality and special case of symmetry	$\bar{\alpha}$	$= 0$
	β_o	$= 0$
	β_{oo}	$= 0$
	$\beta_{ze} = \beta_{zh}$	$= 0$
Three dimensionality	$\bar{\alpha}$	$\neq 0$
	β_o	$\neq 0$
	β_{oo}	$\neq 0$
	$\beta_{ze} = \beta_{zh}$	$\overset{(may)}{=} 0$.

While the use of the dimensionality indicators provides some information regarding the nature of the structure, quantitative interpretation is restricted to one and two-dimensional models. In practice it is frequently possible to interpret the more usual three-dimensional structure in terms of these two and one-dimensional models to some reasonable degree of approximation. In this case, it may be desirable to define the following parameters:

$$\beta_1 \equiv \frac{\rho'_{xx} + \rho'_{yy}}{\rho'_{xy} + \rho'_{yx}} \qquad (2\text{-}55a)$$

$$\beta_2 \equiv \frac{\rho'_M - \rho'_m}{\rho'_M} \quad \text{(anisotropy factor)} \qquad (2\text{-}55b)$$

where ρ'_{ij} are the apparent resistivities corresponding to $Z'_{ij}(\theta_o)$, and ρ'_M and ρ'_m correspond to the maximum and minimum values between ρ'_{xy} and ρ'_{yx}.

3-dimensionality $\beta_1 \neq 0$, measuring the degree of 3-dimensionality.

$\beta_2 = 0 - 1$

2-dimensionality $\beta_1 = 0 \quad (\rho'_{xx} = \rho'_{yy} = 0)$

$\beta_2 \neq 0 \quad (\rho'_{xy} \neq \rho'_{yx})$

1-dimensionality $\beta_1 = 0$

$\beta_2 = 0 \quad (\rho'_{xy} = \rho'_{yx})$

CHAPTER III

INSTRUMENTATION AND DATA ANALYSIS

III-A. Instrumentation

The instruments used for data gathering have been described by Allsopp et al. (1974), and are shown in Fig. (3-1). It is designed to measure three components of the magnetic field (H_x,H_y,H_z) and two components of the electric field (E_x,E_y) of the micropulsation signals in the frequency range from 0.0001 to 10 H_z. A short description of this system will follow.

(1) Magnetic system:

A time varying magnetic field with amplitude of the order of 10^{-2} to 10^{2} gammas is detected with a specially designed induction type sensor (Burke and Rankin 1975) and produces μV level output in the frequency range of interest. Preamplification stage consists of a RATEK RA-11 parametric amplifier and two FET input operational amplifiers, with a total gain of 85 dB. The output is fed to a post amplifier with switchable voltage gains at -20, -10, 0, 10, 20 dB, and then through a Butterworth low pass filter to eliminate the aliasing effect. The overall amplitude and phase responses are shown in Fig. (3-2).

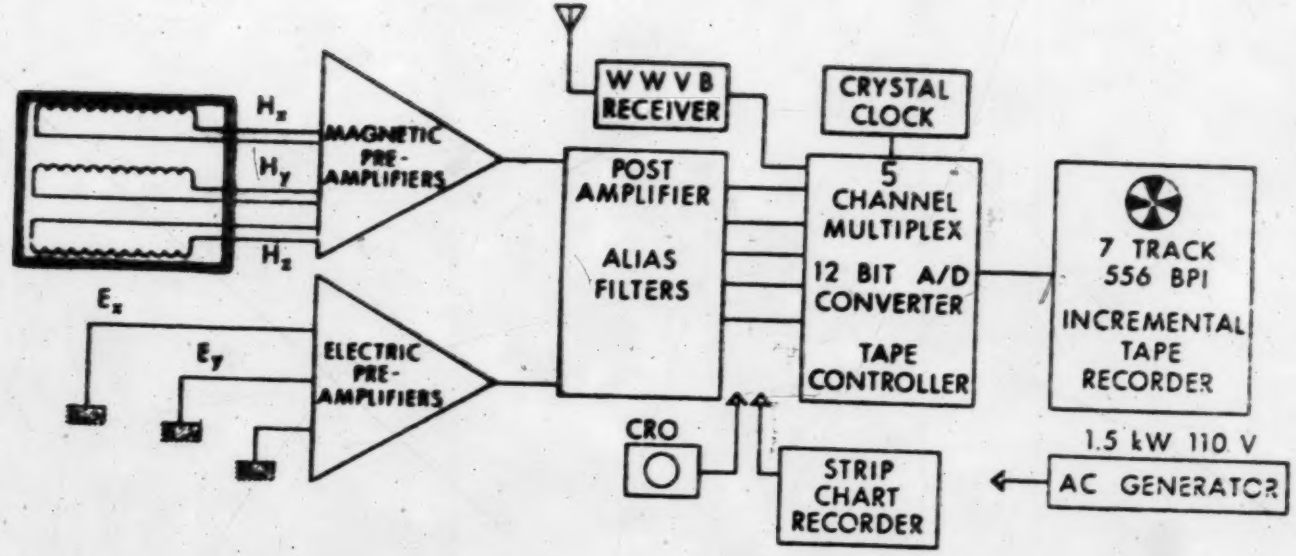

FIG.3-1 MAGNETOTELLURIC FIELD RECORDING SYSTEM

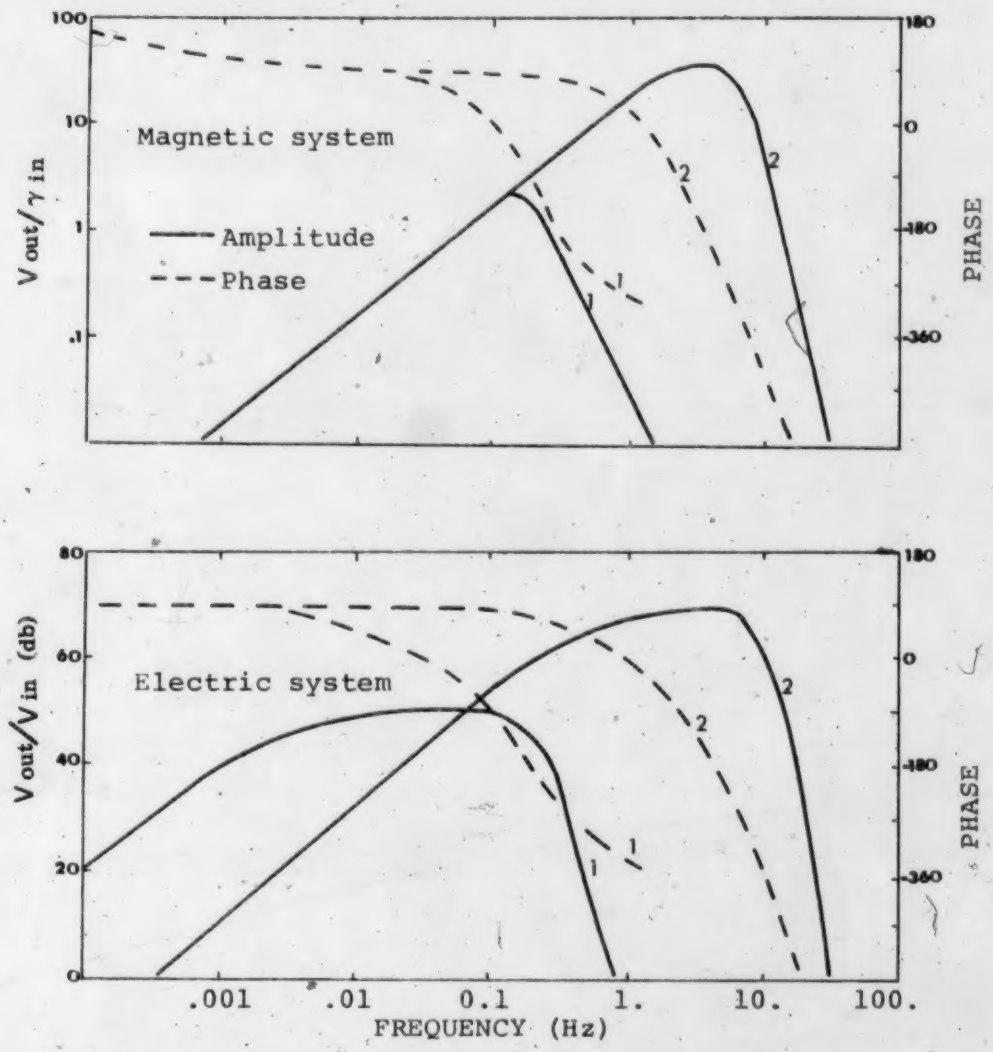

Fig.(3-2). Amplitude and phase responses of the magnetic and electric systems. (1) for low mode and (2) for high mode of recording.

(2) Electric system:

The electric field variations are detected as a voltage difference between copper electrodes in the ground. A chopper stabilized operational amplifier is used for preamplification. The post amplifier and aliasing filter are identical to that of the magnetic system as described above. The overall amplitude and phase responses are shown in Fig. (3-2).

(3) Digital recording:

The recording system consists of the multiplexer, A-D converter, crystal clock and a seven track tape recorder, with a dynamic range of ±10 V. The sampling rates were chosen to be 1.25 and 40 samples/second/channel in low and high mode respectively. A 2700-feet tape with 556 bpi can last up to 20 days or 16 hours depending on the mode of operation.

III-B. Data Analysis

The first step in the interpretation of the data is to obtain power spectral estimates of the measured quantities, H_x, H_y, H_z, E_x, E_y.

(1) Power spectrum computation:

Let f(t) represents the time sequence of a recorded signal. The procedure is as follows.

a) Truncation

Let N represent the number of samples per data set; $T_o = N\Delta t$ is the sample time length (sec) per data set, where Δt is the sampling interval (sec). A data set with length of N samples can be obtained by truncating the possible infinite time sequence f(t)

$$f_o(t) = f(t) \cdot W_o(t) \qquad (3\text{-}1)$$

where

$$W_o(t) = \begin{cases} 1, & (0 \leq t \leq T_o) \\ 0, & (t = \text{otherwise}) \end{cases}$$

The effect of this convolution is removed in the frequency domain.

b) Removing mean and trend

Since only the AC component of the signal is of interest, it is customary to eliminate the DC component at this stage by removing the mean. Removing the trend is done to remove the effect of contributions at periods longer than the fundamental and is accomplished by removing the slope corresponding to the difference between the average of the first and last third points.

c) Tapering

A large discontinuity may occur between the value of the function at the beginning and the end of the

data set; this discontinuity produces undesirable high frequency harmonics in the power spectrum. It is customary to taper the data set making the first and the last points approach the mean value which is now zero; and it is done by using a cosine bell window with one-tenth of the samples tapered at each end of the data set.

d) Fourier transform

The Fast Fourier Transform method is used to transform the time sequence $f_o(t)$, from the time domain into the frequency domain.

$$F_o(\omega_n) = \frac{2}{T_o}\int_0^{T_o} f_o(t)e^{-j\omega_n t}\,dt = F(\omega_n)*W_o(\omega_n) \qquad (3\text{-}2)$$

where $F(\omega)$ and $W_o(\omega)$ are the Fourier transfer function of $f(t)$ and $W_o(t)$ respectively, and $\omega = 2\pi f$. From N data points, N/2 complex coefficients $F_o(\omega_n)$ are obtained with

$\omega_n = n\omega_1$, where $\omega_1 = 2\pi/T_o$, and $n = 1,2,\ldots,N/2$.

The corresponding frequency range is

$$(f_1=1/T_o) \leq f_n \leq (f_N=1/2\Delta t) .$$

The highest frequency f_N is called the Nyquist or folding frequency. Components of higher frequencies than f_N are analog filtered out of the recorded signals, to avoid aliasing effects.

e) Hamming window

The Fourier coefficients $F_o(\omega)$ obtained from a truncated data set are different from the actual ones $F(\omega)$ due to the truncating effect. The correction can be done by multiplication with $W_o(\omega)$ in the frequency domain. However, the Hamming or a similar window can be used as an excellent approximation for this correction. The Fourier transfer of the Hamming window has the form

$$W_h(\omega_n) = 0.54\ W_o(\omega_n) + 0.23[W_o(\omega_{n-1}) + W_o(\omega_{n+1})]. \quad (3\text{-}3)$$

Applying this window by convolution in the frequency domain, the Fourier coefficients of the data signal are obtained as

$$F(\omega_n) = 0.54\ F_o(\omega_n) + 0.23[F_o(\omega_{n-1}) + F_o(\omega_{n+1})]. \quad (3\text{-}4)$$

f) System response correction

The overall system response must be removed to obtain the true Fourier coefficients of the E and H-field quantities.

g) Power spectrum computation

Auto and cross-power spectra are computed as

$$P_{IJ}(\omega_n) = F_I^*(\omega_n) \cdot F_J(\omega_n) \quad (3\text{-}5)$$

where * indicates the complex conjugate and I,J

(=1,2,3,4,5) are integer indexes referring to the data channels. The number of samples per data set used is usually large (say, 4096), so that there are a large number (N/2) of harmonics in the power spectrum. At this point, smoothing is carried out to obtain average power spectral estimates. This reduces the computing time in later stages of the analysis, and eliminates noise effect (see Chapter IV). Ten frequencies are obtained in each frequency decade; the ratio of center frequencies of successive bands is

$$\log \frac{f_{k+1}}{f_k} = \frac{1}{10} \quad .$$

Thus, the bandwidth averaging power spectral estimates at a representative frequency ω_k is

$$\langle P_{IJ}(\omega_k) \rangle = \frac{1}{M_b} \sum_{(\text{band})} P_{IJ}(\omega_n) \qquad (3\text{-}6)$$

where M_b is the number of harmonics involved in the bandwidth averaging.

If more than one data set is used, then the overall averaging spectral estimate is computed as

$$\langle P_{IJ}(\omega_k) \rangle = \frac{1}{M_s} \sum_{m=1}^{M_s} P^m_{IJ}(\omega_k) \qquad (3\text{-}7)$$

where $m = 1,2,\ldots M_s$ represents a given data set and M_s is the number of data sets contributing to this average.

(2) Polarization:

The polarization characteristics of the MT-field have been studied, using power spectral estimates, by Fowler et al. (1967), Paulson (1968), and Rankin and Kurtz (1970). The three important polarization parameters are: Degree of Polarization, Polarization Angle, and Ellipticity.

a) Degree of Polarization (DP)

For quasi-monochromatic EM-signals, the power spectral estimates may consist of polarized and unpolarized portions, and can be represented by a matrix of the following form

$$\begin{pmatrix} \langle P_{xx} \rangle & \langle P_{xy} \rangle \\ \langle P_{yx} \rangle & \langle P_{yy} \rangle \end{pmatrix} = \begin{pmatrix} A & B \\ B^* & C \end{pmatrix} + \begin{pmatrix} D & 0 \\ 0 & D \end{pmatrix} \qquad (3\text{-}8)$$

where x and y refer to the components of either E or H. The first matrix on the right hand side corresponds to the completely polarized contribution, i.e. that part with unit coherency ($AC = B^*B$); while the second matrix corresponds to the incoherent contribution. The degree of polarization is defined as the ratio of the polarized intensity to the total intensity of the signals.

$$DP = \frac{A + C}{\langle P_{xx} \rangle + \langle P_{yy} \rangle} = \left[1 - \frac{4|J|}{(\langle P_{xx} \rangle + \langle P_{yy} \rangle)^2}\right]^{\frac{1}{2}} \qquad (3\text{-}9)$$

where $J = \langle P_{xx} \rangle \langle P_{yy} \rangle - \langle P_{xy} \rangle \langle P_{yx} \rangle$, is the determinant of the generalized power matrix. For a completely polarized signal, the coherency between x and y components is unity so that $J = 0$ and $DP = 1$. For a completely unpolarized signal, where the coherency is zero, $DP = 0$.

b) Polarization Angle (θ_p)

The polarization angle θ_p is defined as the major axis azimuth angle of the polarization ellipse of the polarized field

$$\tan 2\theta_p = \frac{2\,\mathrm{Re}\langle P_{xy} \rangle}{\langle P_{xx} \rangle - \langle P_{yy} \rangle} \qquad (3\text{-}10)$$

c) Ellipticity (ε)

Ellipticity is defined as the ratio of minor to major axis of the polarization ellipse

$$\varepsilon = \tan\left[\tfrac{1}{2} \sin^{-1} \frac{2\,\mathrm{Im}\langle P_{xy} \rangle}{[(\langle P_{xx} \rangle - \langle P_{yy} \rangle)^2 + 4\langle P_{xy} \rangle \langle P_{yx} \rangle]^{\frac{1}{2}}}\right] \qquad (3\text{-}11)$$

ε values ranges from 0 for a linearly polarized field, to 1 for a circularly polarized field. A positive or negative value of ε represents the sense of polarization of righthand or lefthand as measured when looking into the propagating wave.

(3) Impedance computation:

In order to determine the surface impedance matrix elements Z_{ij}, using Eqns. (2-37), two independent data determinations required. However, determination can be done by using power spectral estimates in the frequency domain. Consider the frequency domain expression defined the surface impedance tensor, as

$$E_x = Z_{xx}H_x + Z_{xy}H_y \qquad (3\text{-}12)$$

[(2-37)]

$$E_y = Z_{yx}H_x + Z_{yy}H_y$$

Let each of Eqns. (3-12) be multiplied in turn by the complex conjugate of each of the 5 field quantities $(H_x, H_y, H_z, E_x, E_y)$. If the source field is randomly or partly randomly polarized with respect to the frequency, there is some degree of statistical independence between the cross-powers of the various field components. Consequently, the power spectral estimates $\langle P_{IJ}(\omega)\rangle$ as determined in Eqn. (3-6) will produce 5 linearly independent equations for each of Eqns. (3-12) of the form

1. $\langle E_x^* E_i\rangle = Z_{ix}\langle E_x^* H_x\rangle + Z_{iy}\langle E_x^* H_y\rangle$

2. $\langle E_y^* E_i\rangle = Z_{ix}\langle E_y^* H_x\rangle + Z_{iy}\langle E_y^* H_y\rangle$

3. $\langle H_x^* E_i\rangle = Z_{ix}\langle H_x^* H_x\rangle + Z_{iy}\langle H_x^* H_y\rangle$

$$4. \quad \langle H_y^* E_i \rangle = Z_{ix} \langle H_y^* H_x \rangle + Z_{iy} \langle H_y^* H_y \rangle$$

$$5. \quad \langle H_z^* E_i \rangle = Z_{ix} \langle H_z^* H_x \rangle + Z_{iy} \langle H_z^* H_y \rangle \qquad (3\text{-}13)$$

where i = x,y.

Using Equations 3 and 4 of (3-13) is equivalent to the least square error fitting method (Sims et al. 1971). Eqns. (3-13) provide 10 pairs of simultaneous equations for solution of each impedance element. However, the pairs (1,4), (2,3), and those involving (5) are not suitable since under some circumstances the solutions for impedance functions become indeterminate. There are 4 remaining pairs (1,2), (1,3), (2,4), (3,4) which are well behaved as long as the source field is at least partially unpolarized. Thus, up to 4 independently computed values of each of the impedance elements Z_{ij} can be obtained at each frequency ω_k. It is useful to average

$$Z_{ij}(\omega_k) = \frac{1}{L} \sum_{\ell=1}^{L} Z_{ij}^{\ell}(\omega_k) \qquad (3\text{-}14)$$

where ℓ = 1,2,3,4 represents a given solution and L is the number of acceptable solutions among the possible 4.

In order for a solution to exist by the method described, it is necessary that the smoothing be carried out i.e. at least over 2 frequency estimates, or to use 2 independent data sets. On the other hand,

in order to obtain satisfactory value of Z_{ij}, the bandwidth used for smoothing must be limited to a range for which Z_{ij} does not vary significantly with respect to frequency.

The admittance elements defined by

$$H_z = Y_x E_x + Y_y E_y \qquad (3\text{-}15)$$

[(2-38)]

and the coefficients α_x and α_y in the relation

$$H_z = \alpha_x E_x + \alpha_y E_y \qquad (3\text{-}16)$$

[(2-35)]

are computed in a similar manner and are subject to the same conditions as the impedance elements Z_{ij} just discussed, and the result is

$$Y_i = \frac{1}{L} \sum_{\ell=1}^{L} Y_i^{\ell}(\omega_k) \qquad (3\text{-}17)$$

$$\alpha_i = \frac{1}{L} \sum_{\ell=1}^{L} \alpha_i^{\ell}(\omega_k) \ . \qquad (3\text{-}18)$$

The apparent resistivity for an impedance element Z_{ij} is computed as

$$\rho_{ij}(\omega_k) = \frac{0.2}{f_k} |Z_{ij}(\omega_k)|^2 \quad \text{(in ohm-meter)} \qquad (3\text{-}19)$$

where the unit of Z_{ij} is (millivolt/kilometer)/gamma.

(4) Criteria of data reliability:

Experimental data is inevitably recorded in the presence of noise of one kind or another, and the establishment of reliable criteria for judging the quality of a computed result is important. For the case at hand, noise is defined as any portion of the measured EH-field quantities not conforming to the impedance and admittance relationships defined in Eqns. (3-12), (3-15), and (3-16). Both phasor coherency and predicted coherency, have been proposed and used as a measure of data quality.

a) Phasor Coherency (CP) (Word et al. 1970)

When noise is present in the measured EH-fields, the independently computed solutions of Z_{ij}^{ℓ}, Y_i^{ℓ}, and α_i^{ℓ} are not completely consistent. The degree of scatter between the independent solutions can be used as an effective measure of the reliability of the results. The phasor coherency, representing a measure of the degree of data quality, is defined as

$$CP = 1 - \frac{D}{|R|}$$

where $R = \frac{1}{L} \sum_{\ell=1}^{L} R_\ell$ and $D = \frac{1}{L} \sum_{\ell=1}^{L} |R_\ell - R|$

and R_ℓ represents the ℓ-th solution for Z_{ij}^{ℓ}, Y_i^{ℓ}, or α_i^{ℓ}, and L the number of acceptable solutions. The phasor

coherency has the range of

$$-\infty \leq CP \leq 1 .$$

b) Predicted Coherency (PCH) (Swift 1967)

The predicted coherency is defined as the coherency between the measured field component and the corresponding component predicted from the average value of Z_{ij}^{ℓ}, Y_i^{ℓ}, or α_i^{ℓ}. The PCH for the impedance is given as

$$PCH(E_x^* E_x^p) = \frac{|Z_{xx}\langle E_x^* H_x\rangle + Z_{xy}\langle E_x^* H_y\rangle|}{\{\langle P_{Ex}\rangle [|Z_{xx}|^2 \langle P_{Hx}\rangle + |Z_{xy}|^2 \langle P_{Hy}\rangle + 2Re(Z_{xx}^* Z_{xy} \langle H_x^* H_y\rangle)]\}^{\frac{1}{2}}}$$

$$PCH(E_y^* E_y^p) = \frac{|Z_{yx}\langle E_y^* H_x\rangle + Z_{yy}\langle E_y^* H_y\rangle|}{\{\langle P_{Ey}\rangle [|Z_{yx}|^2 \langle P_{Hx}\rangle + |Z_{yy}|^2 \langle P_{Hy}\rangle + 2Re(Z_{yx}^* Z_{yy} \langle H_x^* H_y\rangle)]\}^{\frac{1}{2}}}$$

and for the admittance

$$PCH(H_z^* H_z^p) = \frac{|Y_x\langle H_z^* E_x\rangle + Y_y\langle H_z^* E_y\rangle|}{\{\langle P_{Hz}\rangle [|Y_x|^2 \langle P_{Ex}\rangle + |Y_y|^2 \langle P_{Ey}\rangle + 2Re(Y_x^* Y_y \langle E_x^* E_y\rangle)]\}^{\frac{1}{2}}}$$

where the superscript p represents the predicted quantity. The PCH has the range of

$$0 \leq PCH \leq 1 .$$

The phasor and predicted coherency represent a measure of the degree to which all influences in the measured EH-fields are related by the same tensor. CP = 1 and PCH = 1 if all solutions of a given R^{ℓ} coincides in both magnitude and phase. But the converse is not necessary, since noise can exist and be coherent between channels. As part of the process of analysis, the ordinary coherencies (E_xH_y) and (E_yH_x) are computed for the raw data. If these ordinary coherencies are low the data is rejected from the subsequent processing stream.

The problem of noise contamination will be discussed in the following chapter.

CHAPTER IV

NOISE DISCUSSION

In the statistical sense, the primary magnetic signals appearing in the magnetotelluric method can be considered as noise. However in arbitrary measuring directions the orthogonal components of the magnetic fields, consisting of primary plus secondary contribution, show a considerable degree of coherence. The components of the electric field at the surface of the earth are substantially secondary and are thus highly coherent with both the orthogonal magnetic component and between themselves. In the subsequent discussion those components of the fields which are coherent in the sense just described will be considered to be signal whereas all other contributions, whether coherent or not, will be considered as noise.

As an example of coherent noise, the 60 Hz power line contribution is frequently present and strenuous efforts must be made to remove it. Other examples are power line spikes and steps, which can affect all channels of information. This noise is usually eliminated by discarding sections of record during the pre-editing processes.

Random noise cannot be eliminated by any process except in a statistical sense, but since it is incoherent

its effect can be taken into account and noisy data can be rejected according to a predetermined criterion for coherency.

IV-A. General Discussion

(1) Covariance and Coherence

The covariance functions for time sequences can be defined by

$$a_I(\tau) = \frac{1}{N} \sum_{t=1}^{N-\tau} X_I(t)\, X_I(t+\tau) \quad \text{auto-covariance} \qquad (4\text{-}1a)$$

$$c_{IJ}(\tau) = \frac{1}{N} \sum_{t=1}^{N-\tau} X_I(t)\, X_J(t+\tau) \quad \text{cross-covariance} \qquad (4\text{-}1b)$$

where X_I and X_J are time sequences with zero mean values, and $\tau = 0,1,2,\ldots$ represents the time lag.

For signals which are quasi-periodic and coherent, $a(\tau)$ and $c(\tau)$ are also quasi-periodic functions of τ. For random noise which is non-coherent, $a(\tau)$ and $c(\tau)$ are also random, and when N is large $a(\tau, \tau \neq 0)$ and $c(\tau)$ becomes very small and can be considered negligible when compared with $a(0)$, where $a(0)$ is the zero lag auto-covariance which is also the energy density of the time sequence.

$$a(0) = \frac{1}{N} \sum_{t=1}^{N} |X(t)|^2 = \sigma^2 \qquad (4\text{-}2)$$

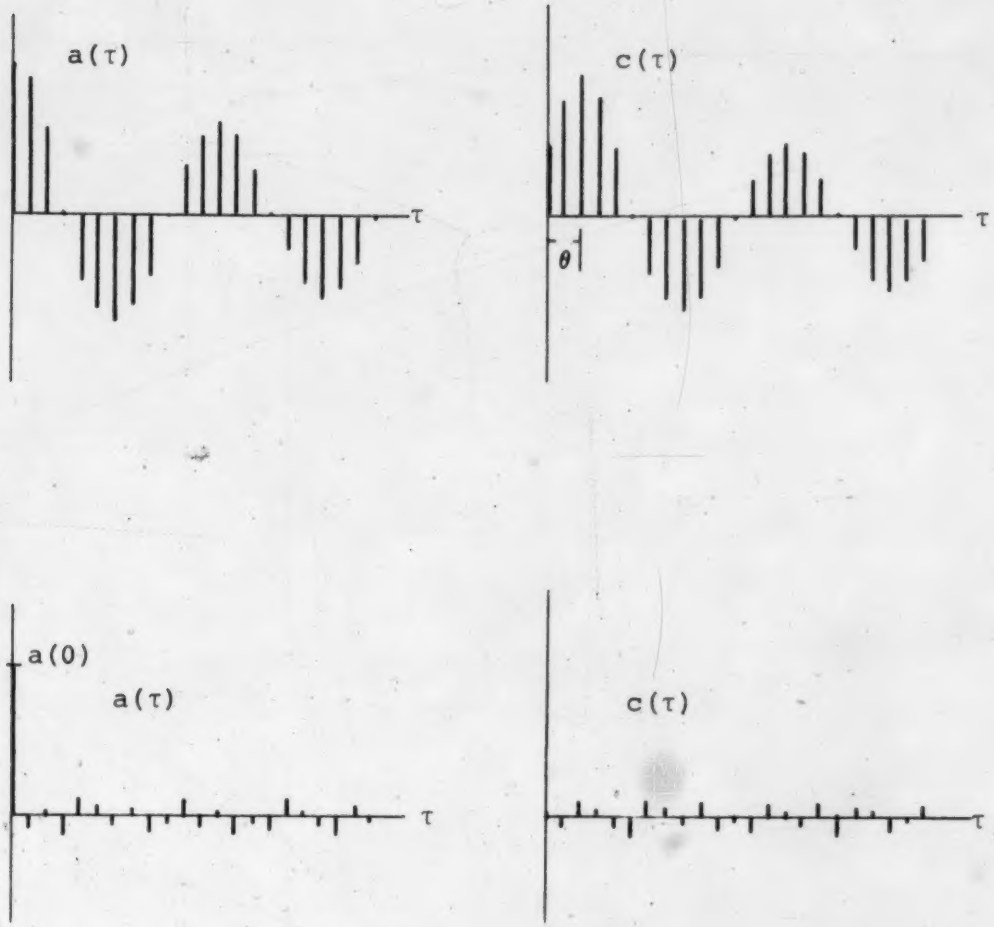

Fig.(4-1). Relative amplitudes of auto-covariance $a(\tau)$ and cross-covariance $c(\tau)$ for two coherent sinusoidal sequences with a phase θ (upper), and for two random noise sequences (lower).

This also turns out to be the variance estimate of X(t) which, if X(t) is stationary, approaches a constant value when N is large.

Fig. (4-1) shows the relative amplitudes of $a(\tau)$ and $c(\tau)$ for two coherent sinuisoidal sequences with a phase difference θ, and for two random noise sequences.

Now consider time sequences which consist of the sum of signal S(t) and random noise $\eta(t)$

$$X_I(t) = S_I(t) + \eta_I(t) \tag{4-3a}$$

$$X_J(t) = S_J(t) + \eta_J(t) \tag{4-3b}$$

The auto- and cross-covariance functions are

$$a_I(\tau) = \frac{1}{N} \sum_{t=1}^{N-\tau} X_I(t)\, X_I(t+\tau)$$

$$= \frac{1}{N} \left[\sum_{t=1}^{N-\tau} S_I(t) S_I(t+\tau) + \sum_{t=1}^{N-\tau} \eta_I(t)\, \eta_I(t+\tau) \right.$$

$$\left. + \sum_{t=1}^{N-\tau} S_I(t)\, \eta_I(t+\tau) + \sum_{t=1}^{N-\tau} \eta_I(t)\, S_I(t+\tau) \right] \tag{4-4a}$$

$$c_{IJ}(\tau) = \frac{1}{N} \sum_{t=1}^{N-\tau} X_I(t) X_J(t+\tau)$$

$$= \frac{1}{N} \left[\sum_{t=1}^{N-\tau} S_I(t) S_J(t+\tau) + \sum_{t=1}^{N-\tau} \eta_I(t)\, \eta_J(t+\tau) \right.$$

$$\left. + \sum_{t=1}^{N-\tau} S_I(t)\, \eta_J(t+\tau) + \sum_{t=1}^{N-\tau} \eta_I(t)\, S_J(t+\tau) \right] \tag{4-4b}$$

The first term in both $a(\tau)$ and $c(\tau)$ is signal and the second term is noise; the last two terms are the noise-signal interference terms and pertain to the noise effect. Except for the second term of the zero lag auto-covariance $a_\eta(0)$, which is also the noise energy density, each of the remaining terms containing η is a sum of random functions as indicated in Eqns.(4-4), and thus decreases as N increases. For sufficiently long time sequences, it will be shown later that terms in Eqns. (4-4) involving random functions can be neglected.

(2) Power Spectrum of Signal and Noise

a) Power spectrum of random noise

For a random time sequence $\eta(t)$, its complex Fourier coefficients are defined by

$$\eta(\omega_n) = \frac{2}{T}\int_0^T \eta(t)e^{-j\omega_n t}\,dt \qquad (4\text{-}5a)$$

which for digitized data becomes

$$\eta(\omega_n) = \frac{2}{N}\sum_{t=1}^{N} \eta(t)e^{-j2\pi nt/N} \,. \qquad (4\text{-}5b)$$

The corresponding power spectrum is defined by

$$P_\eta(\omega_n) = \eta^*(\omega_n)\eta(\omega_n) \,. \qquad (4\text{-}6)$$

$\eta(\omega)$ and $P_\eta(\omega)$ are also random in both amplitude and

phase. For digitized data one obtains for the average noise power

$$\bar{P}_\eta \equiv \bar{\varepsilon} = \frac{2}{N} \sum_{n=1}^{N/2} P_\eta(\omega_n)$$

$$= \frac{2}{N} \cdot \frac{2}{N} \sum_{t=1}^{N} |\eta(t)|^2 = \frac{4}{N} \sigma_N^2 \qquad (4\text{-}7)$$

where

$$\sigma_N^2 \equiv \frac{1}{N} \sum_{t=1}^{N} |\eta(t)|^2 \quad (=a(0))$$

is the variance estimate which approaches a constant value as N becomes sufficiently large. Henceforth we will consider discretely digitized data of finite sample length N.

As mentioned earlier the distribution of the amplitudes of a random noise power spectrum is also random. According to an experimental study of a typically random process described in section A-4 of this chapter, the maximum value in the spectrum $P_\eta(\omega_n) \sim 4\bar{\varepsilon}$. It can be considered that the power spectrum $P_\eta(\omega_n)$ can be represented by the average value $\bar{\varepsilon}$ weighted by a factor K_n^2 so that

$$P_\eta(\omega_n) = K_n^2 \, \bar{\varepsilon} = K_n^2 \, \frac{4}{N} \, \sigma^2 \, . \qquad (4\text{-}8)$$

The K_N^2 form a set of random positive numbers with

$$\frac{2}{N} \sum_{n=1}^{N/2} K_n^2 = 1 \, .$$

Now let the weighting factor for the maximum value of $P_\eta(\omega)$ be represented by K_M^2. The magnitude of K_M^2 is found to be limited; for instance, $K_M^2 \sim 4$ for the case given above. Also, as mentioned earlier, σ^2 has a constant value, and thus it is clear that for a stationary random process the amplitude of the power spectrum as given in Eqn. (4-8) is inversely proportional to N, the number of sample points.

b) Power spectrum of signal

For a monofrequency sinusoidal signal $S(t) = s_o \sin(\omega_o t)$, the Fourier coefficient is

$$S(\omega_o) = \frac{2}{T} \int_0^T s_o \sin(\omega_o t) e^{-j\omega_o t} \, dt \qquad (4\text{-}9)$$

and the magnitude of the power spectrum at this frequency is

$$P_s(\omega_o) = S^*(\omega_o) S(\omega_o) = s_o^2 \qquad (4\text{-}10)$$

which is independent of the number of sample points N. The same condition holds for each harmonic of a more general time sequence.

It is seen from Eqn. (4-8) and Eqn. (4-10) that an obvious distinction exists between signal and random noise. For a signal the amplitude of the spectrum is independent of N, while for random noise, it is inversely proportional to N. This fact can also be

understood by considering that for a continuously periodic signal the power is distributed to only those frequencies that are present in the signal, while for random noise, the power is distributed over all N/2 harmonics with equal probability.

c) Spectral densities with mixed signal and noise

For a mixed signal and noise time sequence as given in Eqn. (4-3)

$$X(t) = S(t) + \eta(t) \tag{4-11a}$$

the Fourier coefficients are

$$X(\omega_n) = S(\omega_n) + \eta(\omega_n) \tag{4-11b}$$

where

$$S(\omega_n) = \frac{2}{T}\int_0^T S(t)e^{-i\omega_n t}\,dt$$

and

$$\eta(\omega_n) = \frac{2}{T}\int_0^T \eta(t)e^{-j\omega_n t}\,dt\ .$$

The auto-power spectrum is

$$P(\omega_n) = X^*(\omega_n)X(\omega_n) = P_s(\omega_n) + P_\eta(\omega_n) \tag{4-12}$$

where the signal is $P_s(\omega_n) = S^*(\omega_n)S(\omega_n)$, and the noise contribution is $P_\eta(\omega_n) = \eta^*(\omega_n)\eta(\omega_n) + S^*(\eta_n)\eta(\omega_n) + \eta^*(\omega_n)S(\omega_n)$. Using the result deduced in the last section,

$$P_S(\omega_n) = s_o^2 \tag{4-13a}$$

$$P_\eta(\omega_n) = \frac{1}{N} 4\sigma^2 K_n^2 + \frac{1}{\sqrt{N}} 4 s_o \sigma K_n \cos(\gamma_n) \tag{4-13b}$$

where γ_n is the phase angle of $S^*(\omega_n)\eta(\omega_n)$ and is random, ranging from 0 to 2π.

The noise-signal ratio of auto-power $(\eta/S)_a$ for a given harmonic is defined as

$$(\eta/S)_a \equiv \frac{P_\eta(\omega_n)}{P_S(\omega_n)} = \frac{1}{N} \cdot \frac{4\sigma^2}{s_o^2} K_n^2 + \frac{1}{\sqrt{N}} \frac{4\sigma}{s_o} K_n \cos(\gamma_n) \tag{4-14}$$

and since $K_n \leq K_M$ and $\cos(\gamma_n)$ can be either positive or negative

$$\left(\frac{4\sigma^2}{Ns_o^2} K_M^2 - \frac{4\sigma}{\sqrt{N}\, s_o} K_M\right) \leq (\eta/S)_a \leq \left(\frac{4\sigma^2}{Ns_o^2} K_M^2 + \frac{4\sigma}{\sqrt{N}\, s_o} K_M\right) \tag{4-15}$$

The general cross-power spectrum between $X_I(t)$ and $X_J(t)$ for a given frequency ω is

$$P_{IJ}(\omega) = X_I^*(\omega) X_J(\omega) = P_{SIJ}(\omega) + P_{\eta IJ}(\omega) \tag{4-16a}$$

where the signal is

$$P_{SIJ}(\omega) = S_I^*(\omega) S_J(\omega) \tag{4-16b}$$

and the noise contribution is

$$P_{\eta IJ}(\omega) = \eta_I^*(\omega)\eta_J(\omega) + S_I^*(\omega)\eta_J(\omega) + \eta_I^*(\omega) S_J(\omega) \tag{4-16c}$$

which can be written as

$$P_{SIJ}(\omega) = s_o^2 e^{j\theta_S}$$

$$P_{\eta IJ}(\omega) = \frac{1}{N} 4\sigma^2 K_{nI} K_{nJ} e^{j\theta_\eta} + \frac{2s_o\sigma}{\sqrt{N}}(K_{nI} e^{j\theta_I} + K_{nJ} e^{j\theta_J})$$

where θ's are the phase angles for the corresponding terms in Eqns. (4-16b,c).

The noise-signal ratio of cross-power for a given harmonic is defined as

$$(\eta/S)_c \equiv \left| \frac{P_{\eta IJ}(\omega)}{P_{SIJ}(\omega)} \right|$$

$$= \left| \frac{1}{N} \frac{4\sigma^2}{s_o^2} K_{nI} K_{nJ} e^{j\theta_\eta} + \frac{1}{\sqrt{N}} \frac{2\sigma}{s_o} (K_{nI} e^{j\theta_I} + K_{nJ} e^{j\theta_J}) \right| \quad (4\text{-}17a)$$

$$\leq \left(\frac{4\sigma^2}{N s_o^2} K_M^2 + \frac{4\sigma}{\sqrt{N}\, s_o} K_M \right) \quad (4\text{-}17b)$$

since $K_{nI}^2, K_{nJ}^2 \leq K_M^2$.

It is seen from Eqns. (4-14) and (4-17) that the noise-signal ratio in the power spectrum depends upon N, the number of sample points used for analysis. In some cases, the power estimate resulting from an averaging is desired; these will be discussed in the next section.

(3) Power Estimate and Averaging Effect

In some cases such as MT prospecting, the power spectrum which is used for further analysis consists of smoothed estimates, averaged over a frequency band (Mb), or averaged at a given frequency over a number of data sets (Ms), or both. The resulting auto-power is estimated by

$$\langle P \rangle = \langle P_S \rangle + \langle P_\eta \rangle \quad . \tag{4-18a}$$

From equations (4-13)

$$\langle P_S \rangle = \frac{1}{Ms} \sum_{k=1}^{Ms} \frac{1}{Mb} \sum_{n=1}^{Mb} P_{Sk}(\omega_n)$$

$$= \frac{1}{M} \sum_{n=1}^{M} P_S(\omega_n) = \overline{s^2} \tag{4-18b}$$

where $P_{Sk}(\omega)$ is the signal power density of the k-th set, $M = Ms \cdot Mb$, and $\sum_{n=1}^{M}$ stands for the double summation.

$$\langle P_\eta \rangle = \frac{1}{M} \sum_{n=1}^{M} P_\eta(\omega_n)$$

$$= \frac{4\sigma^2}{N} \frac{1}{M} \sum_{n=1}^{M} K_n^2 + \frac{4\sigma\bar{s}}{\sqrt{N}} \frac{1}{M} \sum_{n=1}^{M} (K_n \cos(\gamma_n)) \quad . \tag{4-18c}$$

$\frac{1}{M} \sum_{n=1}^{M} K_n^2 \to 1$ as previously shown. Define $\sum_{n=1}^{M} (K_n \cos(\gamma_n)) \equiv \langle K_n \rangle$, Eqn. (4-18c) becomes

$$\langle P_\eta \rangle = \frac{4\sigma^2}{N} \pm \frac{4\sigma\bar{s}}{\sqrt{N}} \frac{\langle K_n \rangle}{M} \quad . \tag{4-19}$$

The noise-signal ratio of the auto-power estimate is estimated from Eqn. (4-18b) and (4-19),

$$\langle N/S\rangle_a \equiv \frac{\langle P_\eta\rangle}{\langle P_S\rangle} = \frac{4\sigma^2}{N\,\overline{s^2}} \pm \frac{4\sigma}{\sqrt{N}\,\bar{s}}\,\frac{\langle K_n\rangle}{M} \tag{4-20a}$$

or, by using the reasonable estimate of $\langle K_n\rangle$

$$\left(\frac{4\sigma^2}{N\,\overline{s^2}} - \frac{4\sigma K_M}{\sqrt{N}\,\bar{s}\,M}\right) \lesssim \langle \eta/S\rangle_a \lesssim \left(\frac{4\sigma^2}{N\,\overline{s^2}} + \frac{4\sigma K_M}{\sqrt{N}\,\bar{s}\,M}\right) . \tag{4-20b}$$

The averaged cross-power estimate is

$$\langle P_{IJ}\rangle = \langle P_{SIJ}\rangle + \langle P_{\eta IJ}\rangle \tag{4-21a}$$

where

$$\langle P_{SIJ}\rangle = \frac{1}{M}\sum_{n=1}^{M} P_{SIJ}(\omega_n) = \frac{1}{M}\sum_{n=1}^{M} (s_n^2 e^{j\theta_{Sn}}) \tag{4-21b}$$

$$\langle P_{\eta IJ}\rangle = \frac{4\sigma^2}{N}\,\frac{1}{M}\sum_{n=1}^{M} (K_{nI}K_{nJ}e^{j\theta_{\eta n}})$$

$$+ \frac{2\sigma\bar{s}}{\sqrt{N}}\,\frac{1}{M}\left(\sum_{n=1}^{M} K_{nI}e^{j\theta_{In}} + \sum_{n=1}^{M} K_{nJ}e^{j\theta_{Jn}}\right) . \tag{4-21c}$$

Since the signals are coherent, and assuming that $e^{j\theta_{Sn}}$ are in phase within a given band, Eqn. (4-21b) can be rewritten as

$$\langle P_{SIJ}\rangle = \overline{s^2}\, e^{j\theta_S} . \tag{4-22a}$$

However, the phases of noise terms are random, so that Eqn. (4-21c) can be written

$$\langle P_{\eta IJ} \rangle = \frac{4\sigma^2}{N} \frac{\langle K_n \rangle^2 e^{j\langle \theta_\eta \rangle}}{M} + \frac{4\sigma \bar{s}}{\sqrt{N}} \frac{\langle K_n \rangle e^{j\langle \theta'_\eta \rangle}}{M} \qquad (4\text{-}22b)$$

where $\langle \theta_\eta \rangle$'s represent the average of the random phases, ranging from 0 to 2π. From Eqns. (4-22a) and (4-22b), the noise-signal ratio of the cross-power is

$$\langle \eta/S \rangle_c \equiv \left| \frac{\langle P_{\eta IJ} \rangle}{\langle P_{SIJ} \rangle} \right| = \left| \frac{4\sigma^2}{N \overline{s^2}} \frac{\langle K_n \rangle^2 e^{j\langle \theta_\eta \rangle}}{M} + \frac{4\sigma}{\sqrt{N}\, \bar{s}} \frac{\langle K_n \rangle e^{j\langle \theta'_\eta \rangle}}{M} \right| \qquad (4\text{-}23a)$$

$$\lesssim \left(\frac{4\sigma^2 K_M^2}{N \overline{s^2}_M} + \frac{4\sigma K_M}{\sqrt{N}\, \bar{s}\, M} \right) . \qquad (4\text{-}23b)$$

Eqns (4-20b) and (4-23b) represent the limits of the noise effect in the auto- and cross-power estimates. However, both terms of $\langle P_{\eta IJ} \rangle$ as given in Eqn. (4-22b) and the second term of $\langle P_\eta \rangle$ as given in Eqn. (4-19) are average values of random functions, and thus become negligible for sufficiently large M. In other words, the noise contribution can be largely removed from the cross-power estimate and partially removed from the auto-power estimate. In addition, there are generally some mechanisms which can further diminish the noise contribution from auto-power estimates through the use of a good cross-power estimate (White 1973).

(4) Experiment

For the purpose of investigating the noise effect quantitatively, three noise-signal mixed sequences were generated.

$$X_I(t) = S_I(t) + \eta_I(t), \qquad I = 1,2,3. \tag{4-24}$$

where

$$S_I(t) = \sum_{n=1}^{N} s_o \sin(\omega_n t + \theta_n), \quad \text{with} \quad s_o^2 = 10.$$

The three independent noise components η_I were taken from the random noise sequence provided by the Computing Services Library of the University of Alberta. The noise sequences are normalized to $\sigma_I^2 = 5$, and $K_M^2 \simeq 4$ for these sequences. The formulas used for computing the noise-signal ratio are:

For individual harmonics

$$(\eta/S)_I = \frac{P_{XI}(\omega) - P_{SI}(\omega)}{P_{SI}(\omega)} \qquad \text{(auto-power)} \tag{4-25a}$$

$$(\eta/S)_{IJ} = \left| \frac{P_{XIJ}(\omega) - P_{SIJ}(\omega)}{P_{SIJ}(\omega)} \right| \qquad \text{(cross-power)} \tag{4-25b}$$

For power estimates

$$\langle \eta/S \rangle_I = \frac{\langle P_{XI} \rangle - \langle P_{SI} \rangle}{\langle P_{SI} \rangle} \qquad \text{(auto-power)} \tag{4-26a}$$

$$\langle \eta/S \rangle_{IJ} = \left| \frac{\langle P_{XIJ} \rangle - \langle P_{SIJ} \rangle}{\langle P_{SIJ} \rangle} \right| \qquad \text{(cross-power)} \tag{4-26b}$$

where

$$P_{XI}(\omega) = X_I^*(\omega)X_I(\omega) \qquad P_{SI}(\omega) = S_I^*(\omega)S_I(\omega)$$

$$P_{XIJ}(\omega) = X_I^*(\omega)X_J(\omega) \qquad P_{SIJ}(\omega) = S_I^*(\omega)S_J(\omega)$$

$$\langle P_{XI}\rangle = \frac{1}{M}\sum^{M} P_{XI}(\omega) \qquad \langle P_{SI}\rangle = \frac{1}{M}\sum^{M} P_{SI}(\omega)$$

$$\langle P_{XIJ}\rangle = \frac{1}{M}\sum^{M} P_{XIJ}(\omega) \qquad \langle P_{SIJ}\rangle = \frac{1}{M}\sum^{M} P_{SIJ}(\omega)$$

The computed results are given in Table (4-1) with various values of M and N. In the Table, the first three columns are the noise-signal ratio of the auto-power for the three channels defined in Eqns.(4-25b) and (4-26b). Data in the line with each M-number are the theoretical values defined in Eqns. (4-15), (4-17b), (4-20b), and (4-23b) with the same values of M, N and $\cos(\gamma_n) = \pm 1$.

IV-B. Investigation of Noise Effect on Impedance Elements

(1) General Solution

The surface impedance elements Z_{ij} are computed from the 4 pairs [(1,2), (1,3), (2,4), (3,4)] of equations (III-B-3)

$$(1) \qquad \langle E_x^* E_i\rangle = Z_{ix}\langle E_x^* H_x\rangle + Z_{iy}\langle E_x^* H_y\rangle$$

TABLE 4-1. NOISE-SIGNAL POWER RATIO

AUTO-POWER			CROSS-POWER		
N=64					
M=1	[(-.6)—(.85)]		[	.85	]
-0.14	0.54▲	0.24	0.17	0.41▲	0.06
-0.10	0.01	-0.29	0.17	0.24	0.39
-0.28	-0.13	-0.02	0.34	0.23	0.18
0.15	-0.39	-0.26	0.17	0.37	0.22
0.15	-0.20	0.28	0.09	0.05	0.21
-0.27	0.14	-0.44▽	0.09	0.34	0.41
M=10	[(-.05)—(.12)]		[	.085	]
-0.06	0.05	0.07	0.05	0.08	0.02
0.07	-0.04	-0.08▽	0.03	0.10▲	0.03
0.11▲	0.02	0.07	0.09	0.09	0.05
N=128					
M=1	[(-.5)—(.6)]		[	.6	]
0.31▲	0.23	-0.07	0.31▲	0.17	0.31
0.30	-0.17	-0.04	0.10	0.18	0.13
-0.07	0.03	0.23	0.03	0.23	0.17
-0.07	-0.08	0.00	0.18	0.11	0.08
-0.34▽	0.06	0.04	0.21	0.23	0.18
0.12	0.07	0.00	0.19	0.13	0.28
M=10	[(-.05)—(.08)]		[	.06	]
0.02	0.09	0.04	0.04	0.06▲	0.03
-0.03	-0.05▽	0.07	0.05	0.03	0.04
0.04	0.01	-0.03	0.02	0.02	0.02
0.12▲	0.01	0.01	0.06	0.01	0.04
N=256					
M=1	[(-.3)—(.4)]		[	.4	]
-0.17	0.20	0.09	0.11	0.15	0.12
0.17	0.22▲	-0.14	0.21	0.03	0.06
-0.17	0.17	0.21	0.06	0.28▲	0.11
0.13	-0.08	-0.03	0.04	0.06	0.05
0.07	-0.12	-0.08	0.04	0.13	0.06
0.01	0.01	-0.36▽	0.08	0.20	0.20
M=10	[(-.03)—(.05)]		[	.04	]
0.01	0.04	-0.01	0.02	0.01	0.01
0.06▲	-0.06▽	0.05	0.04	0.03	0.05▲
-0.01	-0.01	0.01	0.04	0.02	0.02
-0.02	-0.00	0.01	0.04	0.02	0.02

$$(2) \quad \langle E_y^* E_i \rangle = Z_{ix} \langle E_y^* H_x \rangle + Z_{iy} \langle E_y^* H_y \rangle$$

(4-30)

$$(3) \quad \langle H_x^* E_i \rangle = Z_{ix} \langle H_x^* H_x \rangle + Z_{iy} \langle H_x^* H_y \rangle$$

$$(4) \quad \langle H_y^* E_i \rangle = Z_{ix} \langle H_y^* H_x \rangle + Z_{iy} \langle H_y^* H_y \rangle \quad (i=x,y)$$

and 4 solutions for each element are obtained. These are represented by

$$Z_{ij}^{\ell} = \frac{N_{ij}^{\ell}}{D_{ij}^{\ell}} \tag{4-31}$$

where $\ell(=1,2,3,4)$ represents a given pair, and N_{ij}^{ℓ} and D_{ij}^{ℓ} are functions of the power estimates. The generalized power estimates are considered to contain the signal and the noise components, thus D and N can be represented symbolically by

$$N_{ij}^{\ell} = N_{ijo}^{\ell} + \Delta N_{ij}^{\ell} \quad , \quad D_{ij}^{\ell} = D_{ijo}^{\ell} + \Delta D_{ij}^{\ell}$$

where N_{ijo}^{ℓ} and D_{ijo}^{ℓ} are the signal, and ΔN_{ij}^{ℓ} and ΔD_{ij}^{ℓ} are noise components.

When the noise-signal ratio is small, Eqn.(4-31) to first order becomes

$$Z_{ij}^{\ell} = Z_{ij}^{o} + \Delta Z_{ij}^{\ell}$$

$$\simeq \frac{N_{ijo}^{\ell}}{D_{ijo}^{\ell}} + \frac{\Delta N_{ij}^{\ell}}{D_{ijo}^{\ell}} - \frac{N_{ijo}^{\ell}}{D_{ijo}^{\ell}} \frac{\Delta D_{ij}^{\ell}}{D_{ijo}^{\ell}} \quad . \tag{4-32}$$

$Z^{o}_{ij} = N^{\ell}_{ijo}/D^{\ell}_{ijo}$ is the major component of the data and thus is a good approximation from which to deduce uniquely the resistivity structure of the earth.

$\Delta Z_{ij} = \frac{\Delta N^{\ell}_{ij}}{D^{\ell}_{ijo}} - \frac{N^{\ell}_{ijo}}{D^{\ell}_{ijo}} \frac{\Delta D^{\ell}_{ij}}{D^{\ell}_{ijo}}$ is due to the noise and varies with different ℓ value, since noise is random. For the case of $\ell = (3,4)$ and $i = x$, N_{ij} and D_{ij} are:

$$D = \langle P_{Hx}\rangle\langle P_{Hy}\rangle - \langle H^{*}_{x}H_{y}\rangle\langle H^{*}_{y}H_{x}\rangle$$

$$\Delta D = \langle P_{Hx}\rangle\langle P_{Hy}\rangle_{\eta} + \langle P_{Hy}\rangle\langle P_{Hx}\rangle_{\eta} - \langle H^{*}_{x}H_{y}\rangle\langle H^{*}_{y}H_{x}\rangle_{\eta} - \langle H^{*}_{y}H_{x}\rangle\langle H^{*}_{x}H_{y}\rangle_{\eta}$$

$$N_{xx} = \langle P_{Hy}\rangle\langle H^{*}_{x}E_{x}\rangle - \langle H^{*}_{y}E_{x}\rangle\langle H^{*}_{x}H_{y}\rangle$$

$$\Delta N_{xx} = \langle P_{Hy}\rangle\langle H^{*}_{x}E_{x}\rangle_{\eta} + \langle H^{*}_{x}E_{x}\rangle\langle P_{Hy}\rangle_{\eta} - \langle H^{*}_{y}E_{x}\rangle\langle H^{*}_{x}H_{y}\rangle_{\eta} - \langle H^{*}_{x}H_{y}\rangle\langle H^{*}_{y}E_{x}\rangle_{\eta}$$

$$N_{xy} = \langle P_{Hx}\rangle\langle H^{*}_{y}E_{x}\rangle - \langle H^{*}_{x}E_{x}\rangle\langle H^{*}_{y}H_{x}\rangle$$

$$\Delta N_{xy} = \langle P_{Hx}\rangle\langle H^{*}_{y}E_{x}\rangle_{\eta} + \langle H^{*}_{y}E_{x}\rangle\langle P_{Hx}\rangle_{\eta} - \langle H^{*}_{x}E_{x}\rangle\langle H^{*}_{y}H_{x}\rangle_{\eta} - \langle H^{*}_{y}H_{x}\rangle\langle H^{*}_{x}E_{x}\rangle_{\eta}$$

After a tedious calculation, the first order approximation of the four ΔZ^{ℓ}_{ij} are written in the following forms, where the superscript denotes the pairs of equations used from (4-30).

$$\Delta Z_{xy}^{(1,2)} D_o^{(1,2)} = \langle E_y^* H_x \rangle_o \langle P_{Ex} \rangle_\eta - \langle E_x^* H_x \rangle_o \langle E_y^* E_x \rangle_\eta$$

$$- Z_{xy}^o [\langle E_y^* H_x \rangle_o \langle E_x^* H_y \rangle_\eta - \langle E_x^* H_x \rangle_o \langle E_y^* H_y \rangle_\eta]$$

$$- Z_{xx}^o [\langle E_x^* H_x \rangle_o \langle E_y^* H_x \rangle_\eta - \langle E_y^* H_x \rangle_o \langle E_x^* H_x \rangle_\eta]$$

(4-33a)

$$\Delta Z_{xy}^{(1,3)} D_o^{(1,3)} = Z_{xx}^o \langle E_x^* H_x \rangle_o \langle P_{Hx} \rangle_\eta + \langle P_{Hx} \rangle_o \langle P_{Ex} \rangle_\eta$$

$$- Z_{xy}^o [\langle P_{Hx} \rangle_o \langle E_x^* H_y \rangle_\eta - \langle E_x^* H_x \rangle_o \langle H_x^* H_y \rangle_\eta]$$

$$- Z_{xx}^o \langle P_{Hx} \rangle_o \langle E_x^* H_x \rangle_\eta - \langle E_x^* H_x \rangle_o \langle E_x^* H_x \rangle_\eta$$

(4-33b)

$$\Delta Z_{xy}^{(2,4)} D_o^{(2,4)} = - Z_{xy}^o \langle E_y^* H_x \rangle_o \langle P_{Hy} \rangle_\eta + Z_{xy}^o \langle H_y^* H_x \rangle_o \langle E_y^* H_y \rangle_\eta$$

$$+ Z_{xx}^o [\langle H_y^* H_x \rangle_o \langle E_y^* H_x \rangle_\eta - \langle E_y^* H_x \rangle_o \langle H_y^* H_x \rangle_\eta]$$

$$+ \langle E_y^* H_x \rangle_o \langle H_y^* E_x \rangle_\eta - \langle H_y^* H_x \rangle_o \langle E_y^* E_x \rangle_\eta$$

(4-33c)

$$\Delta Z_{xy}^{(3,4)} D_o^{(3,4)} = - Z_{xy}^o \langle P_{Hx} \rangle_o \langle P_{Hy} \rangle_\eta + Z_{xx}^o \langle H_y^* H_x \rangle_o \langle P_{Hx} \rangle_\eta$$

$$+ Z_{xy}^o \langle H_y^* H_x \rangle_o \langle H_x^* H_y \rangle_\eta - Z_{xx}^o \langle P_{Hx} \rangle_o \langle H_y^* H_x \rangle_\eta$$

$$+ \langle P_{Hx} \rangle_o \langle H_y^* E_x \rangle_\eta - \langle H_y^* H_x \rangle_o \langle H_x^* E_x \rangle_\eta$$

(4-33d)

$$\Delta Z_{xx}^{(1,2)} D_o^{(1,2)} = -\langle E_y^* H_y \rangle_o \langle P_{Ex} \rangle_\eta + \langle E_x^* H_y \rangle_o \langle E_y^* E_x \rangle_\eta$$

$$- Z_{xx}^o [\langle E_x^* H_y \rangle_o \langle E_y^* H_x \rangle_\eta - \langle E_y^* H_y \rangle_o \langle E_x^* H_x \rangle_\eta]$$

$$Z_{xy}^o [\langle E_y^* H_y \rangle_o \langle E_x^* H_y \rangle_\eta - \langle E_x^* H_y \rangle_o \langle E_y^* H_y \rangle_\eta]$$

(4-33e)

$$Z_{xx}^{(1,3)} D_o^{(1,3)} = - Z_{xx}^o \langle E_x^* H_y \rangle_o \langle P_{Hx} \rangle_\eta - \langle H_x^* H_y \rangle_o \langle P_{Ex} \rangle_\eta$$

$$- Z_{xy}^o [\langle H_x^* H_y \rangle_o \langle E_x^* H_y \rangle_\eta - \langle E_x^* H_y \rangle_o \langle H_x^* H_y \rangle_\eta]$$

$$+ Z_{xx}^o \langle H_x^* H_y \rangle_o \langle E_x^* H_x \rangle_\eta + \langle E_x^* H_y \rangle_o \langle H_x^* E_x \rangle_\eta$$

(4-33f)

$$Z_{xx}^{(2,4)} D_o^{(2,4)} = Z_{xy}^o \langle E_y^* H_y \rangle_o \langle P_{Hy} \rangle_\eta - Z_{xy}^o \langle P_{Hy} \rangle_o \langle E_y^* H_y \rangle_\eta$$

$$- Z_{xx}^o [\langle P_{Hy} \rangle_o \langle E_y^* H_x \rangle_\eta - \langle E_y^* H_y \rangle_o \langle H_y^* H_x \rangle_\eta]$$

$$+ \langle P_{Hy} \rangle_o \langle E_y^* E_x \rangle_\eta - \langle E_y^* H_y \rangle_o \langle H_y^* E_x \rangle_\eta$$

(4-33g)

$$Z_{xx}^{(3,4)} D_o^{(3,4)} = - Z_{xx}^o \langle P_{Hy} \rangle_o \langle P_{Hx} \rangle_\eta + Z_{xy}^o \langle H_x^* H_y \rangle_o \langle P_{Hy} \rangle_\eta$$

$$+ Z_{xx}^o \langle H_x^* H_y \rangle_o \langle H_y^* H_x \rangle_\eta - Z_{xy}^o \langle P_{Hy} \rangle_o \langle H_x^* H_y \rangle_\eta$$

$$+ \langle P_{Hy} \rangle_o \langle H_x^* E_x \rangle_\eta - \langle H_x^* H_y \rangle_o \langle H_y^* E_x \rangle_\eta$$

(4-33h)

where

$$D_o^{(2,4)} = \langle P_{Hy} \rangle_o \langle E_y^* H_x \rangle_o - \langle E_y^* H_y \rangle_o \langle H_y^* H_x \rangle_o$$

$$D_o^{(3,4)} = \langle P_{Hx} \rangle_o \langle P_{Hy} \rangle_o - \langle H_y^* H_x \rangle_o \langle H_x^* H_y \rangle_o$$

$$D_o^{(1,2)} = \langle E_y^* H_x \rangle_o \langle E_x^* H_y \rangle_o - \langle E_x^* H_x \rangle_o \langle E_y^* H_y \rangle_o$$

$$D_o^{(1,3)} = \langle P_{Hx} \rangle_o \langle E_x^* H_y \rangle_o - \langle E_x^* H_x \rangle_o \langle H_x^* H_y \rangle_o$$

(2) Impedance Solutions for Noise-free Cross-power Estimates

Supposing that noise exists in the auto-power estimate only, and not in the cross-power estimate as is often assumed, then all terms in Eqns. (4-33) having a noise cross-power contribution will vanish. With this assumption, and some rearranging to make all the D's real and positive Eqns. (4-33) can be rewritten as:

$$\Delta Z_{xy}^{(1,2)} = Z_{xy}^o \frac{\langle P_{Ex} \rangle_\eta}{D \cdot 121} + Z_{xx}^o \frac{\langle H_y^* H_x \rangle_o \langle P_{Ex} \rangle_\eta}{D \cdot 122} \qquad (4\text{-}34a)$$

$$\Delta Z_{xy}^{(1,3)} = Z_{xy}^o \frac{\langle P_{Ex} \rangle_\eta}{D \cdot 131} + Z_{xx}^o \left(\frac{\langle H_y^* H_x \rangle_o \langle P_{Ex} \rangle_\eta}{D \cdot 132} + \frac{\langle H_y^* H_x \rangle_o \langle P_{Hx} \rangle_\eta}{D \cdot 133} \right) \qquad (4\text{-}34b)$$

$$\Delta Z_{xy}^{(2,4)} = - Z_{xy}^o \frac{\langle P_{Hy} \rangle_\eta}{D \cdot 241} \qquad (4\text{-}34c)$$

$$\Delta Z_{xy}^{(3,4)} = - Z_{xy}^o \frac{\langle P_{Hy} \rangle_\eta}{D \cdot 341} + Z_{xx}^o \frac{\langle H_y^* H_x \rangle_o \langle P_{Hx} \rangle_\eta}{D \cdot 342} \qquad (4\text{-}33d)$$

$$\Delta Z_{xx}^{(1,2)} = - Z_{xx}^{o} \frac{\langle P_{Ex} \rangle_{\eta}}{D \cdot 123} - Z_{xy}^{o} \frac{\langle H_x^* H_y \rangle_o \langle P_{Ex} \rangle_{\eta}}{D \cdot 124} \qquad (4\text{-}34e)$$

$$\Delta Z_{xx}^{(1,3)} = - Z_{xx}^{o} \frac{\langle P_{Ex} \rangle_{\eta}}{D \cdot 134} + \frac{\langle P_{Hx} \rangle_{\eta}}{D \cdot 135} - Z_{xy}^{o} \frac{\langle H_x^* H_y \rangle_o \langle P_{Ex} \rangle_{\eta}}{D \cdot 136} \qquad (4\text{-}34f)$$

$$\Delta Z_{xx}^{(2,4)} = + Z_{xy}^{o} \frac{\langle H_x^* H_y \rangle_o \langle P_{Hy} \rangle_{\eta}}{D \cdot 242} \qquad (4\text{-}34g)$$

$$\Delta Z_{xx}^{(3,4)} = - Z_{xx}^{o} \frac{\langle P_{Hx} \rangle_{\eta}}{D \cdot 343} + Z_{xy}^{o} \frac{\langle H_x^* H_y \rangle_o \langle P_{Hy} \rangle_{\eta}}{D \cdot 342} , \qquad (4\text{-}34h)$$

where

$$D \cdot 122 = |\langle E_x^* H_y \rangle|^2 - \langle E_x^* H_x \rangle \langle E_y^* H_y \rangle \langle H_y^* E_x \rangle / \langle E_y^* H_x \rangle$$

$$D \cdot 121 = D \cdot 122 / \langle P_{Hy} \rangle$$

$$D \cdot 124 = \langle E_y^* H_x \rangle \langle E_x^* H_y \rangle \langle H_x^* E_x \rangle / \langle E_y^* H_y \rangle - |\langle E_x^* H_x \rangle|^2$$

$$D \cdot 123 = D \cdot 124 / \langle P_{Hx} \rangle$$

$$D \cdot 132 = |\langle E_x^* H_y \rangle|^2 - \langle E_x^* H_x \rangle \langle H_x^* H_y \rangle \langle H_y^* E_x \rangle / \langle P_{Hx} \rangle$$

$$D \cdot 131 = D \cdot 132 / \langle P_{Hy} \rangle$$

$$D \cdot 133 = \langle P_{Hx} \rangle \langle E_x^* H_y \rangle \langle H_y^* H_x \rangle / \langle E_x^* H_x \rangle - |\langle H_x^* H_y \rangle|^2$$

$$D \cdot 135 = \langle P_{Hx} \rangle - \langle E_x^* H_x \rangle \langle H_x^* H_y \rangle / \langle E_x^* H_y \rangle$$

$$D \cdot 136 = \langle P_{Hx} \rangle \langle E_x^* H_y \rangle \langle H_x^* E_x \rangle / \langle H_x^* H_y \rangle - |\langle E_x^* H_x \rangle|^2 .$$

$$D\cdot 134 = D\cdot 136/\langle P_{Hx}\rangle$$

$$D\cdot 241 = \langle P_{Hy}\rangle - \langle E_y^* H_y\rangle\langle H_y^* H_x\rangle/\langle E_y^* H_x\rangle$$

$$D\cdot 242 = \langle P_{Hy}\rangle\langle E_y^* H_x\rangle\langle H_x^* H_y\rangle/\langle E_y^* H_y\rangle - |\langle H_x^* H_y\rangle|^2$$

$$D\cdot 342 = \langle P_{Hx}\rangle\langle P_{Hy}\rangle - \langle H_x^* H_y\rangle\langle H_y^* H_x\rangle$$

$$D\cdot 341 = D\cdot 342/\langle P_{Hx}\rangle$$

$$D\cdot 343 = D\cdot 342/\ P_{Hy} \quad .$$

If M is large, the noise component of the auto-power estimate as presented in Eqns. (4-34) is biased positive as can be seen from Eqn. (4-19)

$$\langle P_\eta\rangle = \frac{4\sigma^2}{N} \pm \frac{4\sigma\bar{s}\langle K_n\rangle}{\sqrt{N}\,M} \qquad (4\text{-}19)$$

The second term on the right hand side can be positive or negative whereas the first term is always positive. An average taken from solutions of Eqns. (3-20) or (4-34)

$$\langle Z_{ij}\rangle = Z_{ij}^o + \frac{1}{L}\sum^{L}(\Delta Z_{ij}^{\ell}) = Z_{ij}^o + \langle Z_{ij}\rangle \qquad (4\text{-}35)$$

provides a better estimate.

As just described, the noise contribution to the auto-power estimate causes noise components ΔZ_{ij}^{ℓ} in the impedance elements, and the average $\langle Z_{ij}^{\ell}\rangle$ can become more accurate than the original Z_{ij}^{ℓ}. Consequently

this improved $\langle Z_{ij} \rangle$ is consistent with the existence of auto-power estimates which contain less noise than the original ones do. Thus, substituting $\langle Z_{ij} \rangle$ back to Eqn. (4-30) gives the following relations:

$$\langle P_{Ex} \rangle = R_x \tag{4-36a}$$

$$\langle P_{Ey} \rangle = R_y \tag{4-36b}$$

$$|\langle Z_{xx} \rangle|^2 \langle P_{Hx} \rangle + |\langle Z_{xy} \rangle|^2 \langle P_{Hy} \rangle + 2\mathrm{Re}[\langle Z_{xx}^* \rangle \langle Z_{xy} \rangle \langle H_x^* H_y \rangle] = R_x \tag{4-36c}$$

$$|\langle Z_{yx} \rangle|^2 \langle P_{Hx} \rangle + |\langle Z_{yy} \rangle|^2 \langle P_{Hy} \rangle + 2\mathrm{Re}[\langle Z_{yx}^* \rangle \langle Z_{yy} \rangle \langle H_x^* H_y \rangle] = R_y \tag{4-36d}$$

where

$$R_x = \mathrm{Re}[\langle Z_{xx} \rangle \langle E_x^* H_x \rangle + \langle Z_{xy} \rangle \langle E_x^* H_y \rangle]$$

$$= |\langle Z_{xx} \rangle \langle E_x^* H_x \rangle + \langle Z_{xy} \rangle \langle E_x^* H_y \rangle|$$

$$= \frac{1}{2}\{\mathrm{Re}[\langle Z_{xx} \rangle \langle E_x^* H_x \rangle + \langle Z_{xy} \rangle \langle E_x^* H_y \rangle] + |\langle Z_{xx} \rangle \langle E_x^* H_x \rangle + \langle Z_{xy} \rangle \langle E_x^* H_y \rangle|\}$$

$$R_y = \mathrm{Re}[\langle Z_{yx} \rangle \langle E_y^* H_x \rangle + \langle Z_{yy} \rangle \langle E_y^* H_y \rangle]$$

$$= |\langle Z_{yx} \rangle \langle E_y^* H_x \rangle + \langle Z_{yy} \rangle \langle E_y^* H_y \rangle|$$

$$= \frac{1}{2}\{\mathrm{Re}[\langle Z_{yx} \rangle \langle E_y^* H_x \rangle + \langle Z_{yy} \rangle \langle E_y^* H_y \rangle] + |\langle Z_{yx} \rangle \langle E_y^* H_x \rangle + \langle Z_{yy} \rangle \langle E_y^* H_y \rangle|\}$$

Solving Eqns. (4-36) for $\langle P \rangle$ provides improved auto-power estimates corresponding to the more accurate $\langle Z_{ij} \rangle$.

A cyclic operation

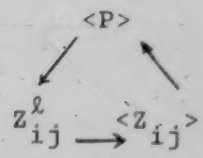

(4-37)

can finally result in solution having the noise substantially removed.

$$\langle P \rangle \rightarrow \langle P \rangle_o \quad , \qquad \langle P_\eta \rangle \rightarrow 0$$

$$\langle Z_{ij} \rangle \rightarrow Z^o_{ij} \quad , \qquad \langle \Delta Z_{ij} \rangle \rightarrow 0$$

These final solutions are consistent with the conditions corresponding to a unit predicted coherency, which are

$$\langle P_{Ex} \rangle = |\langle Z_{xx} \rangle|^2 \langle P_{Hx} \rangle + |\langle Z_{xy} \rangle|^2 \langle P_{Hy} \rangle + 2\,\mathrm{Re}[\langle Z^*_{xx} \rangle \langle Z_{xy} \rangle \langle H^*_x H_y \rangle] \qquad (4\text{-}38a)$$

$$\langle P_{Ey} \rangle = |\langle Z_{yx} \rangle|^2 \langle P_{Hx} \rangle + |\langle Z_{yy} \rangle|^2 \langle P_{Hy} \rangle + 2\,\mathrm{Re}[\langle Z^*_{yx} \rangle \langle Z_{yy} \rangle \langle H^*_x H_y \rangle] \qquad (4\text{-}38b)$$

If the cross-power estimates are noise-free, the following conditions can be simultaneously achieved:

a) Predicted coherency is unity.

b) 4-solutions of Z^{ℓ}_{ij} are identical.

As a consequence the apparent resistivity curves are smooth.

Figs. (4-2) show the result of the operation of Eqn. (4-37). Data was taken from a typical section of MT record. M, at the high frequency end ranges from 1000 to 3000. Such an averaging may remove the noise contribution from the cross-power estimates and leave noise only in the auto-power estimates. The 4-solutions of Z_{ij}^{ℓ} and their average <Z> are plotted from left to right in each row. The first row represents the raw Z_{ij} and the second row represents Z_{ij} after the number of cyclic operations indicated on the individual plots. The scatter in Z_{ij} appears in the raw data, however, after a certain number of the cyclic operations, the noise in the auto-power estimates is substantially removed, and then the solutions of Z_{ij} become unique.

(3) Impedance Solutions as Noise in Both Auto- and Cross-power Estimates

When noise exists in both auto- and cross-power estimates, the solutions of ΔZ_{ij}^{ℓ} are those given by Eqns. (4-33), and an average value given by

$$<Z_{ij}> = Z_{ij}^{o} + <\Delta Z_{ij}>$$

also provides a noise-reduction-effect. Consecutive manipulations as performed by Eqns. (4-36) and (4-37) results in a set of $<Z_{ij}>^{m}$, where m = 1,2,....Mc the number of cycles performed. None of $<Z_{ij}>^{m}$ is

expected to be noise-free, and it is even possible that the noise content is increased. Whether an average given by

$$\langle\langle Z_{ij}\rangle^{m}\rangle = \frac{1}{Mc} \sum_{m=1}^{Mc} \langle Z_{ij}\rangle^{m} \qquad (4\text{-}39)$$

can provide a noise-reduction-effect depends on the form of the noise contribution. However, it is significant that even when no noise reduction is effected the results can be used to establish a confidence limit, which can be used as a criteron for final data selection. The confidence limit is defined by

$$CL \equiv \frac{|\Delta Z_{ij}^{M}|}{|\langle\langle Z_{ij}\rangle\rangle|} \qquad (4\text{-}40)$$

Where ΔZ_{ij}^{M} is the maximum variation among various $\langle Z_{ij}^{\ell}\rangle^{m}$'s.

Fig.(4-3) shows the noise disturbance behavior in the four Z_{ij}^{ℓ}'s and their average $\langle Z\rangle$ for raw data and for the indicated cyclic operations. Data was selected from sections of MT records with high noise contents. The result indicates that data between $t_c \simeq 10$ to 100 sec are acceptable for the example shown.

Fig.(4-4) shows the result which is effected by the cyclic operation of Eqn(4-37). Data was taken from the MT record at the site-10 for both short and long period bands. Fig.(4-4.1) shows the average apparent resistivity ρ_{xy} (corresponding to $\langle Z_{xy} \rangle$) of the raw data, which have low predicted coherencies. Predicted coherency and smoothness of the curve are usually used as criteria for final data selection. If predicted coherency $\gtrsim 0.9$ is taken to be the criteron, none of the data at this site will be accepted.

To examine the effects of the cyclic processing, the low coherency of this data is ignored and a smooth curve is drawn through the data (Fig.4-4.1). Fig.(4-4.2) shows the average apparent resistivity after processing by the cyclic operation. If CL $\equiv \Delta\rho/\rho \lesssim 10\%$ is taken to be the criteron, some of the data is now found to be acceptable, while other parts are still of no use. Using only this acceptable data gives an entirely different picture from the curve of Fig.(4-4.1). The results shown in figure (4-4.2) are also used in figure (5-5.10).

Fig.(4-2). Curves of + $\rightarrow \rho^{\ell}_{xy}$, • $\rightarrow \rho^{\ell}_{yx}$ and $\langle \rho_{xy} \rangle$, $\langle \rho_{yx} \rangle$ for the case where noise exists only in the auto-power. ρ^{ℓ}_{ij} is deduced from Z^{ℓ}_{ij} (in arbitrary units).
Upper set: before cyclic operation.
Lower set: after 10 cyclic operations.
Col. 1-4 are for the pairs appropriate to Eqn(4-30)
Col. 5 is appropriate to the average $\langle Z^{\ell}_{ij} \rangle$.

Fig.(4-3). Same as above for case when noise exists in both auto- and cross-power.

Fig.(4-4.1). Average apparent resistivity ρ^{ℓ}_{xy} (corresponding to $\langle Z^{\ell}_{xy} \rangle$) of raw data for both short (left) and long (right) period bands. The numbers are the predicted coherency values for each indicated period interval. The curves are estimated by taking all the data into account.

Fig.(4-4.2). Same data as above but after 10 cyclic operations. Acceptable data (CL $\gtrsim$10%) are barred. The curves are established by using this acceptable data, and are also used for interpretation as shown in Fig.(5-5.10).

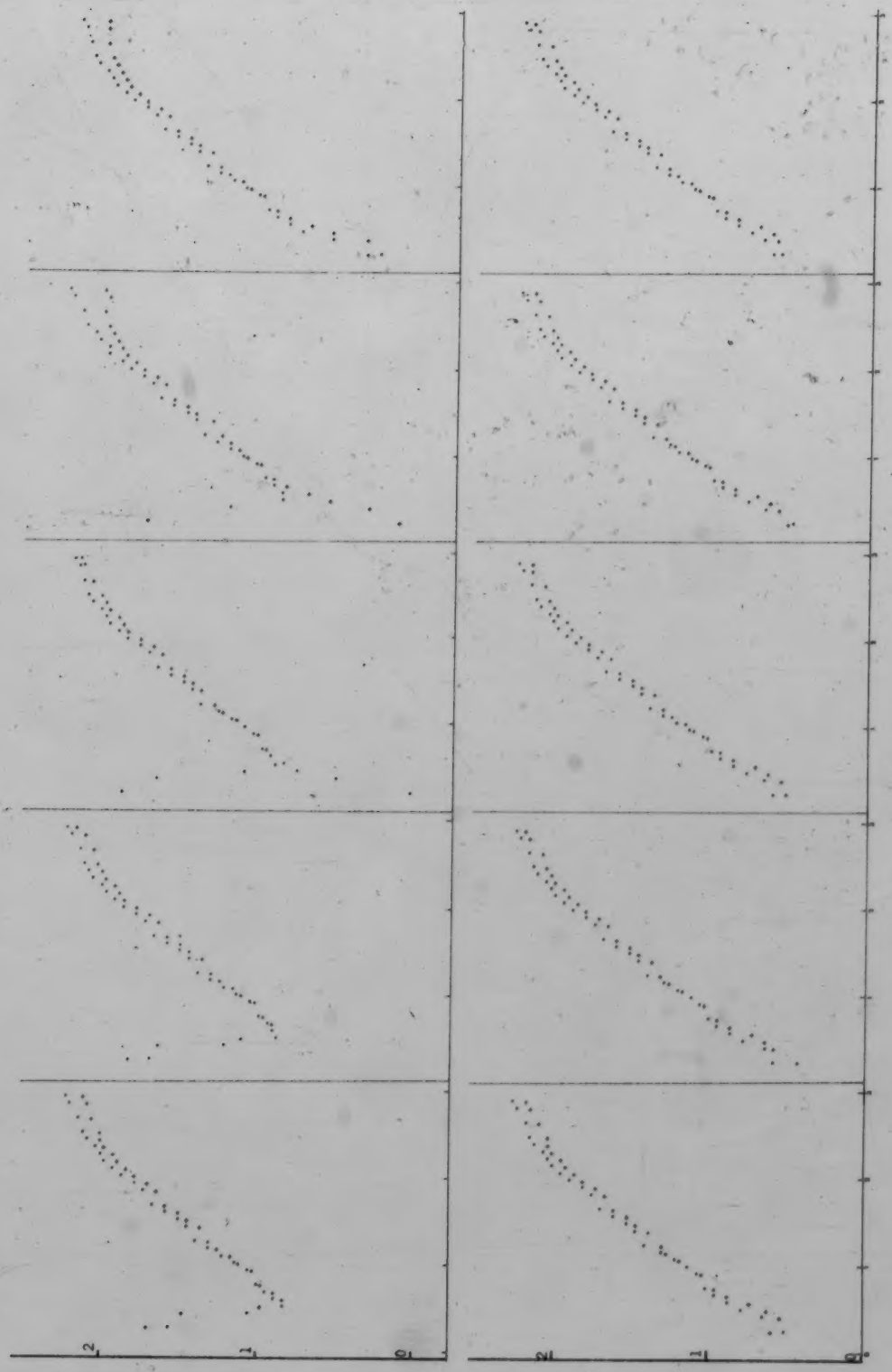

Fig.(4-2).

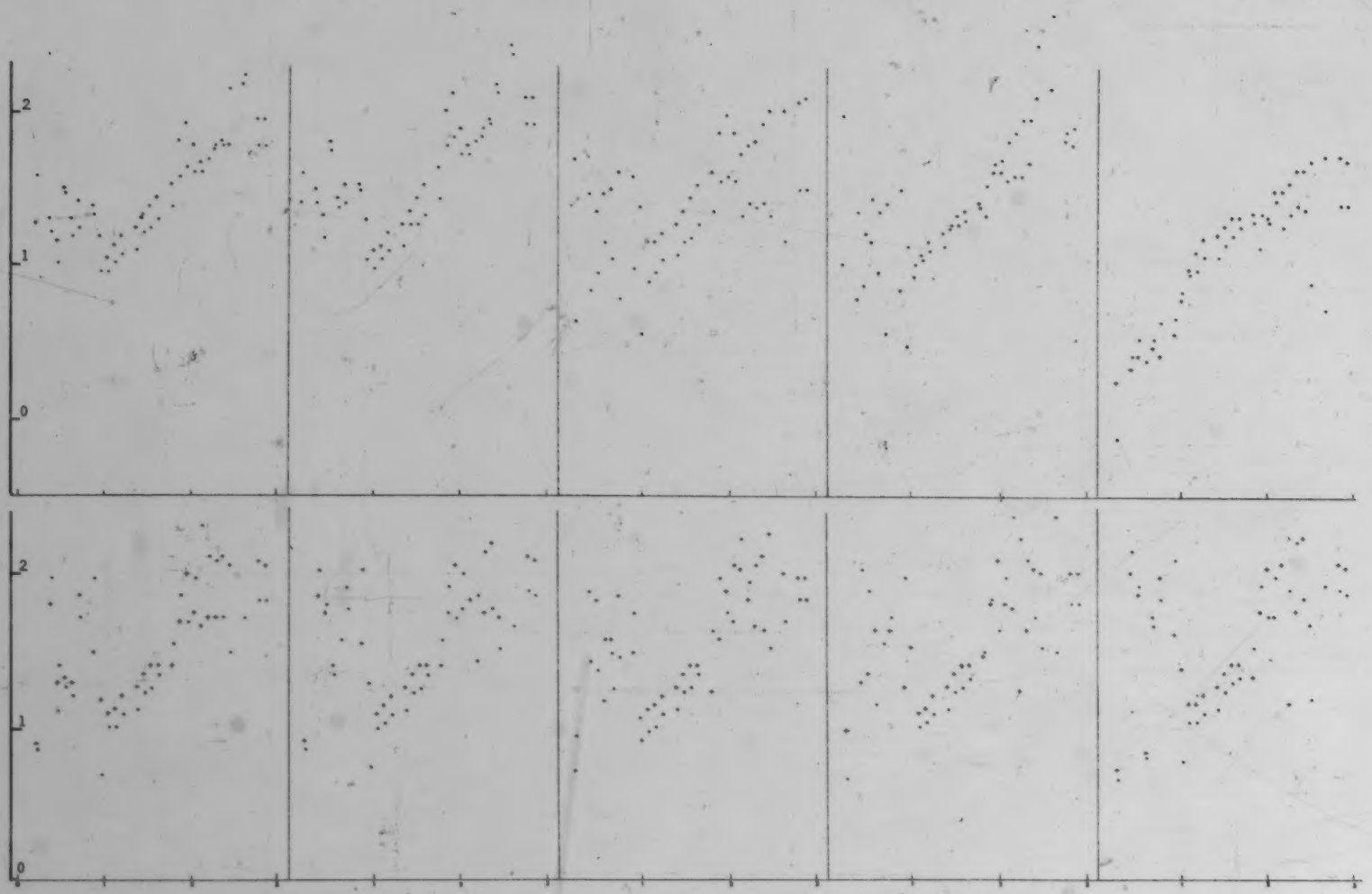

Fig.(4-3). LOG PERIOD (SEC)

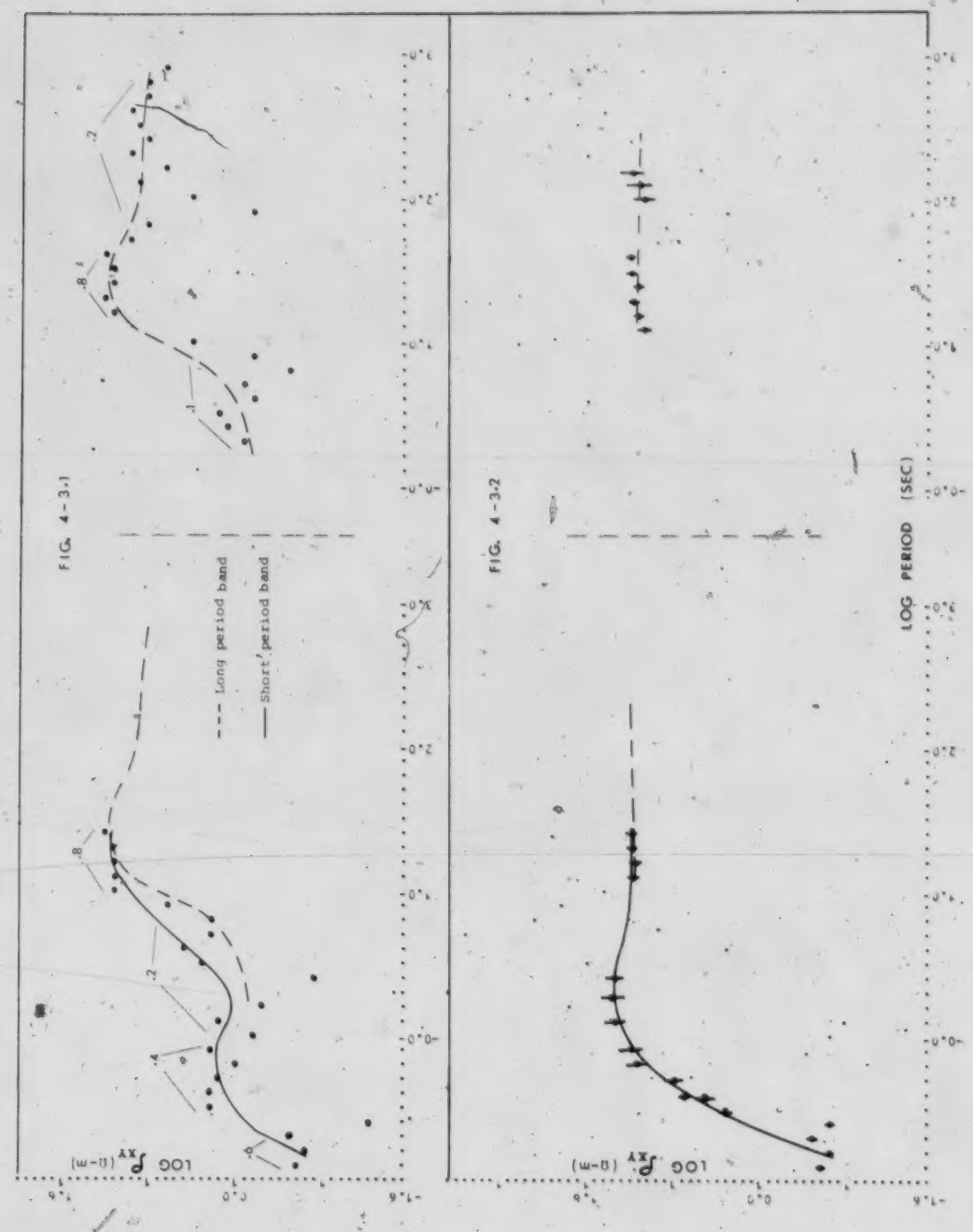
FIG. 4-3.1
FIG. 4-3.2
--- Long period band
— Short period band
LOG PERIOD (SEC)
LOG ρ_{xy} (Ω-m)
LOG ρ_{xy} (Ω-m)

CHAPTER V

MT SOUNDING

V-A. Geological Background

The Black Hills are a pronounced surface feature which rise several thousand feet above the surrounding Great Plains of North America. The location is shown in Fig.(5-1). This island like mountain structure which is approximately 200 km long and 100 km wide extends North West from the South West corner of South Dakota into the North East corner of Wyoming. A considerable number of geological and geophysical studies have been carried out in this region and it is possible to give a general geological description.

As shown in Fig.(5-1.2, 5-1.3, 5-1.4), the central Precambrian core of the Black Hills consists of a succession of highly folded schists, sedimentary in the main, but intruded by a succession of large and small granitic masses. Flanking this Algonkian mass are the upturned truncated edges of the sediments ranging in age from upper Cambrian to Tertiary. The dips of the sediments away from the centre are steeper on the East than on the West. Lidiak (1971) has mapped a metamorphic belt under the sediments and trending somewhat East of the strike of the Black Hills. This belt runs right through the central exposed metamorphic rocks of

the Black Hills, shown in Fig.(5-2).

Gough and Camfield (1971) have found from their deep sounding studies a very pronounced induction anomaly which is in striking agreement with Lidiak's metamorphic belt, as shown in Fig.(5-3). They attribute their results to a suitable graphitic schist in the basement. Mathisrud and Sumner (1967) have found highly conductive graphitic schists in the lead mine district of the Hills, but these were highly localized.

Three heat flow measurements made by Sass et al (1971), were either anomalously high or low. However these measurements were not of high quality and therefore no reliable deductions can be drawn from them. Surface manifestations of thermal activity such as hot springs and elevated ground water temperatures exist in many regions in and around the Black Hills.

The age dating results quoted by Lidiak place the Black Hills' orogeny at 1600 to 1800 m.y. ago. Various silicic intrusives associated with volcanic activity are dated at 1450 m.y. ago. It should be noted that the extension of the metamorphic belt mapped by Lidiak was deduced on the basis of geophysical measurements such as gravity and magnetic and is reasonably consistent with drill hole results and the aeromagnetic survey reported by Zietz et al (1971) and also shown in Fig.(5-2).

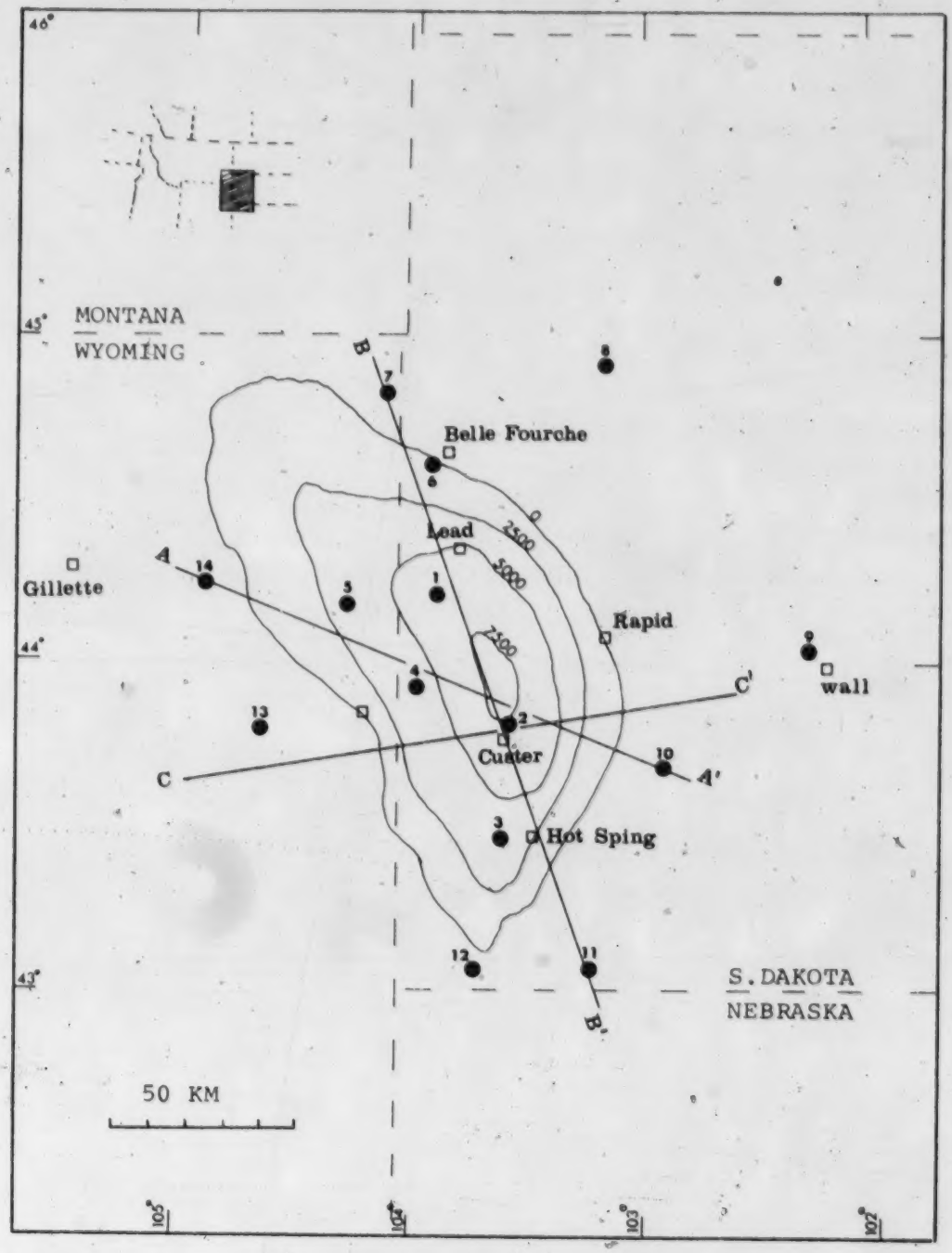

Fig.(5-1). Geological location of the Black Hills and sounding sites (●). Contour interval 2500-ft. Datum is sea level.

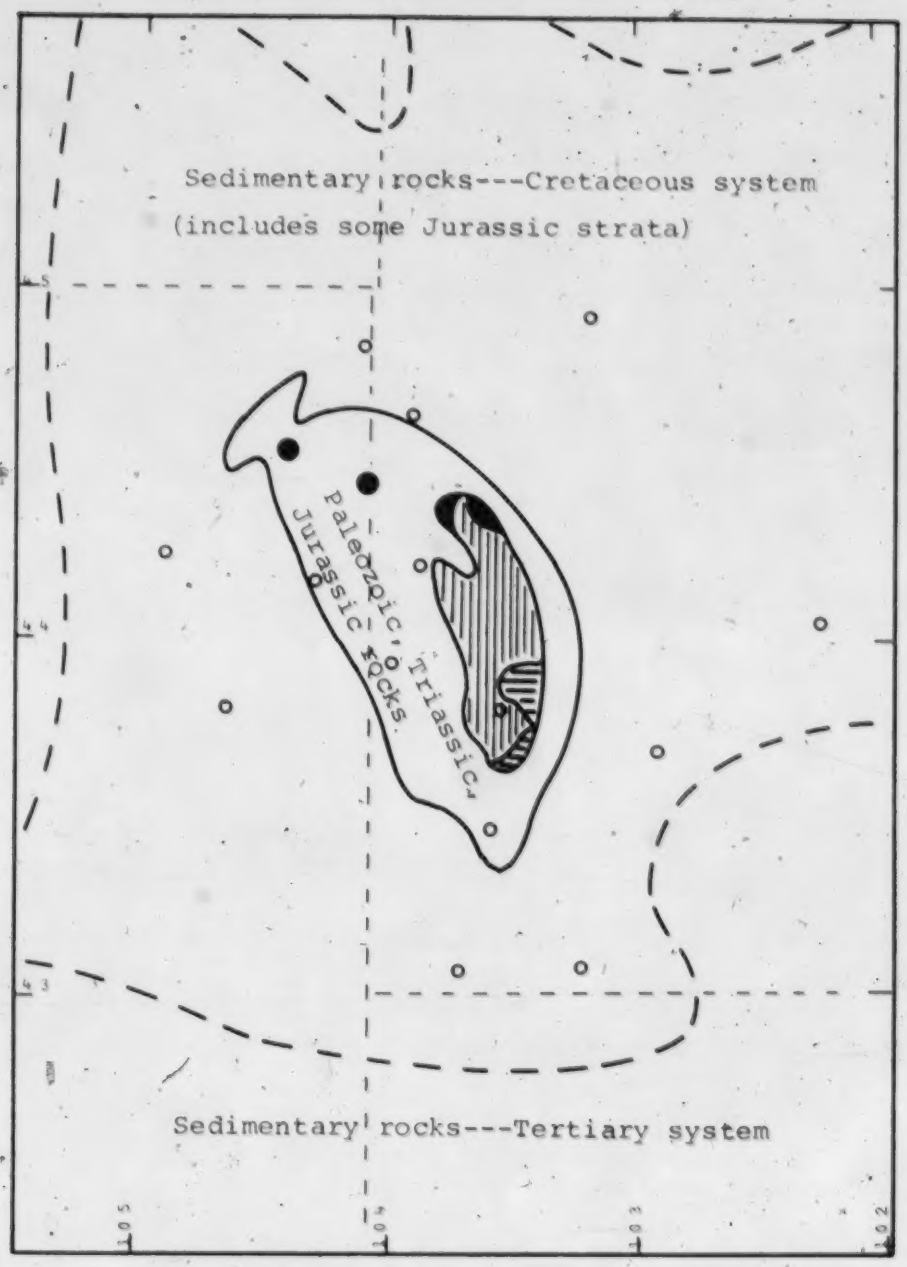

Fig(5-1.2) Areal geologic map of the Black Hills region.

Precambrian rocks--- Sedimentary rocks.

Precambrian rocks--- Igneous and metamorphic.

Intrusive rocks --- Tertiary system.

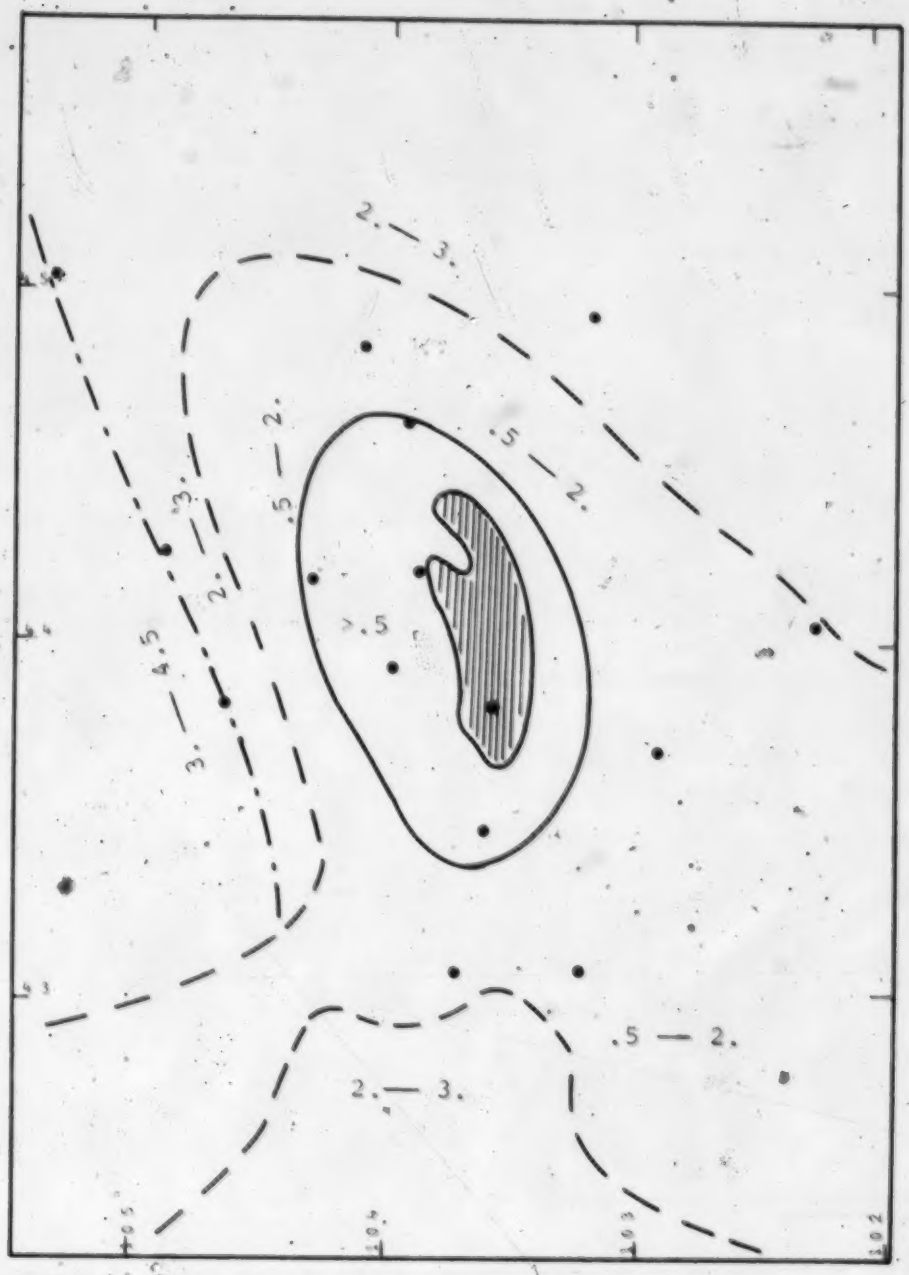

Fig.(5-1.3). Thickness of Phanerozoic rocks.
(Depth to Precambrian basement, in KM).

Black Hills uplift(Precambrian crystalline rocks exposed).

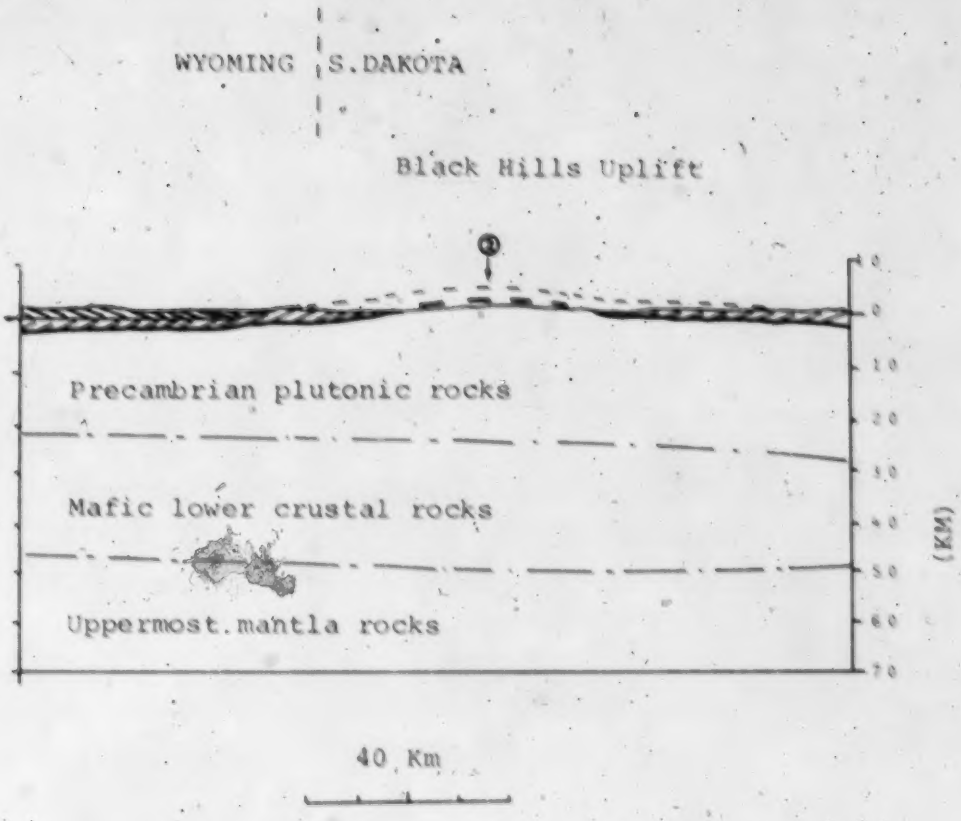

Fig.(5-1.3). Structural cross section along C-C'.

Cenozoic sedimentary rocks, continental, detrital, with local volcanic rocks.

Mesozoic sedimentary rocks, marine and continental, detrital.

[Fig. 5-1.2,3,4; Geologic Atlas of the Rocky Mountain region, Denver, Colorado, 1972]

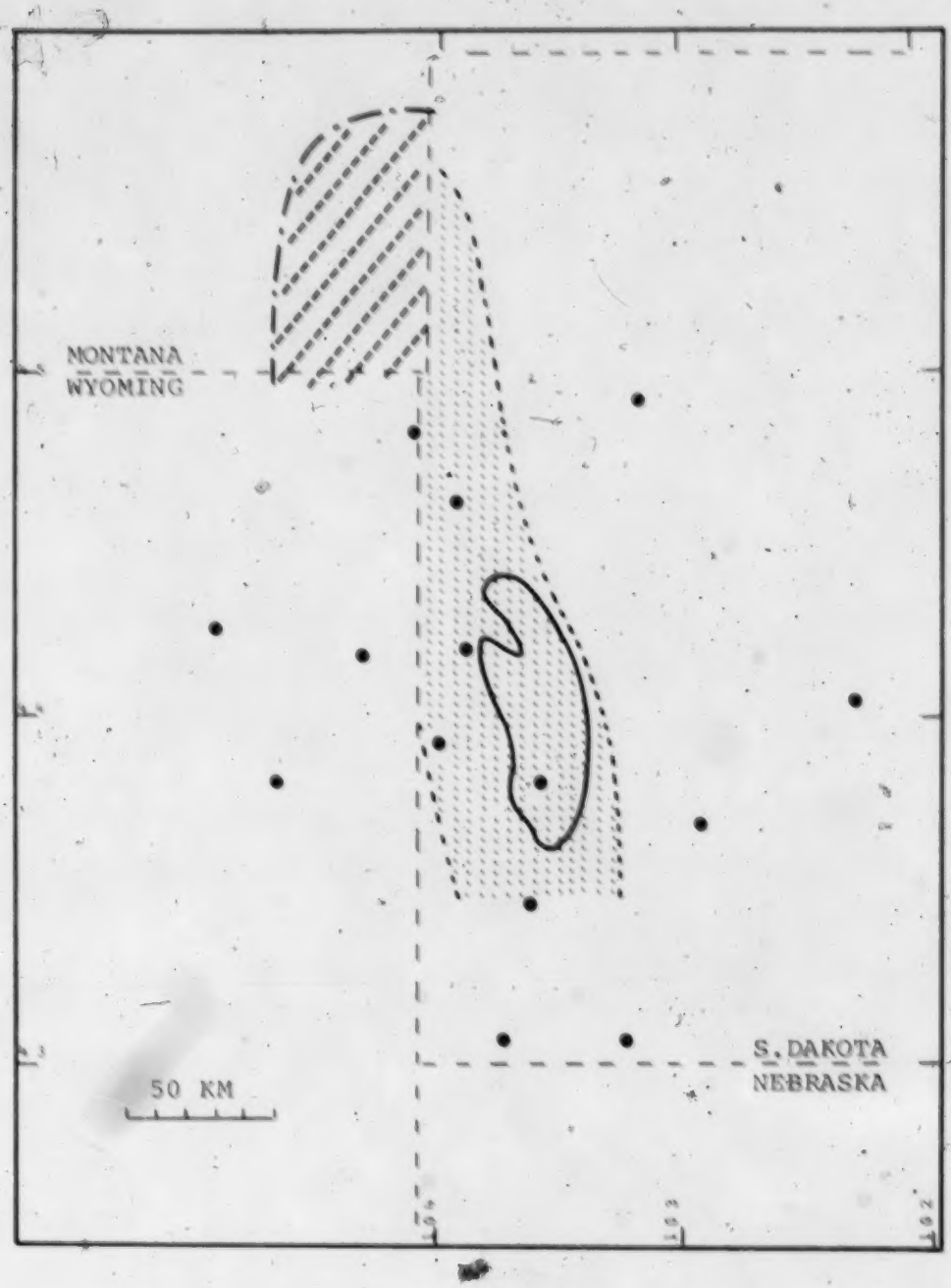

Fig(5-2). The Black Hills uplift.

Metamorphic belt (Lidiak 1971).

Region of high magnetic intensity (Zietz et al).

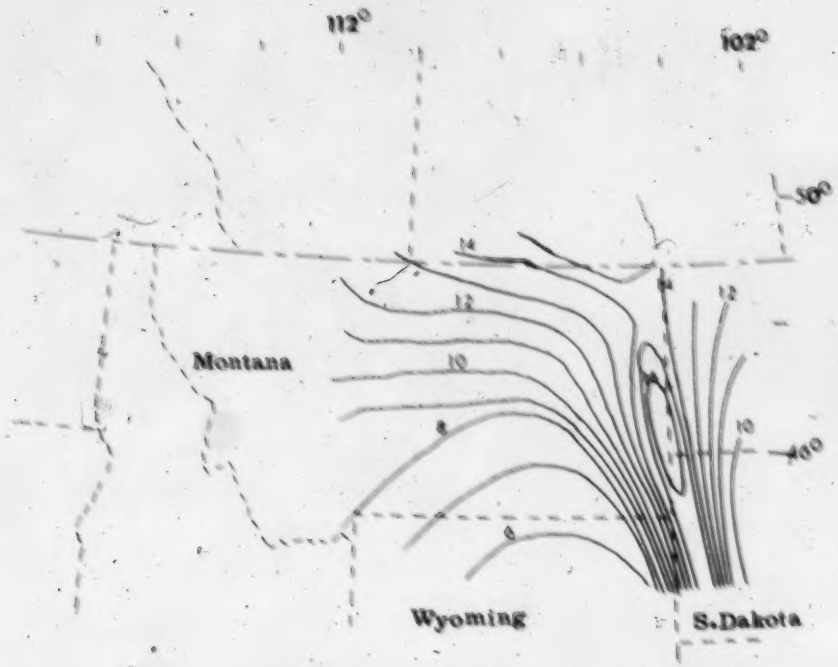

Fig.(5-3). Contour map of Fourier amplitudes of east-west component of magnetic field at period 48 min. Geomagnetic deep sounding result by Gough et al (1971).

Since electromagnetic measurements are affected by structure lying within several skin depths an averaging effect is anticipated and thus one would expect to measure a relatively poorly conducting central region of the Black Hills characteristic of old crystalline material, surrounded by the relatively better conducting material characteristic of more recent sediments. The striking high conductivity anomaly in the central region of the Black Hills will be discussed in the following sections.

IV-B. Data Analysis and Computed Results

Records were selected visually to be of good amplitude and free of spikes and steps. Six data sets were usually obtained at each station in both high and low mode. Details of this are shown in Table (5-1). In all cases a data set consists of 4096 digitized values with the high mode digitized at 40/sec and the low at 1.25/sec. Following the techniques described in Chapter III, the Fourier coefficients were computed using a constant Q filter with Mb = 6 at the low frequency end and Mb $\cong$ 300 at the high frequency end of the spectrum. Fig. (5-4) shows a pair of representative smoothed power density spectra for the E and H fields. The computed numerical results appear in the tables in Appendix B.

While it has been customary in the past to use only the criterion of high predicted coherency between the conjugate pairs of E and H as a basis for acceptance or rejection of data, the cyclic operation presented in Chapter IV permits the inclusion of a considerable amount of data with lower predicted coherencies in the initial stages of computation. The actual criterion adopted in the final stage of computation was that ρ_a was derived from the average values of z_{ij}^{ℓ}, where the individual z_{ij}^{ℓ} lie within 2½% of the average of the 4 possible values. The results of this process can be seen in Figs. (4-2) and (4-3). By this procedure 'good' data was obtained over the complete range of recorded frequencies, except for stations 3 and 9 where only a portion of the spectral range was acceptable.

The apparent resistivities are shown in the 'principal' directions in Figs. (5-5.1 to 5-5.14) for each station. Real principal directions actually exist only for genuinely two-dimensional structures. These directions are given for each station as θ_o in Figs. (5-6.1) to (5-6.2).

In addition to the apparent resistivity, and its principal directions, the directional parameters θ_{ze} and θ_{zh} are also used. These are the directions which produce a maximum coherency between H_z and a component

Table 5-1 (L = long period band, S = short period band)

	Site	Period Band	No. of Data Set Average	Sample Length
1	Nahant	L	6	5.6 h
		S	6	10. m
2	Custer	L	10	9.2 h
		S	6	10. m
3	Kahta	L	7	6.5 h
		S	4	7. m
4	Moon	L	10	9.2 h
		S	6	10. m
5	Smith	L	6	5.6 h
		S	6	10. m
6	Belle Fourche	L	10	9.2 h
		S	6	10. m
7	Colony	L	6	5.6 h
		S	6	10. m
8	Newell	L	6	5.6 h
		S	6	10. m
9	Wall	L	5	4.6 h
		S	6	10. m
10	Cheyenne River	L	6	5.6 h
		S	6	10. m
11	Walker	L	10	9.2 h
		S	6	10. m
12	Ardmore	L	6	5.6 h
		S	4	7. m
13	Clareton	L	10	9.2 h
		S	6	7. m
14	Morecraft	L	10	9.2 h
		S	6	10. m

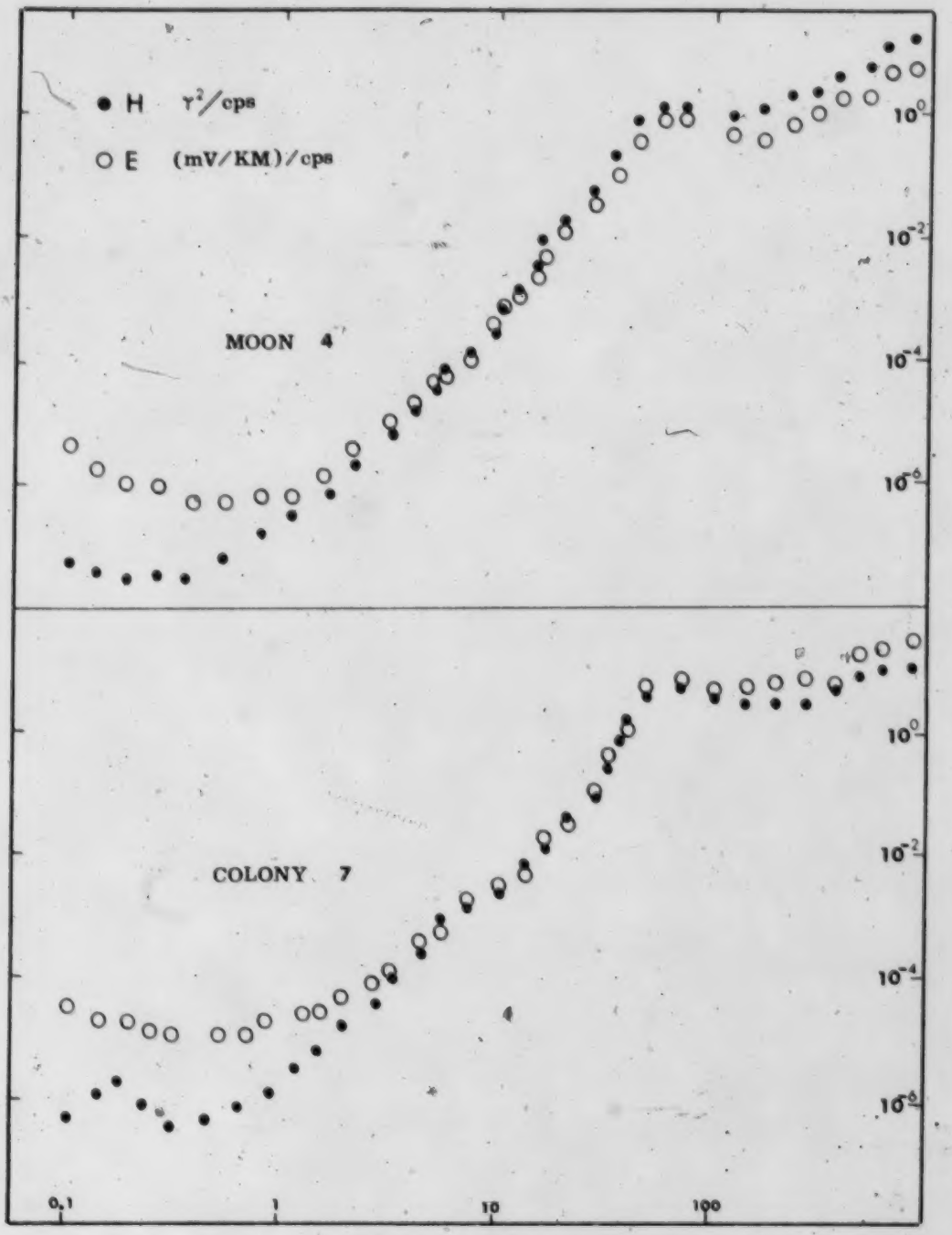

Fig.(5-4). Smoothed power spectral density.

Figs.(5-5). Apparent Resistivities in the Principal Directions vs Period.

O --- ρ maximum of short period band

Δ --- ρ minimum of short period band

● --- ρ maximum of long period band

▲ --- ρ minimum of long period band

—— --- Result of layered model fitting

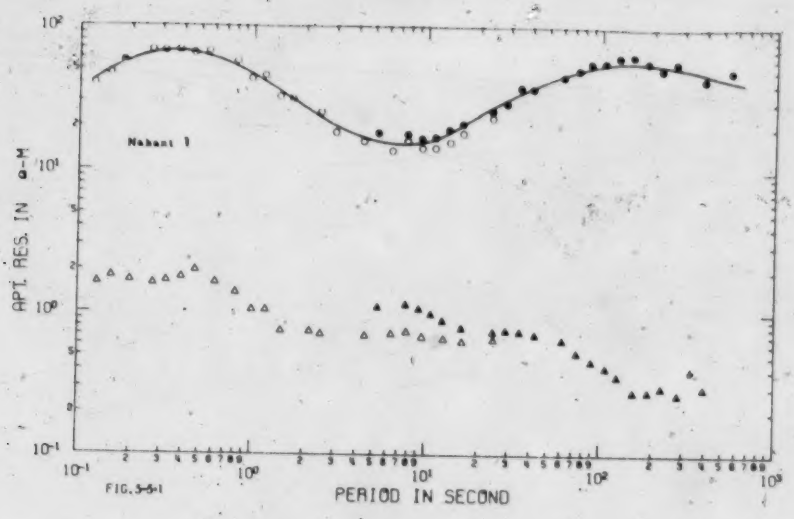

FIG. 5-5-1

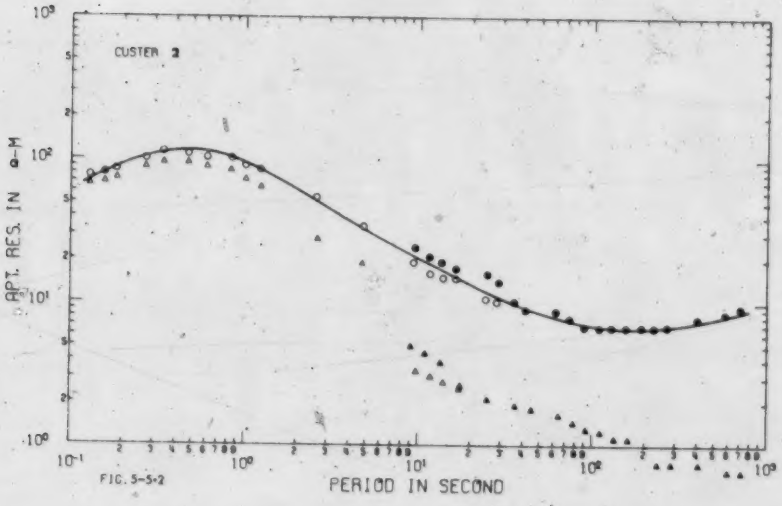

FIG. 5-5-2

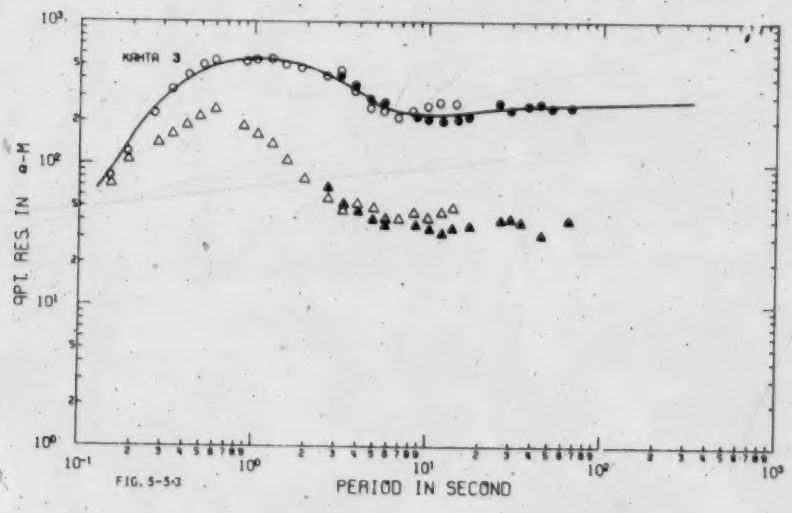

FIG. 5-5-3

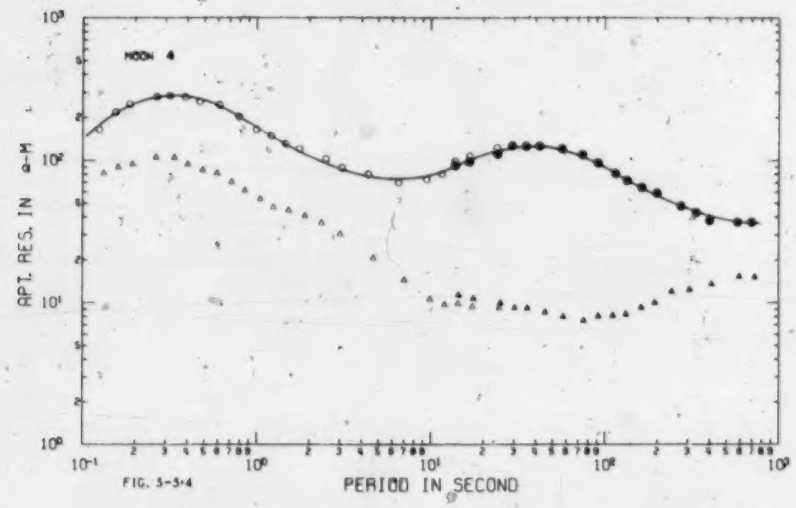

FIG. 5-5-4

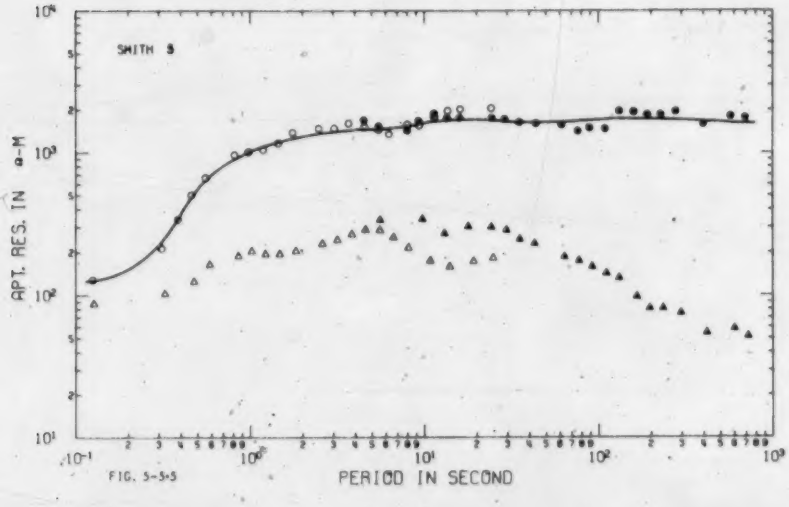

FIG. 5-5-5

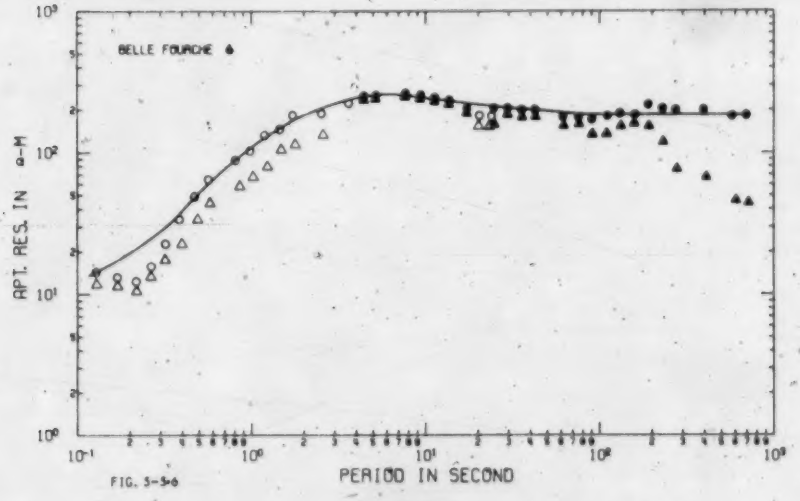

FIG. 5-5-6

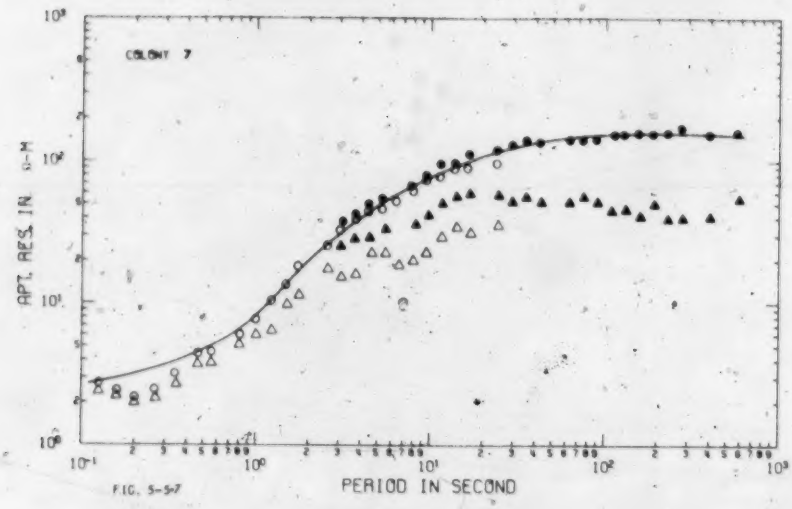

FIG. 5-5-7

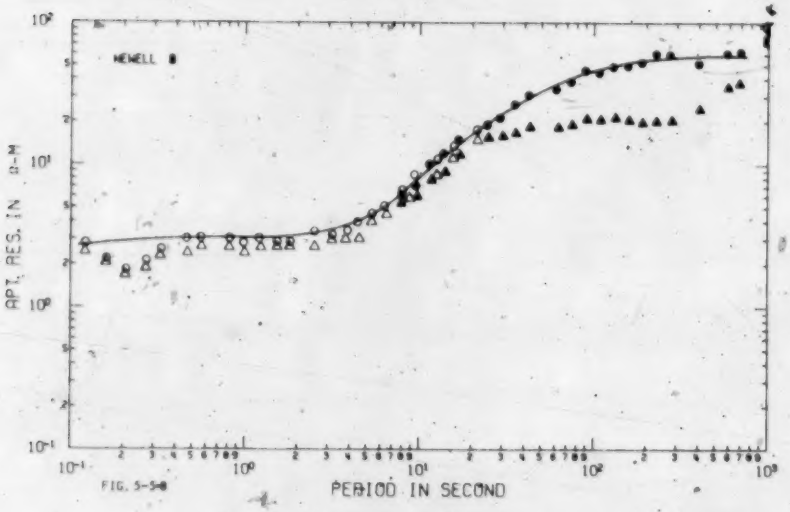

FIG. 5-5-8

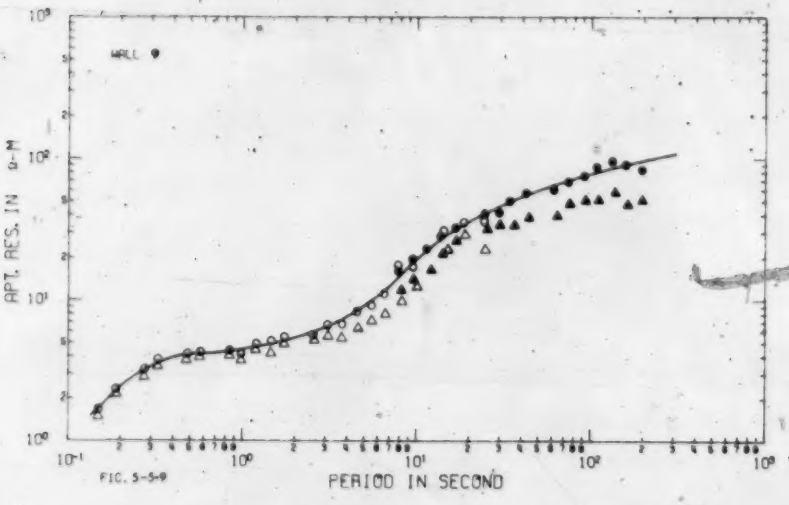

FIG. 5-5-9

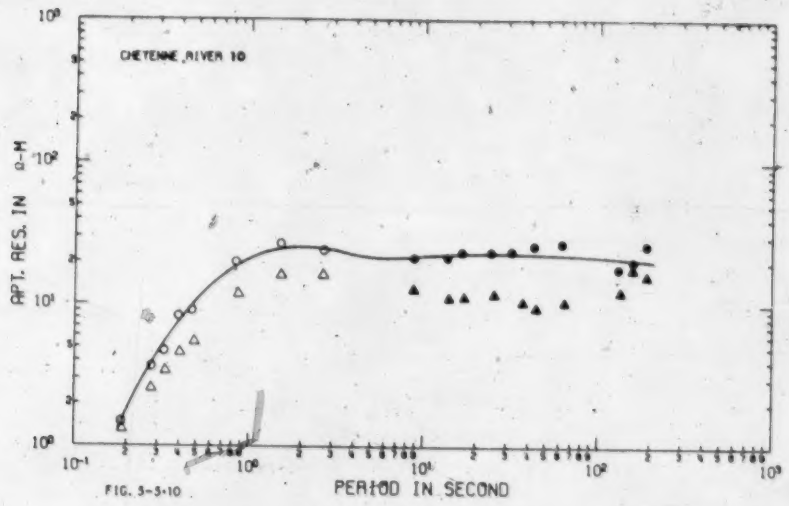

FIG. 3-3-10

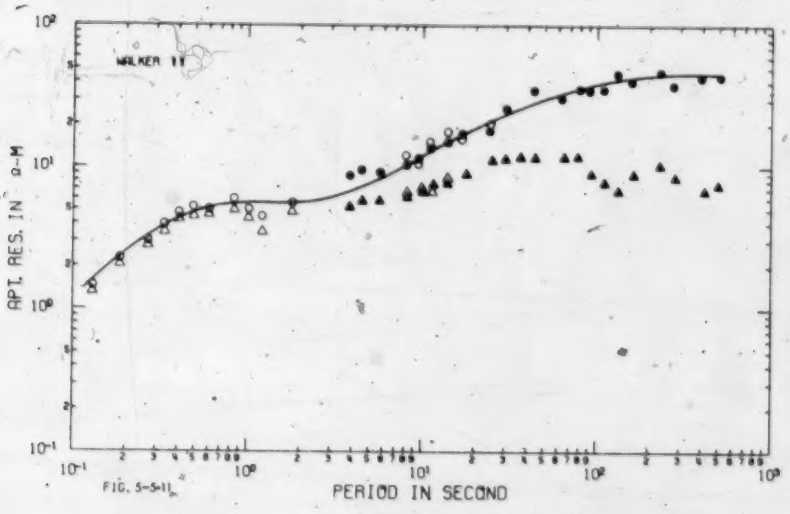

FIG. 3-3-11

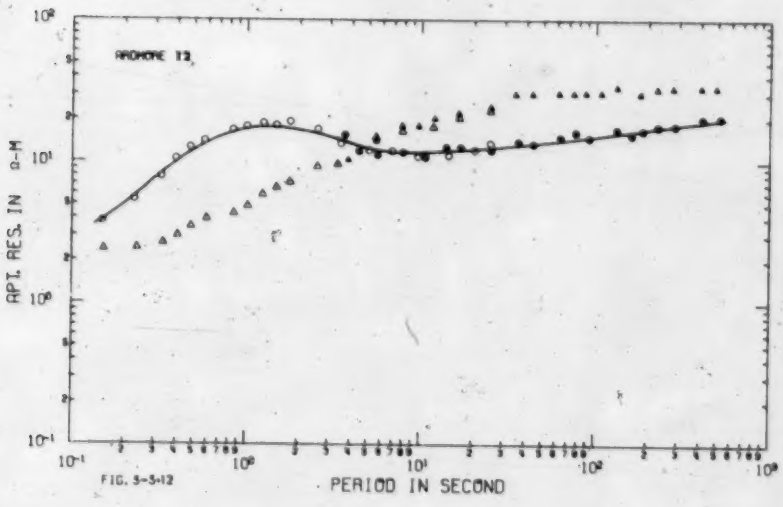

FIG. 3-3-12

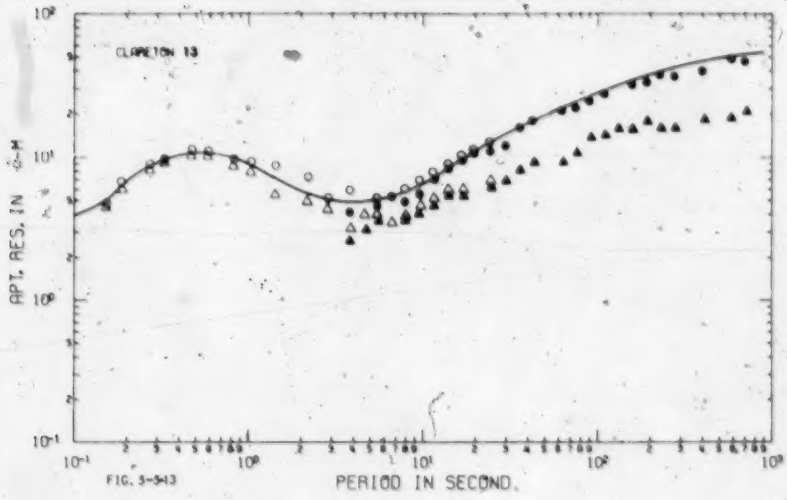

FIG. 3-5-13

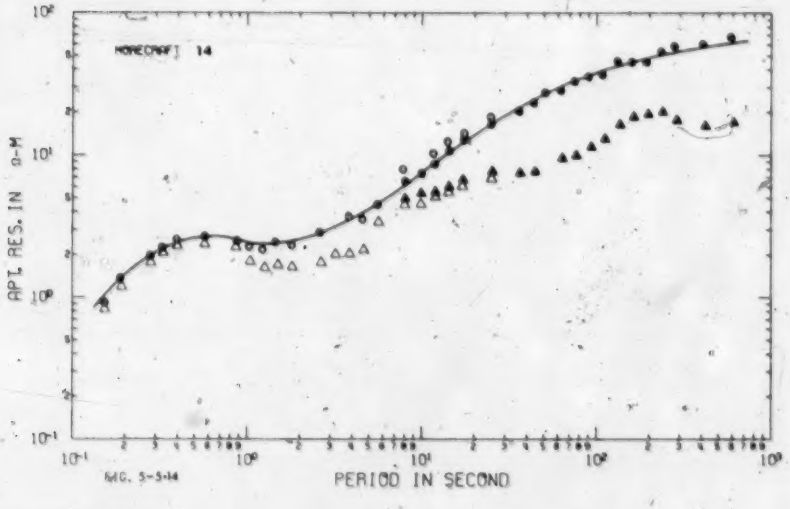

FIG. 3-5-14

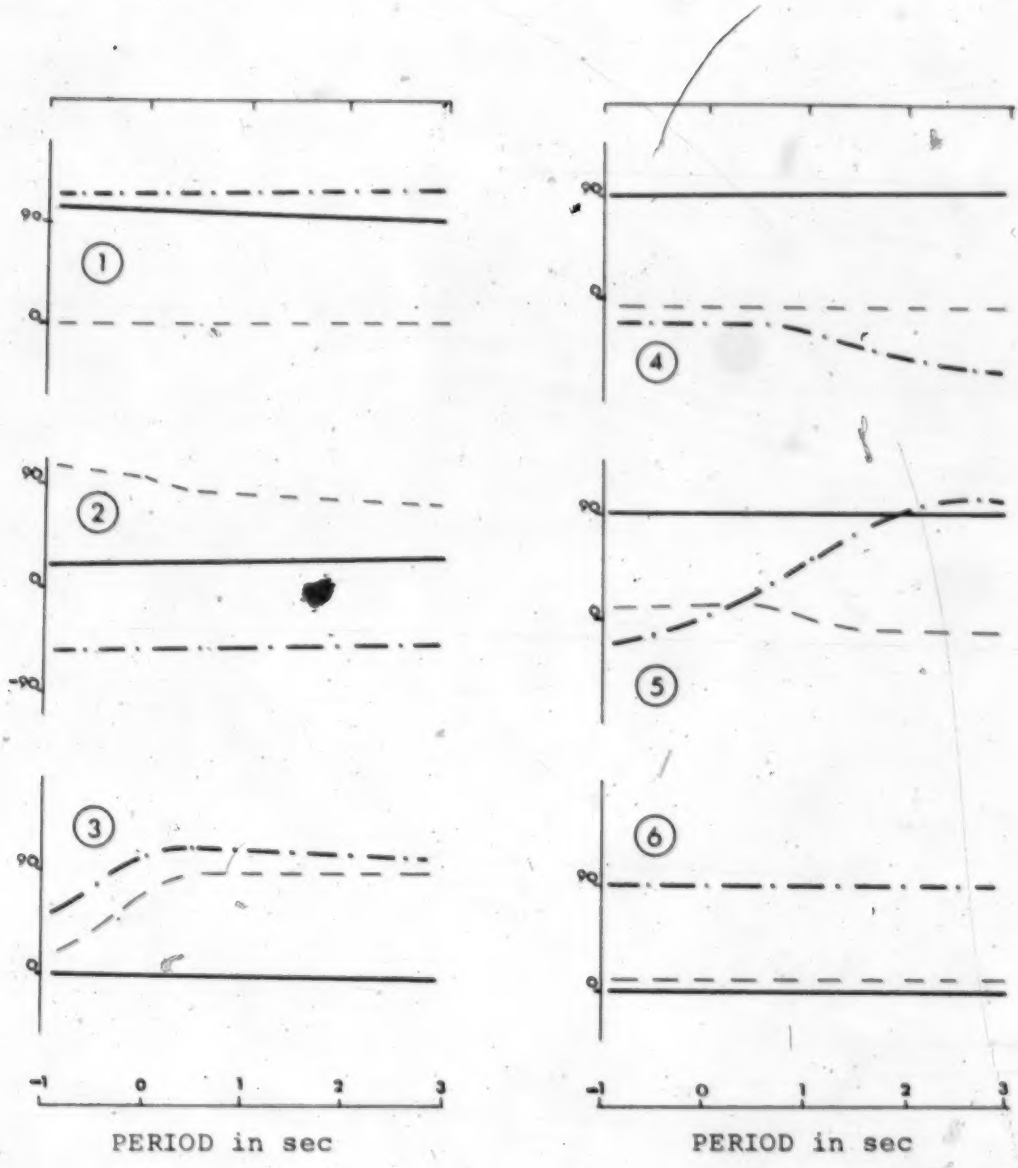

Fig.(5-6.1). Directions of maximum apparent resistivity θ_o (——), maximum admittance θ_{ze} (– – –), and θ_{zh} (—·—) vs period. The numbers in the circles refer to the site number. (Directions in degree measuring from the North)

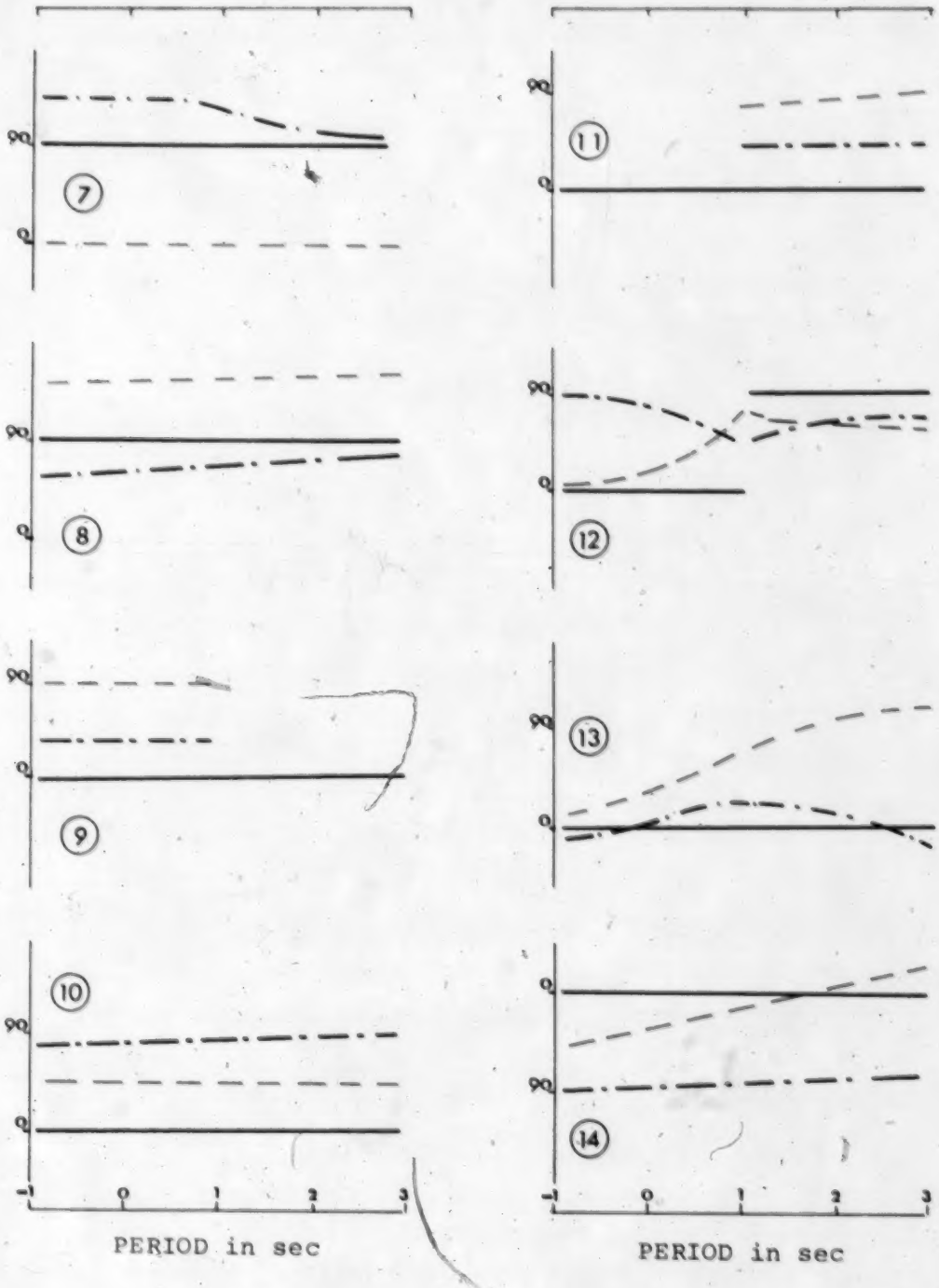

Fig.(5-6.2). (Same as figure 5-6.1).

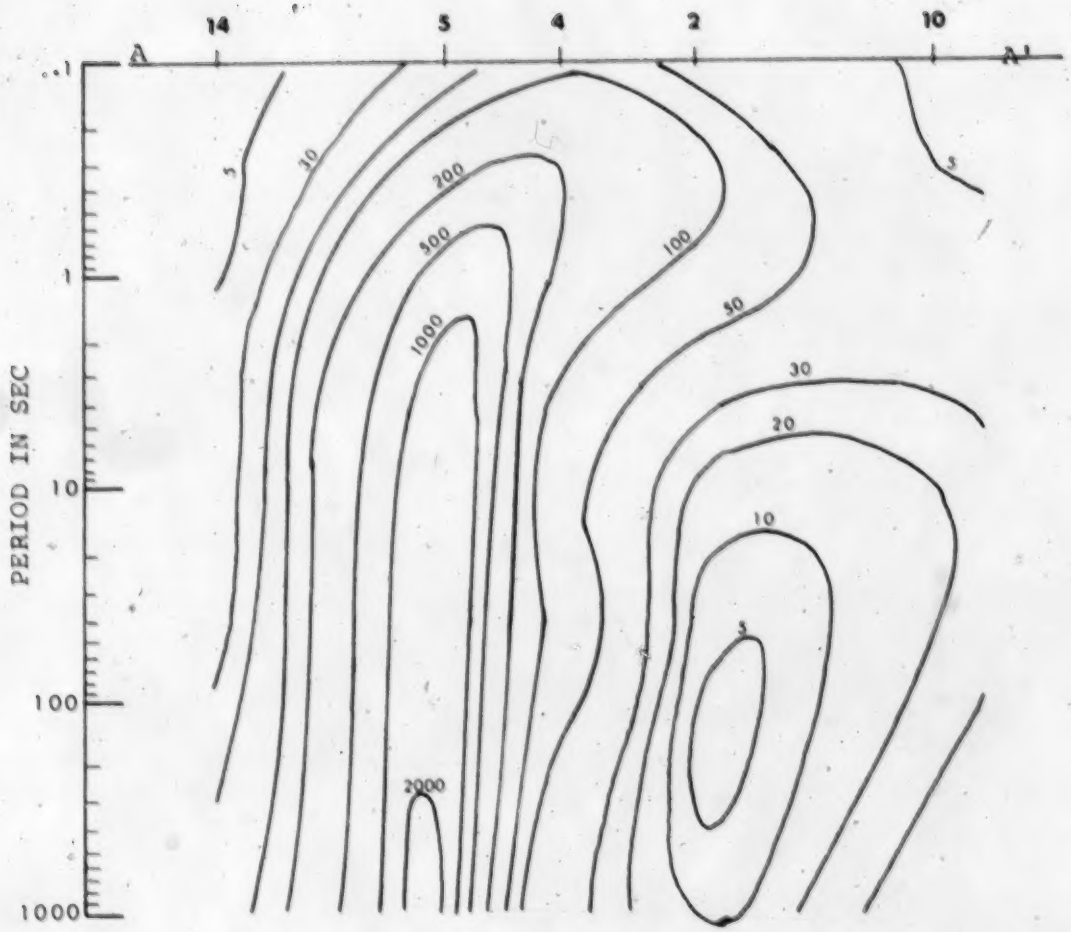

Fig.(5-7.1). Contour map of maximum apparent resistivity (in Ω-M) vs period along A-A' traverse.

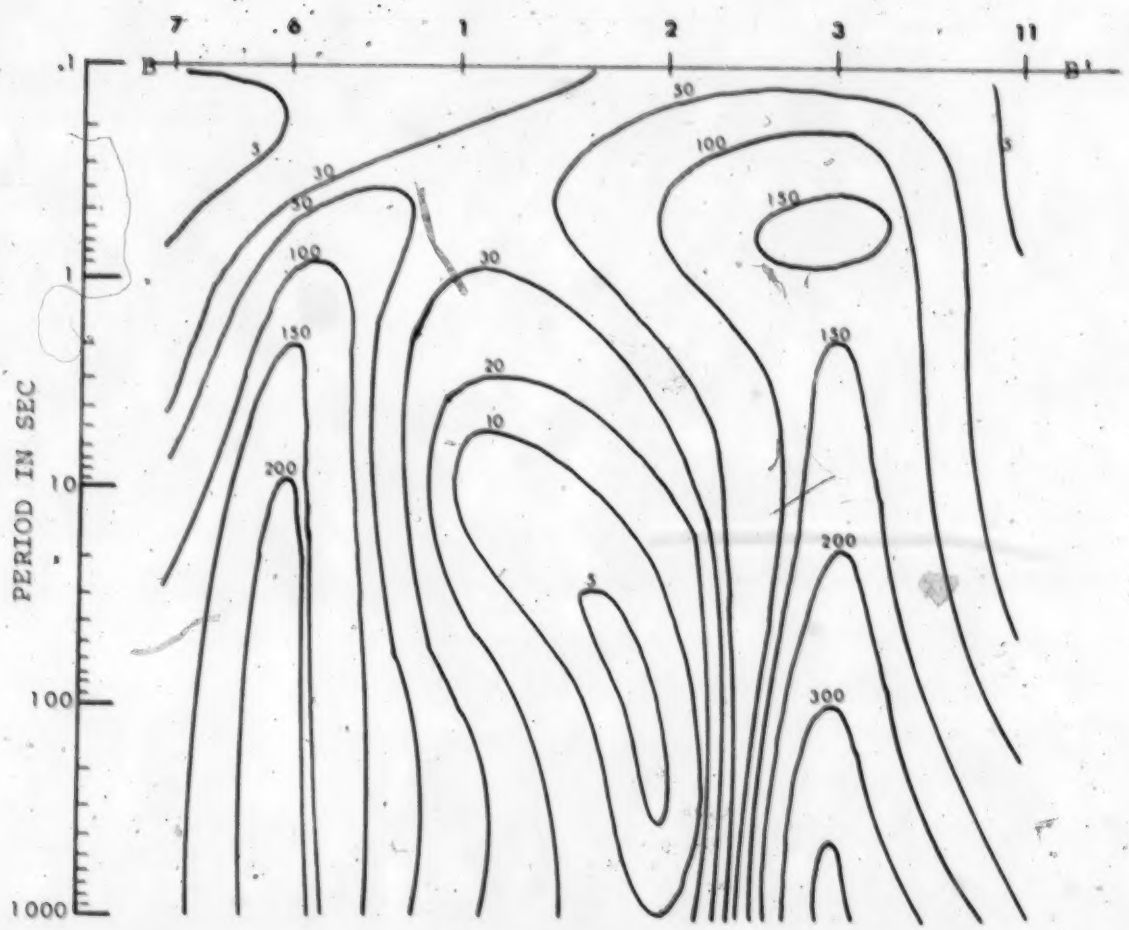

Fig.(5-7.2). Contour map of maximum apparent resistivity (in Ω-M) vs period along B-B' traverse.

of E and H respectively and are also shown in Figs. (5-6.1, 5-6.2) for each station.

Pseudo-sections for the two traverses A-A' and B-B' indicated in Fig. (5-1) are shown in Figs. (5-7.1) and (5-7.2), where apparent resistivity is plotted as a function of period. These are converted to MT resistivity cross sections in Figs. (5-8) and (5-9) and will be discussed in the next section.

V-C. Interpretation and Discussion

(1) Discussions

The results, i.e. the anisotropic character of the apparent resistivity and the dimensional indicators, show that in the area studied, the conductivity structure is 3-dimensional. In the central region of the Hills, at sites 1-5, the two principal apparent resistivities diverge throughout most of the spectral range. The skew factor is large and also θ_o does not coincide with either θ_{ze} or θ_{zh} as they would for a two dimensional earth. In the area external to the Hills, sites 7-14, the apparent resistivity curves coincide for short periods and diverge for longer periods. This is interpreted to imply that in this region the earth is homogeneous, isotropic, and layered near the surface and more complicated at depth. While the dimensional

indicators are in disagreement with this interpretation it must be considered that these indicators are much more sensitive to the minor contributions from 3-dimensional structure. On the east, west, and south sides around the Hills where sites 9-14 are located, the apparent resistivities indicate that below the conductive near surface layers, there is a relatively resistive layer, which in turn is underlain by a conductive third layer. In the area north of the Hills where sites 7 and 8 are located, it seems that the conductive third layer is not present. At the southern corner of the uplift at site 12, the principal axis of the apparent resistivity changes direction by 90° at $t \sim 10$ sec as shown in Figs. (5-5.12) and (5-6.2); such a change only happens at this site.

(2) Earth Model

Taking site 2 as an example and applying the one-dimensional approach, an apparent resistivity curve as shown in Fig. (5-5.2) is used to construct a four layer earth with the parameters as given in Table (5-2). The first two layers would be acceptable due to the isotropic behavior of the apparent resistivities in the first decade of the period. The third layer has a very high conductivity and is located at approximately

3-10 KM, corresponding to a period ranging of about 1-500 sec. In this range the apparent resistivities appear anisotropic. Thus this anomaly may be placed at a distance of 3 KM from the measuring point but in an arbitrary direction in the half space. However, as shown in Fig. (5-7.2), for the same period range θ_o is closer to θ_{ze} rather than to θ_{zh}. According to the results of the two-dimensional model calculations, θ_o coinciding with θ_{ze} is consistent with the measuring site being on the conductive side of the strike of a resistivity anomaly. Thus, this low resistivity anomaly is placed below the measuring site. This result is consistent with that of the group of stations in the anomalous region.

The model parameters of layered earth for each site are calculated and listed in Table (5-2). The maximum apparent resistivity ρ_M corresponds to the direction in which most of the power is concentrated and thus ρ_M is considered to be more reliable for curve fitting. The solid lines in Fig. (5-5) represent the model results.

Pseudo-depth, defined by $\bar{z}(\omega) = \delta(\omega)$ are calculated using the skin depth theory for each one-dimensional profile. The pseudo-depth represents the depth reached by the field with its amplitude reduced by a factor 1/e for a given frequency in a given

layered model. Contours of apparent resistivity and admittance vs pseudo-depth are referred to as MT resistivity cross sections. These are shown for the two given traverses in Figs. (5-8) and (5-9).

While the MT resistivity cross sections are not adequate for detailed interpretation, they do give a qualitative picture which is useful in the total interpretation.

Considering all the results, a final 3-dimensional resistivity section can be constructed. Figs. (5-10) show this construction for two traverses AA' and BB'. Figs. (5-11) show a plane view of the same resistivity distribution at horizontal planes at depths of 1-KM, and 5-KM, and 20-KM, respectively.

(3) Summary and Comments

The cyclic operation developed in Chapter IV has proven very effective in extending the spectral range of data that can be utilized with a high confidence level. This has enabled a more detailed interpretation of the field data from the 1973 field season than had been heretofore considered possible.

In the area surrounding the Black Hills uplift, low resistivity with some layering is found in relatively shallow depths underlain by material of high resistivity. Within the central region was found a

Table 5-2. Parameters of One-dimensional Model

(R = Resistivity, H = Thickness)

Site	R(Ω-M)	H(KM)
Mahant (1)	30-50	.3
	500	3.0
	5	2.0
	2000	30.
	50	
Custer (2)	30-50	.3
	1000-3000	3.
	5	7.
	50	
Kahta (3)	30-50	.3
	1000-2000	8.
	50	4.
	50-400	
Moon (4)	30-50	.3
	2000-4000	3.
	30	6.
	1500	20.
	50	
Smith (5)	30-50	.5
	1000-3000	1.5
	5000-10000	20.
	1500	
Belle Four. (6)	10	.3
	2000-3000	10.
	100	3.
	200	
Colony (7)	4	.5
	2000-3000	20.
	100	
Newell (8)	4	1.5
	2000-3500	5.
	200	10.
	100	
Wall (9)	2	.1
	35	.6
	5	1.
	3000	30.
	30	
Chey. R. (10)	4	.1
	40-50	.1
	200	4.
	5	1.
	50	
Walker (11)	1	.06
	30-50	1.2
	5	1.2
	1500	10.
	30	
Ardmore (12)	2	.1
	150	3.
	4	1.
	1000	10.
	30	
Clareton (13)	2	.1
	40	1.2
	1	.5
	1000	10.
	100	
Morecraft (14)	2	.1
	35	.5
	5	1.2
	1000-2000	10.
	100	

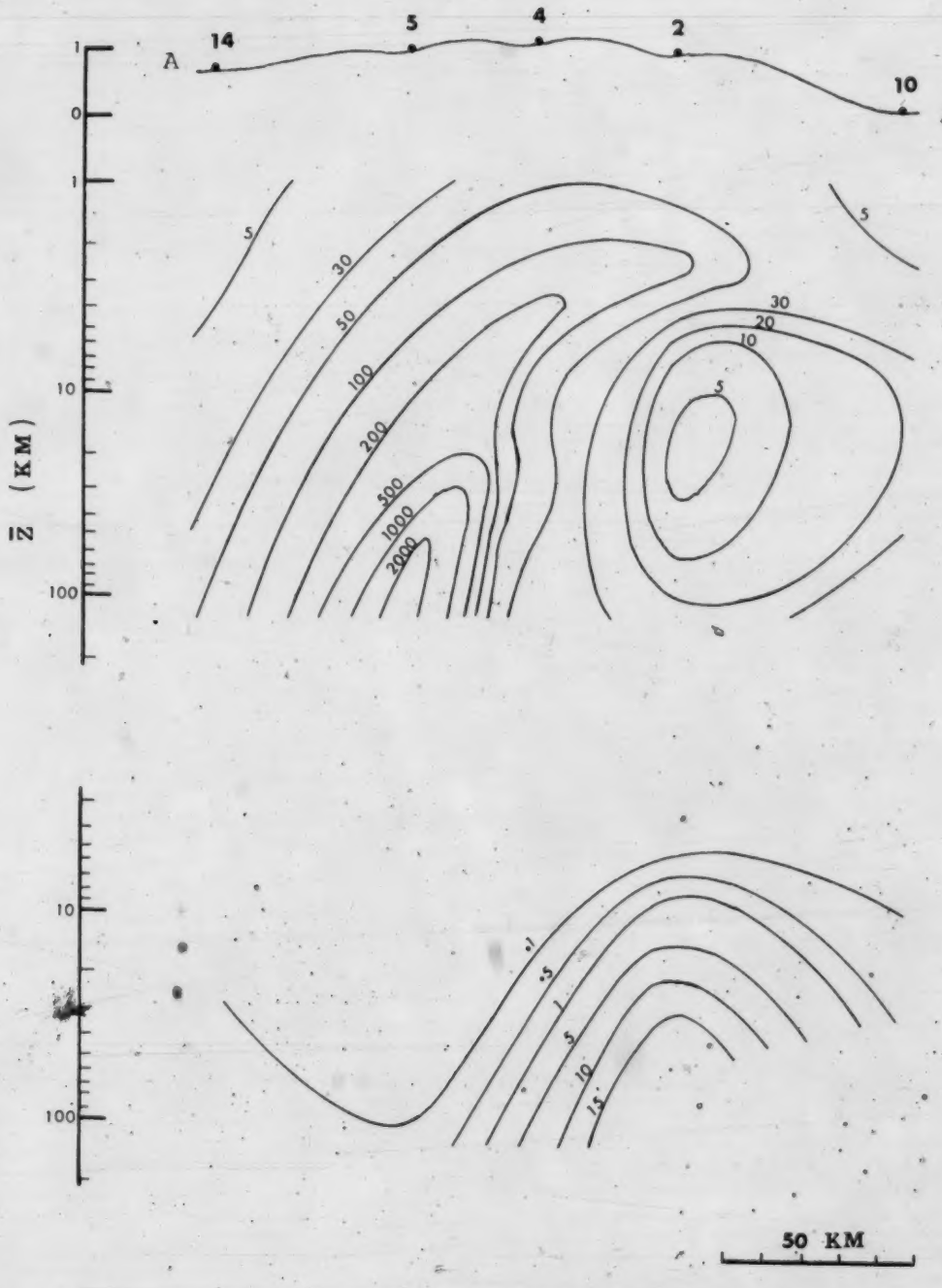

Fig.(5-8). Contours of maximum apparent resistivity (upper, in Ω-M) and maximum admittance (lower, in arbitrary units) vs $\bar{z}$ (pseudo-depth) along A-A' traverse.

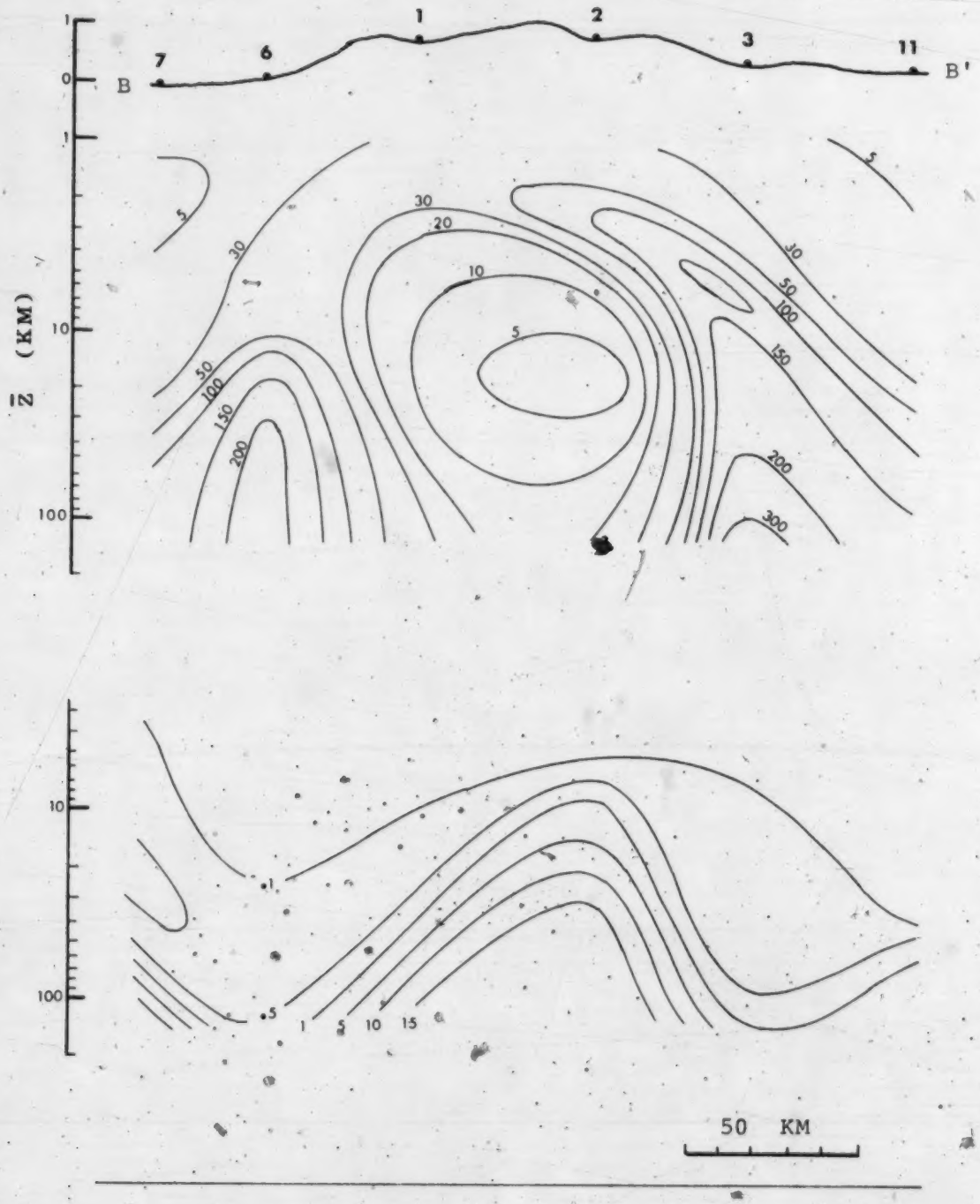

ig. (5-9). Contours of maximum apparent resistivity (upper, in Ω-M) and maximum admittance (lower, in arbitrary units) vs $\bar{z}$ (pseudo-depth) along BB' traverse.

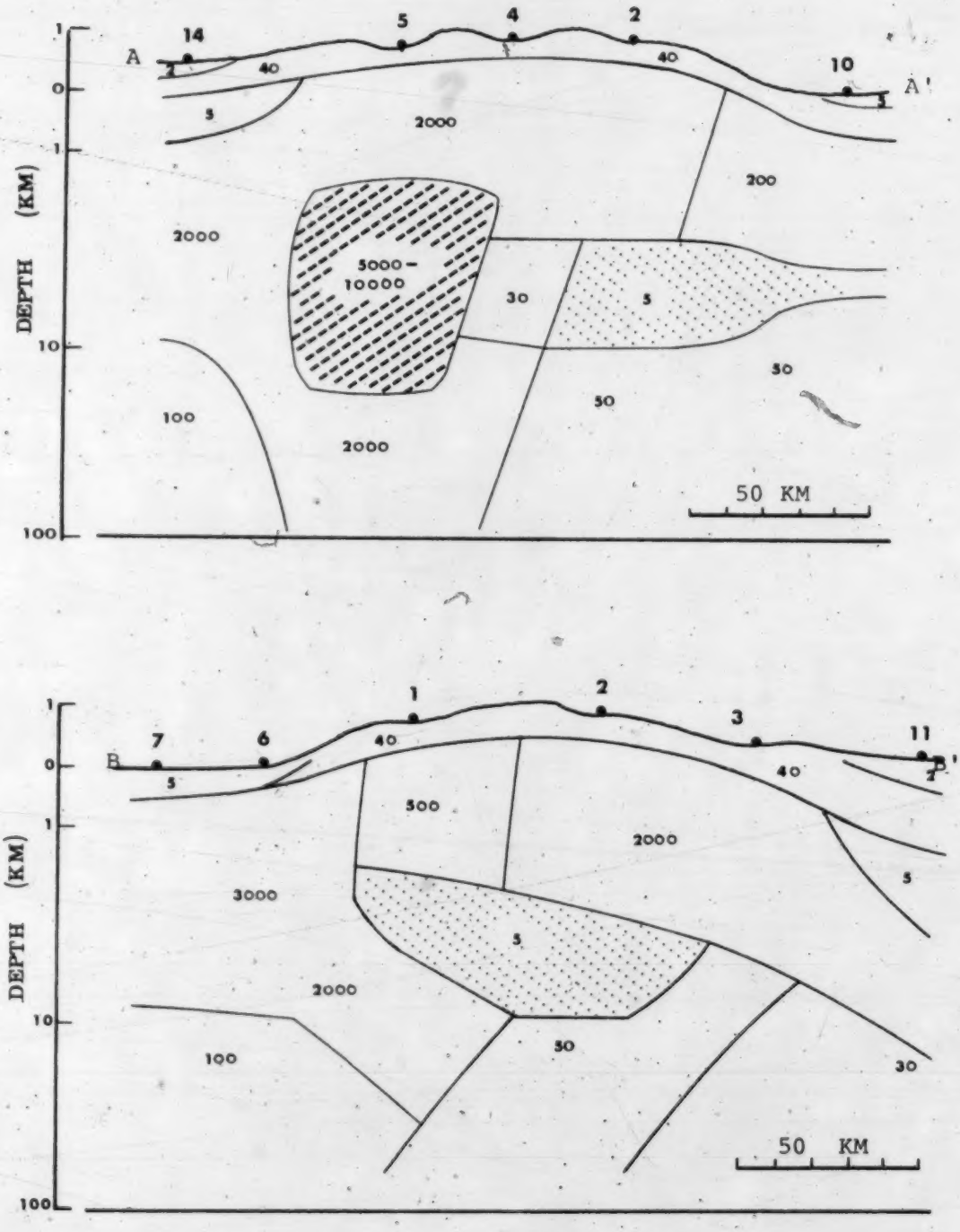

Fig. (5-10). Resistivity (Ω-M) distribution along A-A' (upper) and B-B' (lower) traverses.

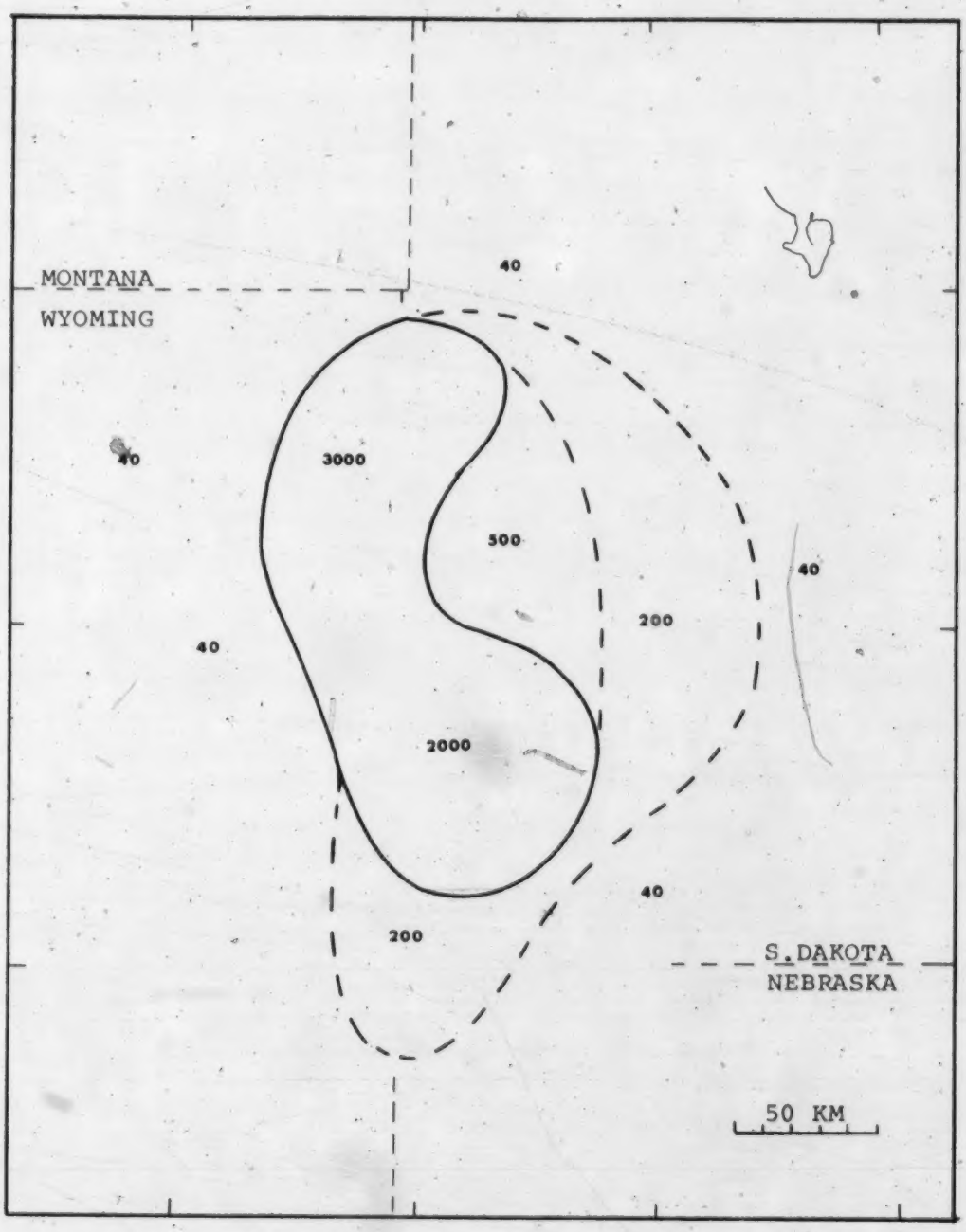

Fig.(5-11.1). Resistivity (Ω-M) distribution in a horizontal plane at a depth of 1-KM from the surface.

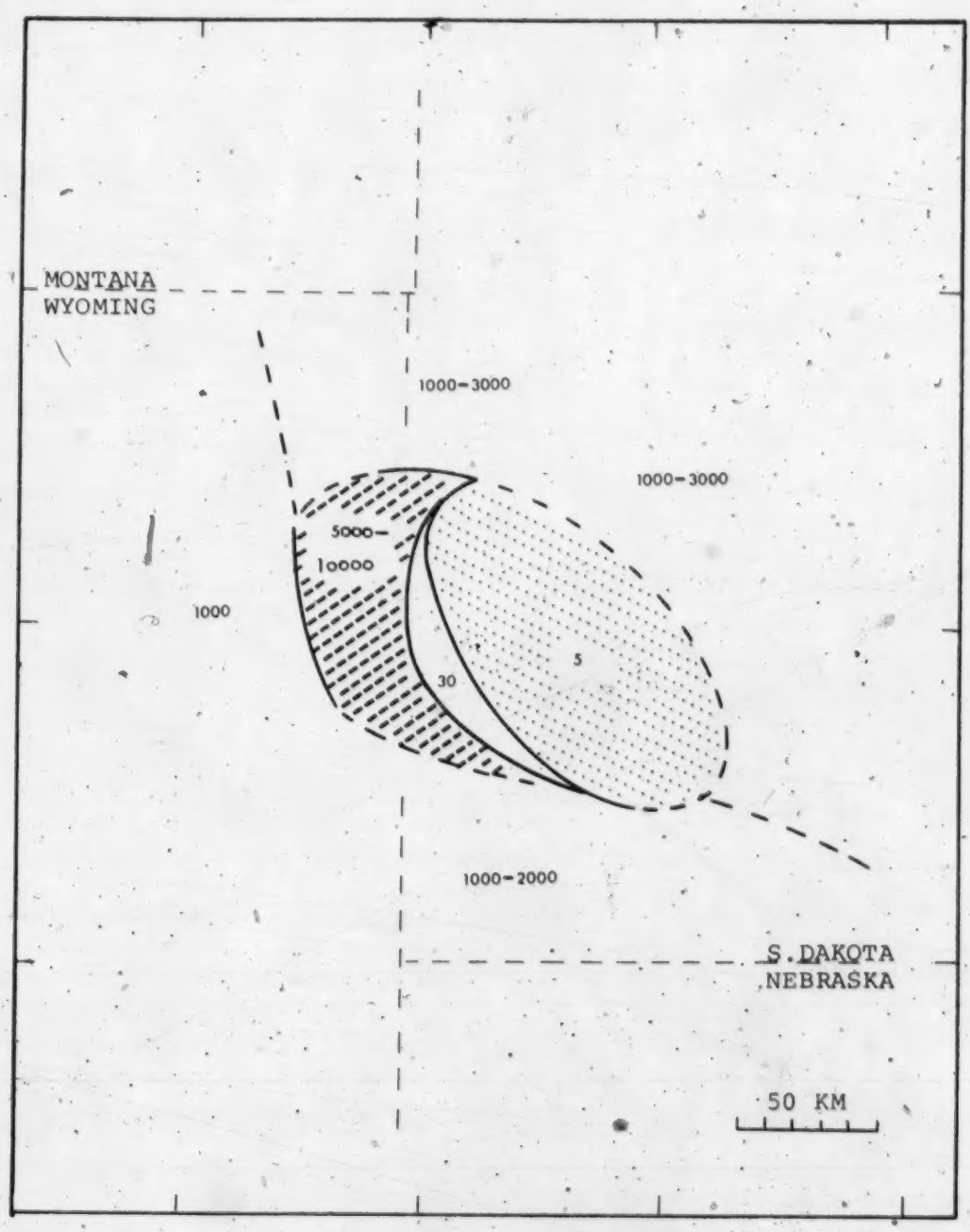

Fig.(5-11.2). Resistivity (Ω-M) distribution in a horizontal plane at a depth of 5-KM from the surface.

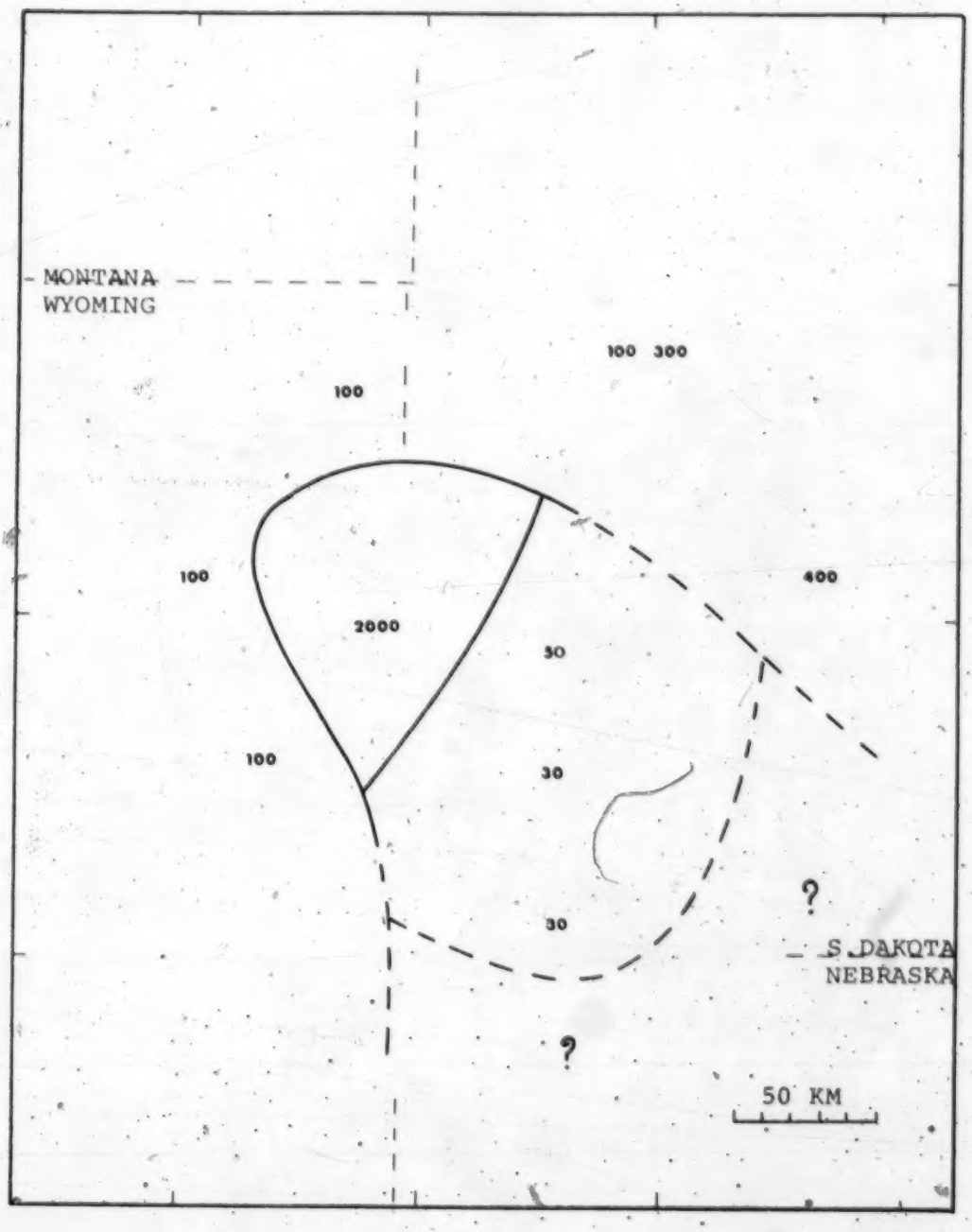

Fig.(5-11-3) Resistivity (Ω-M) distribution in a horizontal plane at a depth of 20-KM from the surface.

thinner layer of low resistivity, a second layer with high resistivity and the closed low resistivity anomaly previously reported by Rankin and Reddy (1973), which is now interpreted to lie at a relatively shallow depth. While the low resistivity of the surface material is expected and usually attributed to the moisture and salt content of the recent sediments, the anomaly in the middle of highly resistive crystalline rocks is more difficult to explain. Since highly conducting material shields the deeper structure, the values assigned to the region below the anomaly are somewhat tentative but it appears that the low resistivity persists downward throughout the entire column of the crust. It is tempting to interpret this low resistive anomaly in terms of a thermal anomaly although other suggestions have been put forward. One other such suggestion by Camfield, Gough and Porath (1971) attributes their elongated induction anomaly to the existence of graphite schists in the basement. The possibility that the anomaly is produced by a distribution of material with an abnormally high value of μ cannot be overlooked and it is proposed to compute models embodying this concept.

The extremely low values of apparent resistivity shown at stations 6, 7 and 8 are associated with peaks in the power density spectrum of the H field at

approximately 6.25 Hz. This is near the Schumann resonance peak reported at 8.6 Hz. This latter phenomenon is associated with waves propagating within the earth-ionosphere cavity due to lightning strokes. If the peak described here is of the same nature as the Schumann resonance, the plane wave theory is not applicable and the results in this region of the spectrum may need modification. Work on this aspect of the problem is to be carried out.

BIBLIOGRAPHY

Allsopp, D.F., M.D. Burke, D. Rankin and I.K. Reddy, 1974. A wide-band digital magnetotelluric recording system. Geophysics Prospecting, 22, 273-278.

Berdichevsky, M.N., 1960. Electrical prospecting with the telluric current method. Gestoptekhizdot, Moscow. (English translation by G.V. Keller, 1965. Quarterly of the Colorado School of Mines, v. 60, p.1.)

Bostick, F.X., Jr., and H.W. Smith, 1962. Investigation of large-scale inhomogeneities in the earth by the magnetotelluric method. Proc. IRE, 50, 2339-2346.

Cagniard, L., 1953. Basic theory of the magnetotelluric method of geophysical prospecting. Geophysics, 18, 605-635.

Camfield, P.A., D.I. Gough, and H. Porath, 1971. Magnetometer array studies in the northwestern United States and southwestern Canada. Geophys. J. Roy. Astron. Soc., 22, 201-221.

Caner, B. and D.R. Auld, 1968. Magnetotelluric determination of the upper mantle conductivity structure at Victoria, British Columbia. Can. J. Earth Sci., 5, 1209-1220.

Cantwell, T., 1960. Detection and analysis of low frequency magnetotelluric signals, Ph.D. thesis, Department of Geology and Geophysics, Massachusetts Institute of Technology.

Chetaev, D.N., 1960. The determination of the anisotropy coefficient and the angle of inclination of a homogeneous anisotropic medium, by measuring impedance of the natural electromagnetic field. Bull. Acad. Sci. USSR, Geophys. Ser. 4, 12, 407-408.

d'Erceville, I., and G. Kunetz, 1962. The effect of a fault on the earth's natural electromagnetic field. Geophysics, 27, 651-655.

Dosso, H.W., 1966. Analog model measurements for electromagnetic variations near faults and dykes. Can. J. Earth Sci., 3, 287-303.

Fowler, R.A., B.J. Kotick, and R.D. Elliott, 1967. Polarization analysis of natural and artificially induced geomagnetic micropulsations. J. Geophys. Res., 72, 2871-2883.

Gough, D.I., and P.A. Camfield, 1972. Convergent geophysical evidence of the metamorphic belt through the Black Hills of South Dakota. J. Geophys. Res., 77, 3168-3170.

Kato, Y., and T. Kikuchi, 1950. On the phase difference of the earth currents induced by changes of the earth's magnetic field. Parts I and II, Sci. Reports of Tohoku University, Ser. 5, Geophysics, 2, 139-145.

Lidiak, E.G., 1971. Buried precambrian rocks of South Dakota. Geol. Soc. Am. Bull. 82, 1411-1420.

Madden, T.R., and P. Nelson, 1964. A defence of Cagniard's magnetotelluric method. Project NR-371-401, Geophysics Laboratory, M.I.T.

Madden, T.R., and C.M. Swift, Jr., 1969. Magnetotelluric studies of the electrical conductivity structure of the crust and upper mantle. in The earth's crust and upper mantle, Geophysical monograph 13, Am. Geophys. Union, 469-479.

Mann, J.E., 1965. The importance of anisotropic conductivity in magnetotelluric interpretation. J. Geophys. Res., 70, 2940-2942.

Mathisrud, G.C., and J.S. Sumner, 1967. Underground induced polarization surveying at the Homestake Mine. Mining Congr. J., 53, 66-69.

Morrison, H.F., E. Wombell, and S.H. Ward, 1968. Analysis of earth impedances using magnetotelluric fields. J. Geophys. Res., 73, 2769-2778.

O'Brien, D.P., and H.F. Morrison, 1967. Electromagnetic fields in an n-layer anisotropic half-space. Geophysics, 32, 668-677.

Paulson, K.V., 1968. The polarization and spectral characteristics of some high-latitude irregular pulsations. Ann. Geophys., 24, 261-266.

Peeples, W.J., and D. Rankin, 1973. A magnetotelluric study in the western Canadian sedimentary basin. Pure and Applied Geophys. (PAGEOPH) 102, 134-147.

Praus, O., and V. Petr, 1969. Magnetotelluric calculations for the interaction of polarized fields with anisotropic layered media. Can. J. of Earth Sci., 6, 759-769.

Price, A.T., 1962. The theory of the magnetotelluric method when source field is considered. J. Geophys. Res., 67, 1907-1918.

Rankin, D., 1962. The magnetotelluric effect of a dyke. Geophysics, 27, 666-676.

Rankin, D., G.D. Garland and K. Vozoff, 1965. An analog model for the magnetotelluric effect. J. Geophys. Res., 70, 1939-1945.

Rankin, D., and R.D. Kurtz, 1970. A statistical study of micropulsations polarizations. J. Geophys. Res.

Rankin, D., and I.K. Reddy, 1969. A magnetotelluric study of resistivity anisotrophy. Geophysics, 34, 438-449.

Rankin, D., and I.K. Reddy, 1970. Polarization of the magnetotelluric fields over an anisotropic earth. PAGEOPH, 78, 58-65.

Reddy, I.K., and D. Rankin, 1972. On the interpretation of magnetotelluric data in the plains of Alberta. Can. J. Earth Sci., 9, 514-527.

Rikitake, T., 1950. Electromagnetic induction within the earth and its relation to the electrical state of the earth's interior. Bull. Earthq. Res. Inst., Tokyo, 28, 45-98.

Rikitake, T., 1951. Changes in earth currents and their relation to the electrical state of the earth's crust. Bull. Earthq. Res. Inst., Tokyo, 29, 270-275.

Sass, J.H., A.H. Lachenbruch, R.J. Munroe, G.W. Greene, and T.H. Moses, Jr., 1971. Heat flow in the western United States. J. Geophys. Res., 76, 6367-6413.

Sims, W.E., and F.X. Bostick, Jr., 1969. Methods of magnetotelluric analysis. Report No. 58, Electronics Research Center, The University of Texas at Austin.

Sims, W.E., F.X. Bostick, Jr., and H.W. Smith, 1971. The estimation of magnetotelluric impedance tensor elements from measured data. Geophysics, 36, 938-942.

Srivastava, S.P., J.L. Douglass, and W.H. Ward, 1963. The application of magnetotelluric and telluric methods in central Alberta. Geophysics, 28, 426-446.

Swift, C.M., Jr., 1967. A magnetotelluric investigation of an electrical conductivity anomaly in the Southwestern United States. Ph.D. thesis, M.I.T.

Takacs, E., 1969. The orientation of the magnetotelluric impedance ellipses. Acta Geodaet., Geophys. et Montanist. Acad. Sci. Hung., Tomus 4, 415-423.

Tikhonov, A.N., 1950. Determination of the electrical characteristics of deep layers of the earth's crust. Dok. Akad. Nauk., USSR, 73, 295-297.

Vozoff, K., and C.M. Swift, Jr., 1968. Magnetotelluric measurements in the north German Basin. Geophysics Pros. 16, 454-473.

Vozoff, K., A. Orange, and H.S. Lahman, 1969. Magnetotelluric deep earth resistivity at eight U.S. "Type-locations". Report No. RU68011, Geoscience Incorporated, Cambridge, Massachusetts.

Vozoff, K.A., 1972. The magnetotelluric method in the explanation of sedimentary basins. Geophysics, 37, 98-141.

Wait, J.R., 1954. On the relation between telluric currents and the earth's magnetic field. Geophysics, 19, 281-285.

White, R.E., 1973. The estimation of signal spectra and related quantities by means of the multiple coherence function. Geophys. Pros., 21, 660-703.

Whitham, K., and F. Anderson, 1966. Magnetotelluric experiments in Northern Ellesmere Island. Geophys. J. Roy. Ast. Soc., 10, 317-345.

Word, D.R., H.W. Smith, and F.X. Bostick, Jr., 1970. An investigation of the magnetotelluric impedance method. Techn. Report No. 82. Electrical Geophysics Research Lab., U. of Texas at Austin.

Zietz, I., B.C. Hearn, M.W. Higgins, G.D. Robinson, and D.A. Swanson, 1971. Interpretation of an aeromagnetic strip across the northwestern United States. Bull. Geol. Soc. Amer., 82, 3347-3372.

Rankin, D., and I.K. Reddy, 1973. Crustal conductivity anomaly under the Black Hills: A magnetotelluric study. Earth and Planetary Sci. Letts., 20, 275-279.

APPENDIX A

MODELLING CONSIDERATION

Numerical modelling results have been published for numerous one and two dimension cases which have already been referred to. In this appendix several examples are presented schematically and discussed.

I. One-Dimensional Model

The typical feature of the one-dimensional solutions for a layered earth is the simple frequency dependence which uniquely reveals information on conductivity and thickness of the layers through the apparent resistivity and phase relations. In Fig. (A-1a), a pair of two-layer models and their apparent resistivity curves are shown. For sufficiently high frequencies, the corresponding skin depth is sufficiently small, so that the lower layer is not sensed and the apparent resistivity is asymptotic to ρ_1. For sufficiently low frequencies, the corresponding skin depth is large and the upper layer has little effect, so that the apparent resistivity approaches ρ_2. The variation with frequency is smooth. A greater thickness of the upper layer, as in model-B compared to model-A, causes the apparent resistivity curve to be

displaced as shown. It is clear that the transition from ρ_1 to ρ_2 is a function of the thickness of the upper layer.

Fig. (A-1b) shows the result of a highly conductive and a highly resistive intervening layer. In both cases the apparent resistivity curves approach the same high and low frequency limits, while for intermediate frequencies the effect of the intervening layer is seen. The apparent resistivity never reaches the true values of ρ_2 or $\bar{\rho}_2$ as long as layer 2 is not very thick, but the effect of this layer will always be present as long as it is not extremely thin. The extension to a multi-layer model can be easily visualized.

II. Two-Dimensional Model

Fig. (A-2) shows a solution for a vertical fault. Some notable features are as follows:

a) The apparent resistivity is asymptotic to the appropriate resistivity value at large distances from the fault. It varies smoothly with position along a traverse crossing the fault in the case of $E_{||}$ (E-field parallel to the strike), but varies discontinuously for the $H_{||}$ case (E-field perpendicular to the strike), as shown in Fig. (A-2).

b) The vertical component of the magnetic field H_z exists only for $E_{||}$, with the maximum value appearing near the fault, decreasing to zero in both directions. The horizontal H-field perpendicular to the strike H_y also varies significantly near the fault for the $E_{||}$ case. Most of these effects can be understood by examining the current flow as shown in the figure. For $H_{||}$ and $E_{\perp}$ the current flows across the interface and since the current is continuous, no H_z is induced. Since $\sigma_1 \neq \sigma_2$ and $E_y = \sigma J_y$, E_y is discontinuous across the fault with the condition $E_1\rho_1 = E_2\rho_2$. The apparent resistivity $\rho_{\perp}$, which depends on E_y^2, changes abruptly across the fault and approaches the appropriate value at large distances on either side of the interface.

Fig. (A-3) shows a pseudo-section for a fault. The horizontal scale is the distance along a traverse as used in Fig. (A-2), and the vertical scale is frequency (corresponding to depth) with the highest frequency at the top. The related data values are plotted beneath each site location for each frequency, and the values are contoured.

Fig. (A-4) shows the effect of an overburden above the fault. The result of the overburden is to smooth and attenuate the anomalous effects as shown; the degree of smoothing increases with the thickness

and conductivity of the overburden.

Fig. (A-5) shows a conductive thin dike buried in the vertical position, and Fig. (A-6) shows a resistive dike. 'Thin' describes the condition where the dike is small compared to a wave length at a given frequency. The effect can also be understood by examining the current flow situation. For a conductive dike, the thin sheet-like conductive material immersed in a resistive basement does not affect the currents flowing perpendicular to the sheet; but it does play an essential role when the currents flow parallel to the strike. The resulting anomalous patterns for $\rho_{||}$ and H_z is shown in Fig. (A-5). For the resistive dike, the situation is the converse; currents which flow across the dike are affected. The $\rho_{\perp}$ patterns are shown in Fig. (A-6).

Fig. (A-7) shows a two-dimensional model of a sloping contrast and the anomalous effects at a typical frequency. Fig. (A-8) shows the anomalous effects for various frequencies at one location; the values are plotted as a function of frequency.

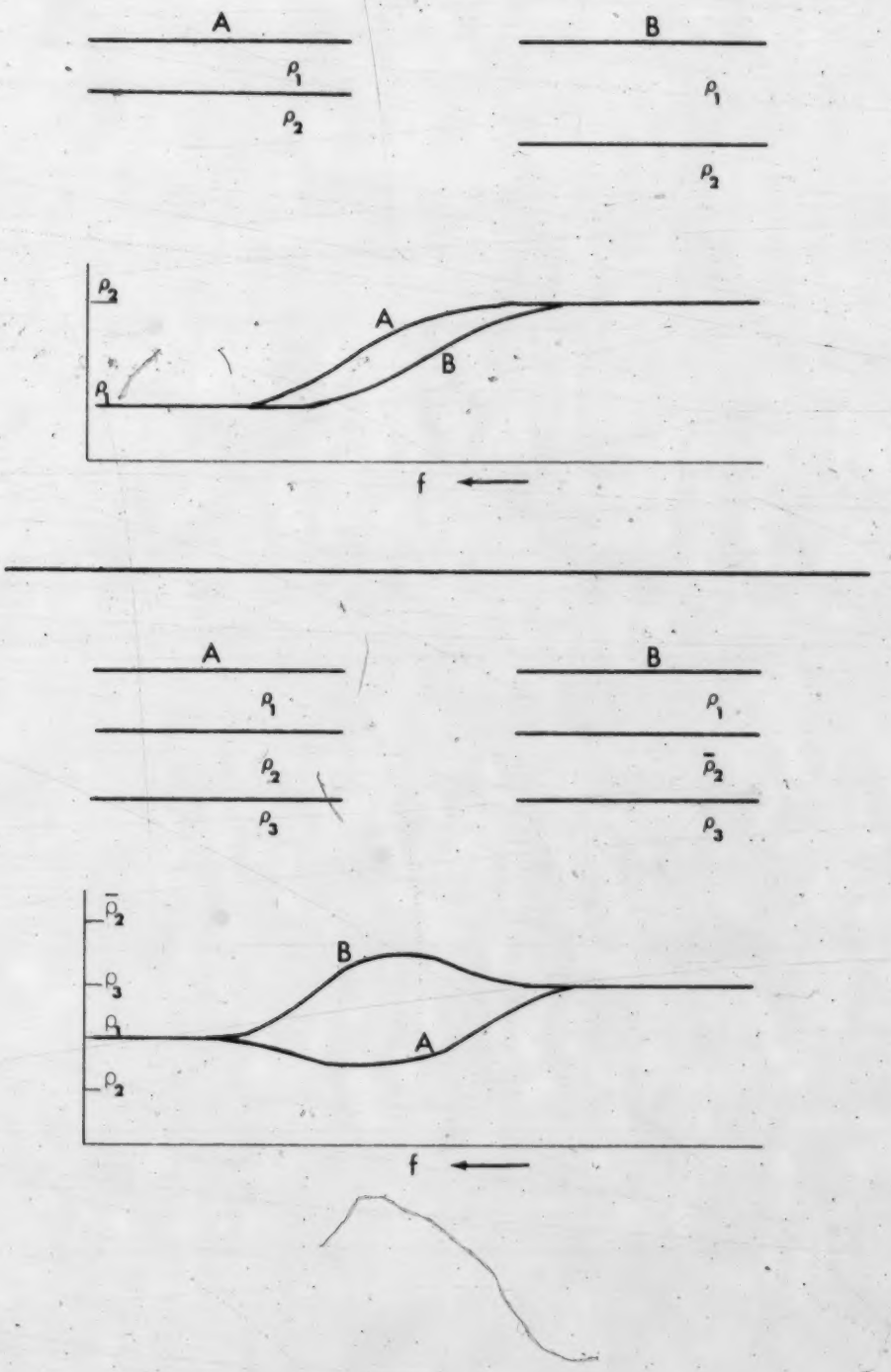

Fig.(A-1). a) Schematic response curves for two-layer models (upper). b) three-layer models (lower).

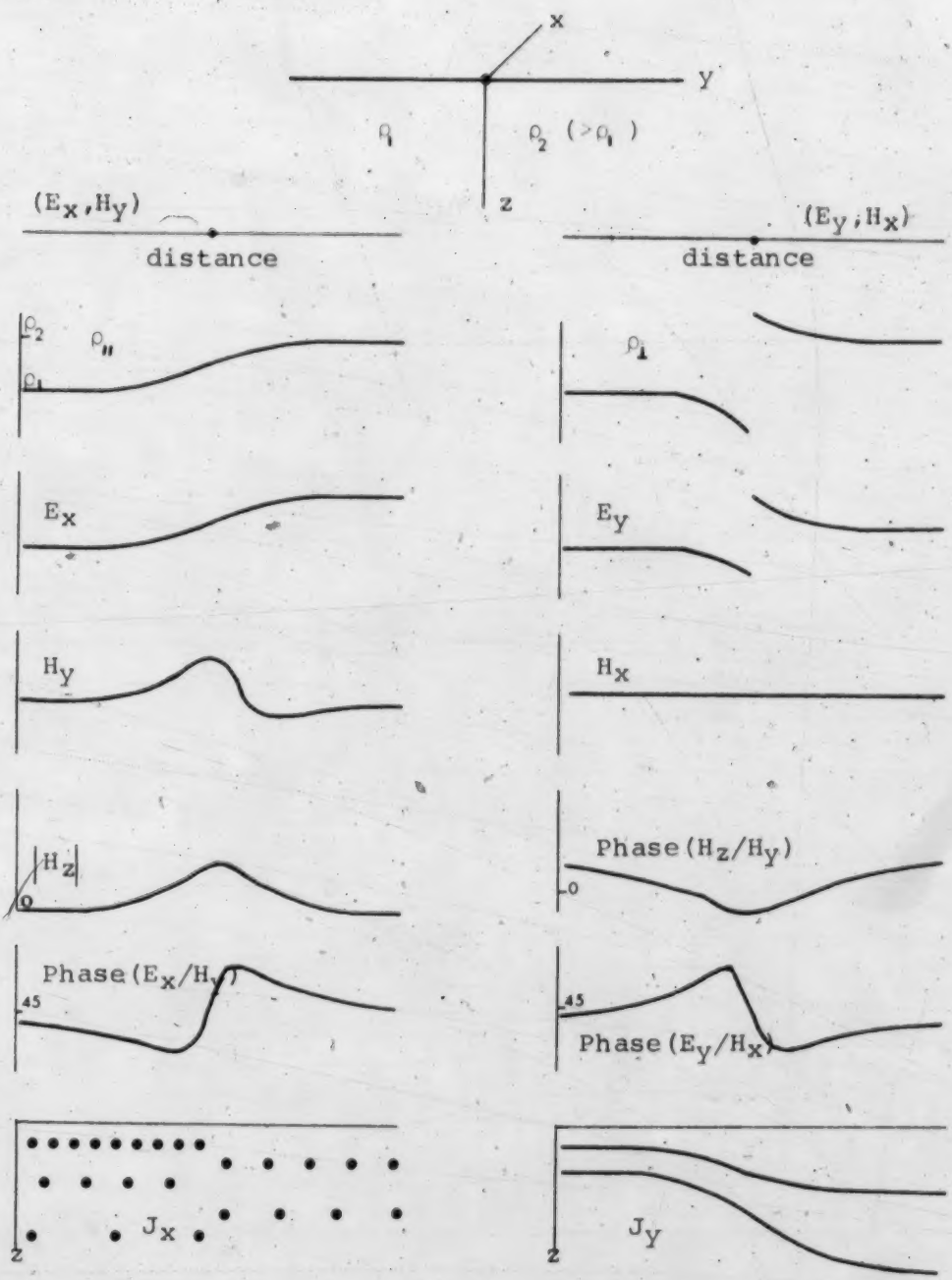

Fig.(A-2). Schematic pseudo-sections for a vertical fault.

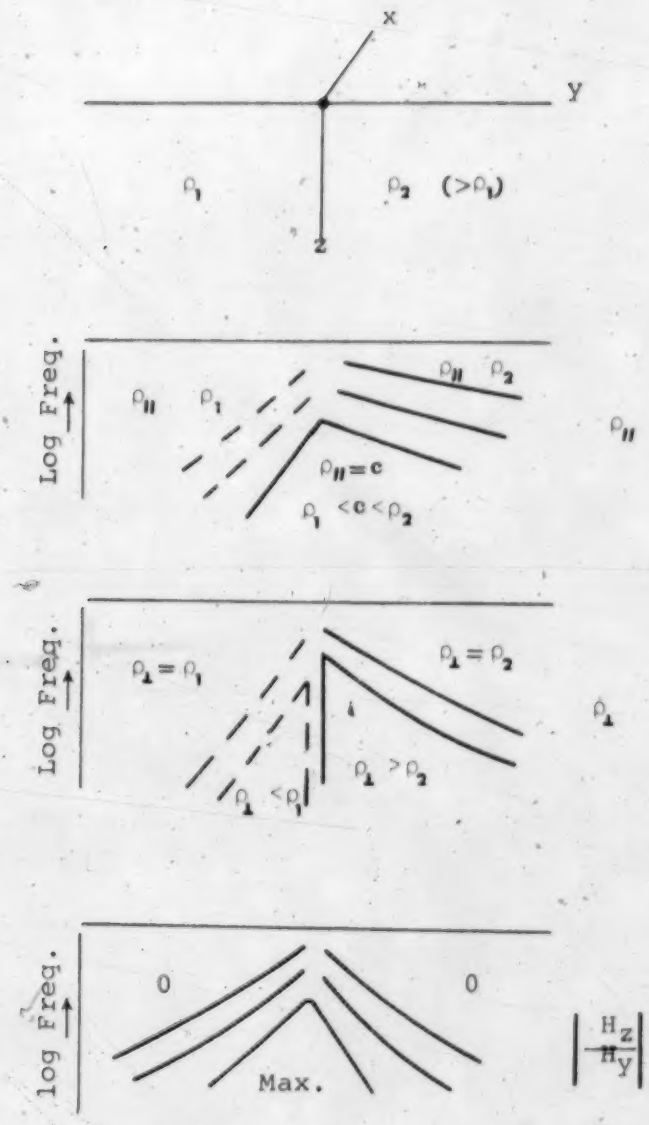

Fig.(A-3). Schematic pseudo-sections for a vertical fault.

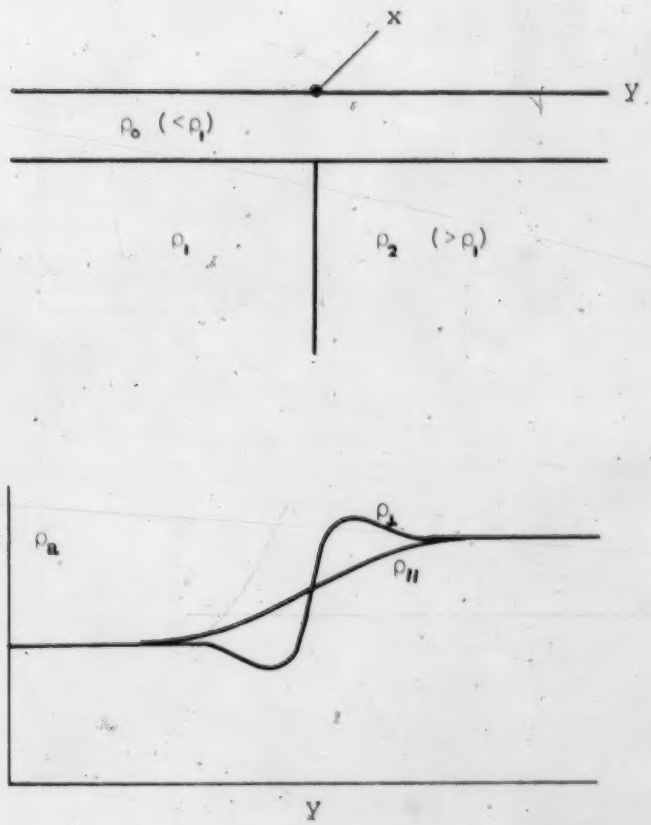

Fig(A-4) Effect of overburden on a vertical fault.

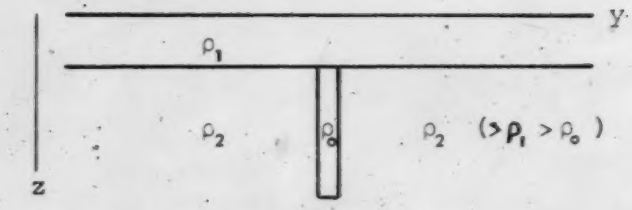

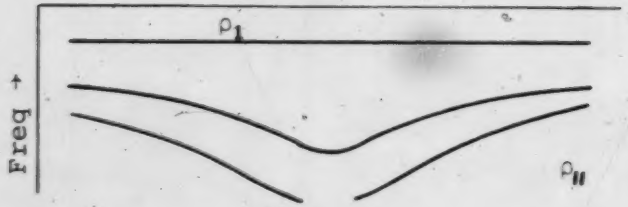

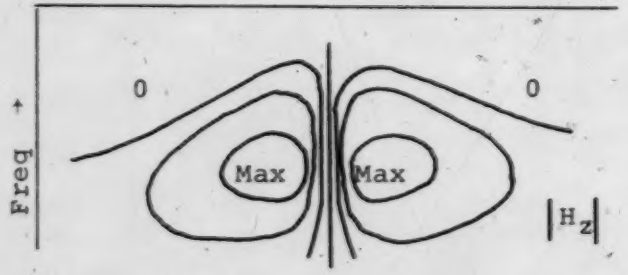

Fig.(A-5). Schematic pseudo-section for a conductive dike.

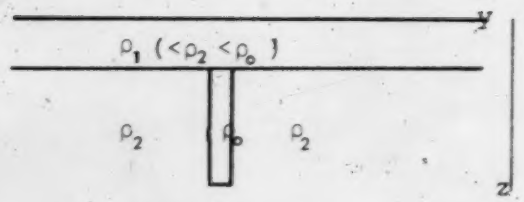

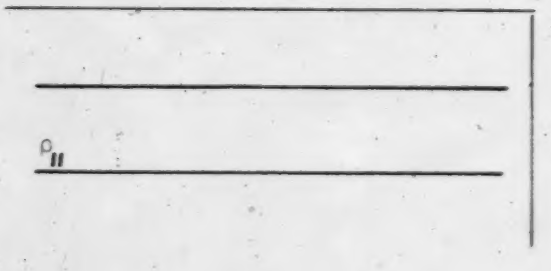

Fig.(A-6). Schematic pseudo-section for a buried resistive dike.

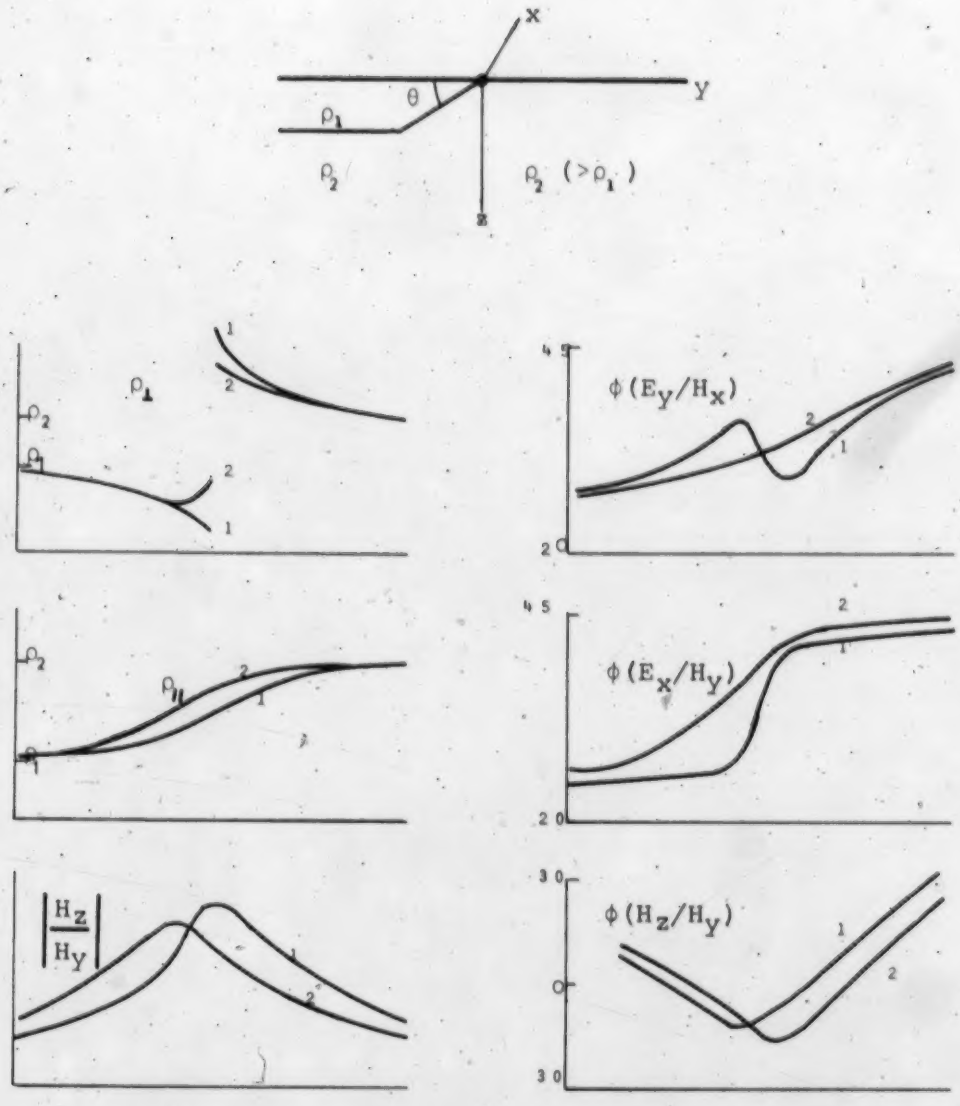

Fig.(A-7). Schematic pseudo-sections for a sloping contact. 1→θ=90°, 2→θ=45°.

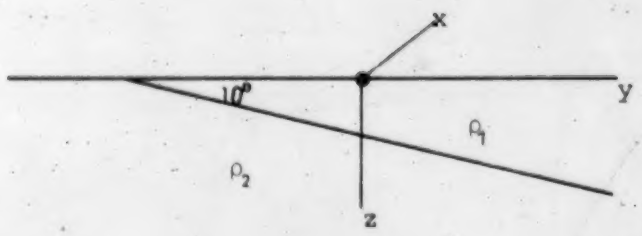

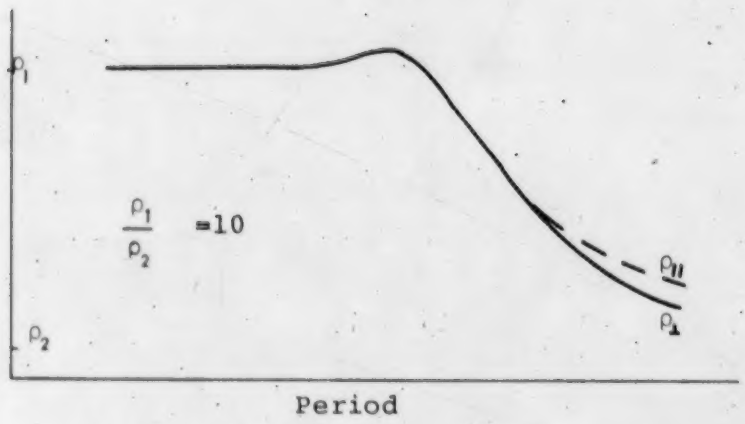

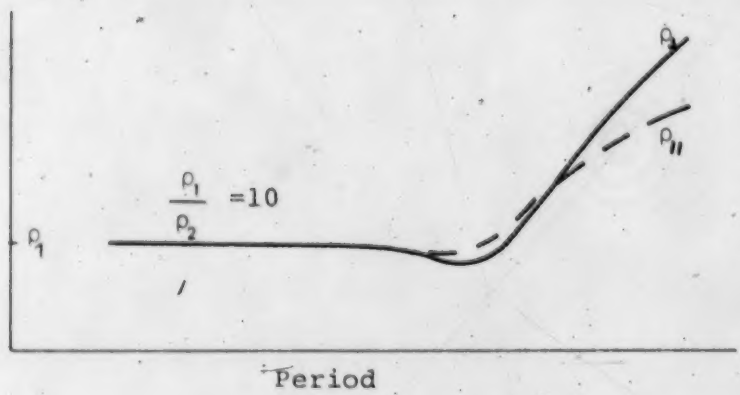

Fig.(A-8). Schematic response curves for a sloping contact.

APPENDIX B

TABULATED ANALYSIS RESULTS

PRD --- Period (sec).

R12 --- Maximum apparent resistivity (Ω-M) for $\theta=\theta_o$.

PH12 --- Phase angle of R12.

R21 --- Minimum apparent resistivity (Ω-M) for $\theta=\theta o$.

PH21 --- Phase angle of R21.

RE1 --- Maximum admittance for $\theta=\theta_{ze}$.

RH1 --- Maximum value of α for $\theta=\theta_{zh}$.

ANG --- θ_o, from the geographical North.

ANGE --- θ_{ze}.

ANGH --- θ_{zh}.

SKW --- $\bar{\alpha}$, skew facter.

BTA --- β_o (Eqn 2-54b).

RAN --- β_1 (Eqn 2-55a).

AIS --- β_2 (Eqn 2-55b).

PRD	R12	PH12	R21	PH21	PE1	PH1	ANG	ANG2	ANGH	SKW	BTA	RAN	AIS
1337.75	23.47	-102.	9.58	39.	12.67	1.53	105.	150.	110.	0.71	0.06	0.43	0.41
875.76	20.41	-126.	11.76	38.	13.02	2.11	100.	165.	135.	0.77	0.02	0.57	0.58
668.87	66.62	-140.	23.45	137.	13.78	1.92	60.	165.	135.	1.00	0.25	0.48	0.35
546.13	39.03	-128.	0.78	162.	10.73	2.16	60.	165.	140.	0.43	0.11	0.09	0.02
463.41	62.57	-124.	0.39	179.	9.84	1.62	70.	175.	145.	0.26	0.14	0.04	0.01
357.53	72.62	-125.	0.26	-121.	11.03	1.44	70.	170.	65.	0.27	0.18	0.05	0.00
291.92	68.82	-131.	0.44	-102.	19.85	1.87	65.	165.	35.	0.40	0.25	0.11	0.01
229.42	82.21	-144.	0.38	-111.	16.23	1.79	70.	165.	35.	0.44	0.32	0.14	0.00
189.19	91.36	-145.	0.37	-109.	8.87	1.22	70.	165.	45.	0.39	0.29	0.11	0.00
168.44	84.35	-143.	0.37	-111.	5.32	0.80	70.	165.	60.	0.39	0.26	0.11	0.00
133.80	78.28	-143.	0.60	-99.	3.57	0.67	65.	165.	75.	0.38	0.21	0.09	0.01
106.29	75.71	-145.	0.64	-103.	2.19	0.56	65.	160.	110.	0.38	0.17	0.08	0.01
84.43	71.43	-147.	0.69	-109.	0.83	0.51	65.	150.	125.	0.39	0.13	0.07	0.01
67.06	61.24	-153.	0.93	-111.	1.62	0.49	65.	160.	110.	0.47	0.15	0.11	0.02
53.27	53.87	-154.	0.91	-118.	1.52	0.41	65.	165.	90.	0.47	0.08	0.09	0.02
42.32	48.26	-156.	0.98	-119.	0.99	0.32	65.	165.	95.	0.49	0.09	0.10	0.02
33.61	40.04	-156.	1.01	-123.	0.74	0.42	65.	155.	90.	0.51	0.09	0.10	0.03
26.70	34.87	-154.	0.93	-126.	0.49	0.30	65.	155.	100.	0.55	0.12	0.12	0.03
21.21	28.51	-154.	1.03	-129.	0.32	0.32	65.	150.	105.	0.55	0.16	0.12	0.04
16.85	25.62	-154.	1.24	-126.	0.32	0.28	65.	150.	100.	0.59	0.18	0.13	0.05
13.38	21.55	-148.	1.34	-129.	0.50	0.36	65.	165.	45.	0.66	0.26	0.17	0.06
10.63	21.80	-139.	1.70	-117.	0.23	0.40	70.	15.	65.	0.66	0.32	0.19	0.08
8.44	24.77	-136.	2.32	-112.	0.11	0.47	70.	135.	50.	0.62	0.28	0.15	0.09
6.71	27.28	-133.	2.46	-108.	0.14	0.72	75.	165.	35.	0.62	0.28	0.16	0.09
5.33	28.20	-137.	4.32	-117.	0.18	0.83	75.	175.	30.	0.53	0.31	0.13	0.15
20.90	19.00	-142.	0.60	-132.	2.23	0.84	65.	175.	10.	0.48	0.17	0.08	0.03
17.07	14.49	-135.	0.52	-130.	2.33	1.00	65.	175.	5.	0.46	0.19	0.09	0.04
14.48	14.15	-131.	0.45	-125.	2.32	1.23	65.	170.	170.	0.40	0.20	0.08	0.03
11.17	31.40	-128.	0.74	-126.	2.49	2.03	70.	170.	5.	0.34	0.42	0.15	0.02
9.12	28.24	-83.	0.76	-113.	2.19	2.96	80.	165.	10.	0.26	0.54	0.21	0.03
7.17	14.78	-138.	0.82	-131.	1.73	5.23	85.	155.	5.	0.50	0.24	0.11	0.06
5.91	59.52	-118.	2.01	-144.	0.57	2.56	75.	60.	160.	0.56	0.37	0.19	0.03
5.26	17.00	-121.	0.55	-131.	1.03	1.70	70.	175.	95.	0.40	0.16	0.07	0.03
4.18	7.65	-107.	0.23	-107.	0.71	1.71	80.	45.	170.	0.62	0.17	0.15	0.03
3.32	19.94	-118.	0.43	-109.	0.61	1.61	80.	150.	5.	0.48	0.17	0.10	0.02
2.64	27.94	-107.	0.33	-118.	1.52	1.00	80.	150.	30.	0.58	0.16	0.15	0.01
2.10	36.19	-118.	0.48	-113.	0.93	3.83	80.	165.	165.	0.52	0.16	0.12	0.01
1.66	35.95	-126.	0.76	-106.	0.37	1.21	85.	155.	0.	0.51	0.21	0.12	0.02
1.32	49.28	-121.	1.16	-102.	0.16	1.25	80.	145.	155.	0.58	0.19	0.15	0.02
1.05	45.55	-118.	1.06	-122.	0.26	0.86	80.	165.	120.	0.53	0.13	0.11	0.02
0.83	63.79	-119.	3.18	-120.	0.28	0.67	85.	170.	90.	0.54	0.07	0.09	0.05
0.66	75.75	-131.	2.62	-133.	0.16	1.00	85.	160.	0.	0.57	0.08	0.11	0.03
0.53	68.36	-135.	2.66	-106.	0.03	0.56	85.	155.	35.	0.56	0.06	0.10	0.04
0.42	72.06	-142.	1.89	-132.	0.03	0.62	85.	140.	150.	0.57	0.06	0.11	0.03
0.33	82.41	-151.	1.72	-137.	0.08	0.47	85.	165.	25.	0.52	0.10	0.11	0.02
0.26	79.57	-161.	1.71	-151.	0.04	0.49	85.	150.	135.	0.50	0.06	0.09	0.02
0.21	64.55	-174.	1.60	-153.	0.07	0.71	85.	160.	30.	0.50	0.08	0.09	0.02
0.17	52.85	178.	2.09	-160.	0.02	0.46	85.	125.	5.	0.49	0.08	0.08	0.04
0.13	38.18	167.	1.83	-167.	0.05	0.27	85.	165.	35.	0.50	0.10	0.09	0.05
0.11	24.62	156.	1.47	-180.	0.03	0.25	85.	165.	50.	0.58	0.05	0.10	0.06
0.08	14.94	152.	1.07	-180.	0.03	0.27	85.	160.	110.	0.55	0.08	0.09	0.07
0.07	7.71	141.	0.66	160.	0.02	0.10	85.	175.	155.	0.70	0.05	0.12	0.09

/ MARANT--52 FILE-

PRD	R12	PH12	R21	PH21	REF	PH1	ANG	ANGE	ANGH	SKW	BTA	RAN	AIS
1337.75	13.61	43.	0.46	62.	9.07	0.60	20.	90.	25.	0.75	0.11	0.19	0.03
875.76	11.74	35.	0.59	65.	9.75	0.41	25.	90.	20.	0.83	0.06	0.22	0.05
668.87	10.27	34.	0.71	58.	6.23	0.25	25.	90.	165.	0.96	0.04	0.25	0.07
546.13	9.13	36.	0.76	57.	3.61	0.23	25.	85.	135.	1.08	0.07	0.30	0.08
463.41	8.60	37.	0.82	54.	3.04	0.24	25.	85.	130.	1.15	0.08	0.31	0.10
357.53	7.79	39.	0.86	56.	1.75	0.24	30.	80.	135.	1.29	0.07	0.36	0.11
291.92	7.73	42.	0.87	59.	1.13	0.24	30.	65.	130.	1.32	0.06	0.37	0.11
229.42	7.42	45.	1.01	62.	1.00	0.19	30.	110.	145.	1.49	0.03	0.42	0.14
189.19	7.56	48.	1.18	62.	0.76	0.20	30.	115.	150.	1.61	0.02	0.44	0.16
168.44	7.75	49.	1.28	62.	0.28	0.18	30.	0.	145.	1.67	0.04	0.45	0.16
133.80	7.57	51.	1.35	63.	0.63	0.20	30.	50.	130.	1.77	0.07	0.47	0.18
106.29	7.91	56.	1.41	62.	0.68	0.18	30.	100.	170.	1.74	0.12	0.45	0.18
84.43	8.76	58.	1.61	62.	0.24	0.13	30.	50.	135.	1.76	0.15	0.45	0.18
67.06	9.83	59.	1.76	62.	0.43	0.16	30.	100.	175.	1.75	0.17	0.44	0.19
53.27	10.06	63.	1.98	65.	0.43	0.25	25.	75.	150.	1.74	0.16	0.42	0.20
42.32	11.48	64.	2.21	66.	0.93	0.20	25.	85.	65.	1.65	0.16	0.38	0.19
33.61	13.24	66.	2.37	66.	0.84	0.37	25.	100.	0.	1.53	0.18	0.36	0.18
26.70	15.17	67.	2.80	66.	1.07	0.38	25.	85.	60.	1.51	0.19	0.35	0.18
21.21	15.83	67.	2.99	68.	0.43	0.27	25.	75.	100.	1.46	0.20	0.32	0.19
16.85	17.79	71.	3.82	71.	0.13	0.35	20.	110.	155.	1.52	0.19	0.30	0.21
13.38	17.15	71.	5.30	73.	0.43	0.64	20.	100.	160.	1.98	0.16	0.32	0.31
10.63	21.30	-103.	17.95	-117.	0.48	1.28	105.	20.	145.	5.27	0.09	0.48	0.88
8.44	102.00	-117.	26.03	-116.	0.41	0.95	110.	55.	155.	2.21	0.05	0.48	0.26
6.71	303.06	-95.	82.58	-131.	0.13	0.58	110.	165.	155.	1.46	0.23	0.43	0.24
5.33	940.45	-134.	123.41	-110.	0.19	0.22	105.	70.	65.	1.42	0.28	0.45	0.13
20.90	12.54	66.	1.53	68.	0.23	0.38	20.	45.	115.	0.98	0.24	0.23	0.12
17.07	9.90	71.	1.61	69.	0.37	0.46	20.	45.	110.	1.05	0.26	0.22	0.16
14.48	8.84	72.	1.86	68.	0.53	0.89	20.	5.	130.	1.33	0.22	0.26	0.21
11.17	9.11	79.	2.05	85.	0.93	1.42	15.	140.	140.	1.37	0.29	0.29	0.22
9.12	10.77	67.	5.46	105.	0.80	0.94	15.	165.	115.	1.26	0.41	0.34	0.51
7.17	196.61	-89.	10.63	-103.	0.92	2.68	95.	120.	10.	0.51	0.01	0.08	0.05
5.91	111.49	-86.	26.74	-121.	1.00	3.10	100.	145.	5.	1.05	0.10	0.20	0.24
5.26	30.48	-74.	28.04	-106.	1.25	2.58	105.	175.	100.	1.72	0.06	0.23	0.92
4.18	57.50	-75.	15.29	-177.	0.58	2.47	95.	40.	150.	0.64	0.27	0.27	0.27
3.32	1395.09	-69.	60.34	162.	0.48	0.53	80.	5.	110.	0.62	0.12	0.24	0.04
2.64	41.20	-117.	16.87	-44.	0.53	2.16	85.	100.	175.	0.41	0.35	0.14	0.41
2.10	65.50	-118.	30.99	-147.	0.14	0.66	100.	0.	165.	1.84	0.07	0.31	0.47
1.66	85.69	-104.	29.32	-166.	0.08	0.21	100.	80.	155.	1.12	0.33	0.45	0.34
1.32	60.31	-81.	28.11	-106.	0.02	0.45	95.	125.	170.	2.27	0.04	0.39	0.47
1.05	28.03	-132.	17.82	-103.	0.02	0.42	100.	110.	170.	1.18	0.06	0.11	0.64
0.83	29.29	-121.	26.25	-116.	0.03	0.34	100.	0.	120.	4.69	0.07	0.06	0.90
0.66	44.98	55.	31.00	61.	0.01	0.12	10.	155.	145.	1.92	0.16	0.07	0.69
0.53	69.78	52.	44.38	59.	0.01	0.37	10.	45.	100.	1.09	0.11	0.03	0.64
0.42	75.09	51.	55.66	51.	0.02	0.66	10.	130.	10.	1.69	0.09	0.02	0.74
0.33	77.91	42.	52.95	43.	0.10	2.84	10.	165.	125.	1.56	0.08	0.03	0.68
0.26	56.42	35.	52.91	33.	0.04	1.13	5.	145.	155.	6.67	0.17	0.05	0.94
0.21	37.57	26.	31.10	26.	0.00	0.09	5.	50.	125.	9.19	0.13	0.20	0.83
0.17	49.23	27.	32.09	3.	0.00	0.08	5.	55.	70.	0.35	0.09	0.01	0.65
0.13	51.43	20.	27.40	-6.	0.00	0.07	5.	150.	115.	0.09	0.13	0.02	0.53
0.11	31.67	15.	22.09	-16.	0.00	0.08	5.	65.	145.	0.04	0.10	0.01	0.70
0.08	23.39	16.	16.70	-24.	0.00	0.13	5.	145.	130.	0.12	0.10	0.01	0.71
0.07	8.91	22.	4.86	-62.	0.00	0.18	10.	135.	90.	0.55	0.38	0.21	0.55

2 CUSTER--18 FILE-
01:11.56 20.32 RC=0

PRD	R12	PH12	R21	PH21	RE1	PH1	ANG	ANGE	ANGH	SKW	BTA	RAN	AIS
1337.75	83.25	85.	0.11	44.	2.17	0.17	170.	80.	120.	0.44	0.46	0.21	0.00
875.76	119.53	93.	0.72	-152.	1.52	0.17	5.	85.	100.	0.57	0.65	0.37	0.01
668.87	229.84	90.	10.46	54.	0.73	0.19	165.	55.	115.	1.23	0.09	0.51	0.05
546.13	196.32	73.	3.14	44.	1.00	0.15	175.	85.	130.	0.90	0.12	0.31	0.02
463.41	113.71	82.	1.15	126.	1.11	0.13	0.	90.	125.	0.75	0.05	0.24	0.01
357.53	1289.91	161.	286.22	-150.	1.31	0.15	75.	95.	120.	1.37	0.41	0.60	0.22
291.92	345.80	59.	9.47	116.	1.15	0.22	0.	100.	100.	0.81	0.07	0.27	0.03
229.42	77.64	57.	0.63	-111.	0.58	0.19	30.	95.	105.	1.02	1.13	1.14	0.01
189.19	116.66	66.	15.48	58.	0.24	0.10	165.	110.	70.	1.24	0.10	0.29	0.13
168.44	135.05	77.	12.65	63.	0.16	0.09	170.	110.	25.	0.89	0.15	0.20	0.09
133.80	92.42	48.	22.81	21.	0.02	0.13	165.	100.	170.	1.76	0.09	0.45	0.25
106.29	1809.22	58.	660.86	78.	0.09	0.13	165.	85.	35.	2.71	0.37	0.75	0.37
84.43	723.04	69.	98.23	74.	0.03	0.07	165.	35.	15.	1.29	0.44	0.46	0.14
67.06	239.05	68.	43.11	51.	0.05	0.12	175.	95.	95.	1.14	0.36	0.31	0.18
53.27	329.57	76.	27.44	63.	0.03	0.11	175.	80.	45.	0.63	0.37	0.20	0.08
42.32	416.60	62.	28.92	57.	0.06	0.09	175.	95.	75.	0.62	0.35	0.19	0.07
33.61	277.47	45.	45.83	51.	0.05	0.09	170.	75.	60.	1.13	0.37	0.31	0.17
26.70	345.63	58.	47.19	64.	0.03	0.11	175.	90.	80.	0.64	0.30	0.15	0.14
21.21	227.21	60.	19.16	47.	0.03	0.11	175.	95.	90.	0.34	0.05	0.03	0.08
16.85	176.51	47.	39.75	47.	0.04	0.15	0.	80.	115.	1.12	0.10	0.15	0.23
13.38	200.23	37.	34.92	47.	0.02	0.08	0.	20.	135.	1.09	0.13	0.19	0.17
10.63	138.33	54.	31.91	54.	0.01	0.13	5.	45.	130.	1.46	0.10	0.24	0.23
8.44	245.93	59.	27.37	50.	0.02	0.19	0.	100.	100.	0.56	0.06	0.07	0.11
6.71	301.61	62.	40.56	48.	0.01	0.13	0.	130.	110.	0.71	0.12	0.12	0.10
5.33	327.62	60.	35.57	59.	0.01	0.15	175.	15.	95.	0.50	0.11	[illegible]	0.11
41.80	994.73	-97.	77.54	-121.	0.28	0.74	5.	140.	65.	0.71	0.59	[illegible]	0.08
27.37	420.21	-117.	77.41	-128.	0.18	1.07	170.	100.	30.	0.78	0.29	[illegible]	0.18
20.90	349.13	-111.	62.73	-126.	0.17	0.80	175.	95.	135.	0.71	0.36	0.19	0.18
17.07	413.44	-115.	57.56	-124.	0.18	1.27	175.	105.	115.	0.37	0.23	0.07	0.14
14.48	408.12	-117.	55.63	-121.	0.21	1.05	175.	80.	15.	0.20	0.16	0.03	0.13
11.17	346.91	-109.	47.60	-122.	0.24	1.36	0.	90.	160.	0.11	0.16	0.02	0.14
9.12	258.92	-110.	50.46	-123.	0.22	1.22	0.	90.	170.	0.19	0.22	0.05	0.19
7.17	240.27	-119.	47.40	-109.	0.13	0.87	175.	100.	155.	0.52	0.25	0.09	0.20
5.91	180.97	-122.	47.37	-115.	0.19	0.92	175.	105.	150.	1.04	0.20	0.14	0.26
5.26	267.45	-119.	65.24	-128.	0.14	1.04	175.	105.	145.	0.46	0.06	0.03	0.24
4.18	411.19	-80.	58.74	-121.	0.07	0.57	175.	100.	165.	0.41	0.20	0.07	0.14
3.32	602.97	-123.	53.77	-121.	0.04	0.40	175.	105.	140.	0.59	0.08	0.08	0.09
2.64	437.61	-115.	62.69	-145.	0.03	0.27	175.	105.	140.	0.69	0.24	0.15	0.14
2.10	365.06	-133.	81.92	-126.	0.04	0.20	170.	115.	140.	1.12	0.09	0.14	0.24
1.66	452.23	-118.	114.50	-120.	0.01	0.19	170.	115.	130.	1.16	0.04	0.13	0.25
1.32	682.45	-136.	158.92	-118.	0.00	0.13	170.	80.	100.	1.16	0.08	0.17	0.23
1.05	592.53	-148.	168.53	-130.	0.00	0.14	175.	110.	95.	0.67	0.01	0.05	0.29
0.83	541.99	-153.	207.44	-139.	0.00	0.09	170.	80.	55.	1.21	0.03	0.10	0.38
0.66	693.38	-157.	267.59	-145.	0.00	0.18	170.	165.	55.	1.14	0.08	0.09	0.39
0.53	590.16	-161.	211.75	-157.	0.00	0.15	170.	25.	60.	1.14	0.18	0.11	0.36
0.42	519.29	-177.	206.01	-159.	0.00	0.16	175.	10.	55.	0.94	0.09	0.07	0.40
0.33	473.61	173.	184.62	-168.	0.00	0.21	175.	5.	75.	0.85	0.08	0.06	0.39
0.26	196.17	157.	100.41	-176.	0.00	0.12	170.	15.	20.	1.22	0.10	0.09	0.82
0.21	132.72	153.	115.44	177.	0.00	0.15	175.	10.	55.	1.10	0.10	0.07	0.87
0.17	76.51	152.	88.05	170.	0.00	0.14	175.	15.	60.	0.83	0.07	0.02	0.89
0.13	33.12	154.	31.47	166.	0.00	0.13	175.	20.	60.	1.28	0.10	0.03	0.95
0.11	15.67	163.	14.47	172.	0.01	0.17	175.	20.	65.	0.94	0.09	0.02	0.78
0.08	6.51	-168.	4.81	-157.	0.01	0.15	175.	15.	65.	0.90	0.06	0.02	0.71
0.07	5.69	-142.	1.28	-119.	0.06	2.87	5.	130.	160.	0.58	0.15	0.07	0.22

PRD	R12	PH12	R21	PH21	RE1	PH1	ANG	ANGE	ANGH	SNW	HTA	RAN	AIS
1337.75	54.20	-131.	18.72	-141.	6.38	0.73	100.	165.	105.	2.59	0.08	0.48	0.35
875.76	38.27	-132.	18.16	-149.	5.59	0.69	105.	160.	95.	3.06	0.03	0.50	0.47
668.87	38.89	-140.	17.43	-152.	5.62	0.69	105.	160.	100.	3.27	0.04	0.50	0.45
546.13	50.58	-124.	15.01	-158.	4.51	0.66	100.	160.	100.	1.55	0.16	0.39	0.30
463.41	37.48	-121.	15.84	-158.	3.10	0.62	100.	165.	95.	1.76	0.25	0.47	0.42
357.53	51.82	-121.	18.58	-154.	2.69	0.67	100.	165.	90.	1.76	0.25	0.46	0.36
291.92	36.56	-105.	19.07	-144.	1.79	0.56	105.	175.	90.	1.62	0.30	0.43	0.52
229.42	40.21	-110.	9.27	-137.	1.67	0.39	105.	170.	55.	1.52	0.06	0.35	0.23
189.19	86.84	-125.	8.63	-164.	1.18	0.53	95.	170.	40.	0.83	0.14	0.21	0.10
168.48	65.97	-133.	7.61	-159.	0.96	0.52	95.	170.	45.	1.32	0.05	0.40	0.12
133.80	67.41	-132.	9.54	-139.	0.81	0.41	100.	0.	100.	1.00	0.07	0.18	0.14
106.29	108.21	-140.	8.22	-142.	0.85	0.34	95.	170.	90.	0.82	0.05	0.16	0.08
84.43	115.94	-132.	6.65	-142.	0.63	0.25	95.	170.	145.	0.64	0.08	0.12	0.06
67.06	135.14	-133.	9.69	-136.	0.49	0.29	95.	170.	130.	0.66	0.13	0.12	0.07
53.27	139.45	-128.	10.64	-133.	0.46	0.39	95.	170.	145.	0.54	0.14	0.09	0.08
42.32	137.96	-128.	11.19	-128.	0.38	0.43	95.	170.	155.	0.55	0.12	0.08	0.08
33.61	145.55	-133.	10.62	-130.	0.27	0.36	95.	170.	165.	0.48	0.07	0.06	0.07
26.70	118.81	-142.	9.33	-128.	0.24	0.25	95.	170.	175.	0.63	0.07	0.10	0.08
21.21	100.48	-145.	12.29	-127.	0.09	0.25	95.	5.	15.	0.60	0.06	0.08	0.12
16.85	102.21	-139.	21.30	-132.	0.06	0.19	100.	15.	40.	0.39	0.10	0.03	0.21
13.38	117.92	-132.	41.19	-138.	0.07	0.16	100.	10.	65.	0.21	0.25	0.06	0.35
10.63	129.44	-125.	54.34	-153.	0.06	0.09	100.	5.	115.	0.44	0.38	0.15	0.42
8.44	77.78	-129.	56.33	-156.	0.07	0.44	105.	160.	160.	0.28	0.35	0.12	0.72
6.71	583.12	-67.	66.69	-75.	0.09	0.72	85.	155.	150.	1.32	0.07	0.35	0.14
5.33	94.94	-86.	39.32	-88.	0.06	0.42	90.	155.	145.	3.50	0.57	0.87	0.41
41.80	198.05	-132.	19.33	-132.	0.28	0.39	95.	170.	130.	0.53	0.09	0.07	0.10
27.37	139.61	-130.	13.36	-130.	0.28	0.43	95.	170.	165.	0.54	0.09	0.07	0.10
20.90	115.83	-129.	10.45	-127.	0.25	0.44	95.	165.	170.	0.50	0.08	0.06	0.09
17.07	99.58	-130.	9.99	-124.	0.20	0.39	95.	160.	165.	0.48	0.06	0.05	0.10
14.48	87.04	-132.	9.41	-127.	0.22	0.41	95.	160.	155.	0.51	0.08	0.06	0.11
11.17	70.27	-132.	11.26	-124.	0.19	0.63	95.	145.	165.	0.65	0.12	0.08	0.16
9.12	57.35	-136.	17.74	-127.	0.06	0.39	90.	80.	20.	0.58	0.09	0.03	0.31
7.17	75.18	-126.	48.97	-104.	0.18	1.74	90.	55.	170.	0.17	0.04	0.00	0.65
5.91	103.54	75.	97.28	85.	0.14	2.29	0.	175.	110.	0.57	0.13	0.04	0.94
5.26	106.47	-146.	76.24	-97.	0.15	2.81	90.	165.	130.	0.33	0.15	0.04	0.72
4.18	222.22	-137.	97.85	-99.	0.12	2.05	90.	155.	135.	0.40	0.25	0.08	0.44
3.32	135.90	-131.	96.30	-102.	0.28	0.78	95.	170.	100.	1.01	0.06	0.07	0.71
2.64	166.63	-126.	69.01	-97.	0.15	0.26	90.	155.	110.	0.54	0.07	0.03	0.41
2.10	138.16	-127.	64.58	-98.	0.08	1.34	90.	15.	105.	0.37	0.03	0.01	0.47
1.66	137.85	-121.	50.24	-102.	0.05	0.48	90.	155.	10.	0.41	0.06	0.02	0.36
1.32	168.27	-121.	51.33	-109.	0.03	0.57	90.	25.	55.	0.24	0.14	0.02	0.31
1.05	185.45	-126.	60.79	-112.	0.02	0.64	90.	135.	160.	0.21	0.09	0.01	0.33
0.83	221.20	-128.	72.24	-115.	0.01	0.33	90.	155.	125.	0.19	0.09	0.01	0.33
0.66	248.43	-131.	91.11	-118.	0.01	0.46	90.	135.	145.	0.32	0.08	0.01	0.37
0.53	269.25	-135.	92.40	-127.	0.01	0.45	85.	105.	155.	0.24	0.11	0.01	0.34
0.42	281.59	-140.	103.36	-134.	0.00	0.32	90.	100.	155.	0.41	0.09	0.02	0.37
0.33	297.14	-149.	110.81	-137.	0.00	0.12	85.	25.	165.	0.34	0.08	0.01	0.37
0.26	299.73	-157.	46.93	-143.	0.00	0.08	85.	0.	50.	0.14	0.07	0.01	0.16
0.21	269.28	-166.	83.42	-154.	0.00	0.07	85.	175.	10.	0.29	0.08	0.01	0.31
0.17	223.30	-176.	96.83	-162.	0.00	0.09	90.	50.	30.	0.44	0.08	0.02	0.43
0.13	170.67	174.	87.12	-173.	0.00	0.06	90.	65.	15.	0.50	0.07	0.01	0.51
0.11	115.61	163.	63.53	174.	0.00	0.06	90.	10.	60.	0.55	0.08	0.02	0.55
0.08	74.78	157.	39.84	166.	0.00	0.02	85.	35.	50.	0.31	0.08	0.01	0.53
0.07	30.14	141.	17.36	156.	0.00	0.79	85.	80.	50.	0.84	0.03	0.03	0.58

4 HOON--58

FILE-

PRD	R12	PH12	R21	PH21	RE1	RH1	ANG	ANGE	ANGH	SKW	BTA	RAN	AIS
1337.75	2811.59	-116.	141.86	-87.	1.20	0.36	70.	170.	90.	0.57	0.13	0.11	0.05
875.76	1827.99	-130.	51.00	-114.	1.05	0.42	70.	170.	100.	0.64	0.28	0.19	0.03
668.87	2019.80	-136.	80.21	-140.	0.92	0.37	70.	170.	100.	0.93	0.47	0.42	0.04
546.13	1880.26	-138.	79.45	-151.	0.51	0.32	75.	170.	110.	1.03	0.68	0.65	0.04
463.41	1673.46	-135.	52.23	-135.	0.34	0.36	80.	170.	100.	0.85	0.65	0.52	0.03
357.53	2201.22	-151.	165.66	-178.	0.40	0.34	70.	170.	115.	1.20	0.72	0.78	0.08
291.92	2722.22	-150.	99.79	-154.	0.56	0.37	70.	175.	110.	0.83	0.42	0.34	0.04
229.42	2320.67	-139.	56.50	-132.	0.40	0.34	75.	170.	115.	0.53	0.41	0.20	0.02
189.19	2368.10	-131.	76.90	-110.	0.37	0.40	85.	170.	100.	0.55	0.53	0.28	0.03
168.44	2358.59	-123.	181.59	-97.	0.35	0.47	95.	170.	95.	0.83	0.51	0.37	0.08
133.80	1274.30	-130.	176.15	-104.	0.33	0.58	90.	170.	95.	1.03	0.65	0.55	0.14
106.29	1415.68	-146.	165.81	-109.	0.31	0.71	85.	170.	85.	0.77	0.54	0.37	0.12
84.43	1240.21	-129.	307.71	-103.	0.18	0.45	95.	170.	85.	1.19	0.43	0.36	0.25
67.06	1671.71	-133.	190.48	-98.	0.14	0.35	90.	170.	65.	0.62	0.41	0.22	0.11
53.27	1617.78	-130.	275.68	-107.	0.08	0.33	90.	170.	70.	0.87	0.39	0.26	0.17
42.32	1529.96	-135.	324.04	-105.	0.07	0.34	90.	170.	90.	0.76	0.37	0.22	0.21
33.61	1990.72	-130.	446.54	-98.	0.07	0.44	95.	165.	85.	0.90	0.30	0.21	0.22
26.70	1847.05	-129.	435.33	-104.	0.05	0.40	95.	170.	80.	0.94	0.23	0.17	0.24
21.21	1755.93	-130.	530.43	-112.	0.02	0.32	95.	175.	80.	1.08	0.13	0.13	0.30
16.85	1934.01	-131.	566.51	-115.	0.01	0.24	95.	0.	70.	1.15	0.07	0.13	0.29
13.38	2019.58	-127.	939.71	-121.	0.01	0.23	100.	0.	75.	2.64	0.07	0.27	0.47
10.63	1577.39	-135.	895.53	-124.	0.01	0.22	95.	35.	70.	1.68	0.06	0.08	0.57
8.44	1499.75	-134.	636.56	-130.	0.01	0.19	95.	25.	75.	1.48	0.22	0.15	0.42
6.71	1699.28	-140.	785.23	-134.	0.01	0.18	95.	30.	70.	1.44	0.27	0.15	0.46
5.33	1823.80	-144.	1121.78	-140.	0.01	0.19	95.	30.	80.	2.43	0.31	0.19	0.62
41.80	4567.47	-139.	261.41	-110.	0.08	0.56	90.	0.	50.	0.36	0.27	0.09	0.06
27.37	3173.89	-135.	172.82	-107.	0.07	0.57	90.	0.	40.	0.28	0.22	0.06	0.05
20.90	2617.80	-134.	125.51	-106.	0.07	0.57	90.	5.	35.	0.22	0.23	0.05	0.05
17.07	2344.42	-130.	83.89	-110.	0.06	0.56	85.	10.	25.	0.16	0.03	0.01	0.04
14.48	1994.22	-134.	90.72	-112.	0.05	0.55	85.	20.	25.	0.16	0.10	0.02	0.05
11.17	1665.83	-129.	121.80	-100.	0.03	0.59	90.	15.	15.	0.10	0.06	0.01	0.07
9.12	1650.71	-117.	204.34	-129.	0.02	0.57	90.	90.	10.	0.37	0.19	0.05	0.12
7.17	1452.07	-125.	248.67	-122.	0.02	0.56	90.	90.	5.	0.35	0.19	0.05	0.17
5.91	1583.31	-133.	310.32	-128.	0.01	0.48	95.	105.	15.	0.56	0.15	0.06	0.20
5.26	1824.87	-133.	330.50	-123.	0.01	0.36	90.	35.	45.	0.51	0.12	0.05	0.18
4.18	2061.17	-136.	310.76	-132.	0.01	0.26	90.	175.	105.	0.35	0.16	0.04	0.15
3.32	1658.07	-142.	235.95	-126.	0.00	0.21	90.	25.	120.	0.25	0.08	0.02	0.14
2.64	1669.58	-136.	245.80	-135.	0.02	0.28	85.	175.	25.	0.85	0.40	0.25	0.15
2.10	1703.37	-138.	233.45	-155.	0.01	0.41	85.	10.	85.	0.67	0.32	0.17	0.14
1.66	1206.78	-157.	184.78	-142.	0.01	0.28	85.	175.	105.	0.41	0.09	0.03	0.15
1.32	956.30	-161.	166.21	-156.	0.01	0.29	85.	160.	140.	0.74	0.08	0.09	0.17
1.05	1104.80	-163.	274.73	-163.	0.00	0.22	85.	100.	175.	0.74	0.16	0.08	0.25
0.83	1039.98	-168.	216.46	-166.	0.01	0.16	85.	5.	125.	0.51	0.09	0.04	0.21
0.66	757.37	180.	190.22	-172.	0.00	0.11	90.	20.	170.	0.36	0.10	0.02	0.25
0.53	553.89	179.	115.94	-171.	0.00	0.06	85.	10.	160.	0.52	0.12	0.05	0.21
0.42	339.85	179.	88.37	-175.	0.00	0.07	85.	25.	165.	0.50	0.15	0.04	0.26
0.33	217.35	174.	43.22	-172.	0.00	0.07	80.	10.	45.	0.30	0.15	0.03	0.20
0.26	133.36	-177.	25.60	-165.	0.00	0.03	85.	10.	175.	0.40	0.14	0.04	0.19
0.21	62.55	-159.	19.74	-155.	0.00	0.04	85.	40.	140.	1.51	0.12	0.18	0.32
0.17	50.61	-143.	19.96	-127.	0.00	0.04	85.	30.	135.	1.98	0.08	0.27	0.39
0.13	135.88	-126.	46.16	-119.	0.00	0.05	85.	25.	25.	0.48	0.04	0.01	0.38
0.11	170.83	-131.	63.16	-120.	0.00	0.08	90.	85.	175.	0.24	0.09	0.01	0.37
0.08	239.12	-130.	92.39	-118.	0.00	0.11	85.	50.	0.	0.37	0.04	0.01	0.39
0.07	163.93	-143.	78.54	-127.	0.00	0.59	85.	70.	140.	0.35	0.05	0.01	0.48

5 SMITH-64

FILE-

PRD	R12	PH12	R21	PH21	PE1	PH1	ANG	ANG2	ANGH	SKW	RPA	RAN	AIS
1337.75	193.97	44.	41.18	76.	1.47	0.58	165.	50.	75.	0.53	0.20	0.08	0.21
875.76	199.13	37.	40.75	73.	0.99	0.64	165.	40.	90.	0.29	0.16	0.04	0.20
668.87	211.82	33.	47.32	69.	0.76	0.64	165.	20.	85.	0.27	0.08	0.02	0.22
546.13	224.03	31.	69.38	73.	0.67	0.60	165.	10.	95.	0.04	0.08	0.01	0.31
463.41	279.70	31.	77.73	71.	0.62	0.90	165.	175.	95.	0.05	0.08	0.01	0.28
357.53	223.90	27.	90.46	65.	0.64	0.67	165.	10.	75.	0.25	0.01	0.01	0.40
291.92	257.38	28.	143.44	66.	0.52	0.72	170.	10.	90.	0.40	0.08	0.02	0.56
229.42	292.74	42.	188.57	58.	0.42	0.74	170.	5.	75.	0.94	0.07	0.03	0.64
189.19	309.98	52.	217.62	45.	0.42	1.01	170.	175.	90.	3.15	0.16	0.14	0.70
168.44	264.33	45.	179.27	48.	0.39	0.98	165.	170.	80.	2.41	0.10	0.07	0.68
133.80	210.03	37.	159.26	54.	0.39	0.95	165.	0.	70.	1.36	0.13	0.06	0.76
106.29	190.30	43.	165.35	56.	0.35	0.96	170.	0.	75.	1.94	0.15	0.08	0.87
84.43	202.09	40.	180.37	55.	0.30	0.94	170.	0.	75.	1.63	0.13	0.06	0.89
67.06	218.69	42.	174.32	55.	0.28	1.03	170.	0.	80.	1.74	0.09	0.06	0.80
53.27	226.53	46.	204.78	54.	0.26	1.18	170.	175.	85.	3.07	0.05	0.06	0.90
42.32	226.77	45.	201.91	54.	0.25	1.17	170.	0.	80.	3.09	0.06	0.06	0.89
33.61	232.66	44.	214.92	54.	0.21	1.17	170.	175.	80.	2.48	0.09	0.05	0.92
26.70	236.73	45.	236.54	53.	0.17	1.09	170.	175.	85.	3.93	0.09	0.08	1.00
21.21	246.80	-127.	241.12	-135.	0.15	1.05	80.	0.	80.	3.87	0.12	0.09	0.98
16.85	266.07	-128.	233.61	-137.	0.14	1.03	80.	5.	80.	3.60	0.14	0.10	0.88
13.38	282.95	-130.	260.02	-139.	0.14	1.24	80.	5.	85.	4.45	0.13	0.14	0.92
10.63	299.03	-132.	266.08	-140.	0.12	1.21	85.	0.	90.	4.46	0.16	0.13	0.89
8.44	300.25	-135.	284.41	-146.	0.05	0.87	85.	130.	105.	3.02	0.14	0.11	0.95
6.71	310.34	-138.	276.36	-144.	0.06	1.06	85.	135.	110.	4.61	0.14	0.09	0.89
5.33	323.03	-143.	251.60	-149.	0.06	1.22	85.	160.	105.	3.74	0.13	0.11	0.78
41.80	275.43	-120.	288.25	-131.	0.22	1.07	85.	10.	80.	3.57	0.19	0.17	0.90
27.37	195.68	-119.	172.92	-128.	0.22	1.06	85.	10.	80.	4.18	0.16	0.15	0.88
20.90	179.65	-124.	150.42	-130.	0.20	1.06	80.	10.	80.	5.10	0.12	0.13	0.84
17.07	162.49	-121.	153.45	-129.	0.18	1.09	80.	5.	80.	4.13	0.09	0.10	0.94
14.48	172.96	-121.	141.64	-129.	0.19	1.11	80.	5.	80.	3.65	0.11	0.11	0.82
11.17	153.65	49.	148.02	53.	0.13	1.04	170.	0.	90.	8.78	0.06	0.11	0.96
9.12	140.06	47.	137.89	47.	0.11	1.05	170.	170.	95.	45.67	0.07	0.16	0.98
7.17	111.06	33.	103.01	67.	0.07	0.75	170.	155.	95.	0.86	0.26	0.13	0.93
5.91	134.48	30.	90.36	52.	0.09	0.69	175.	35.	85.	1.50	0.12	0.11	0.70
5.26	165.18	30.	109.83	40.	0.10	1.00	170.	25.	55.	2.41	0.15	0.12	0.66
4.18	200.69	-142.	126.78	-143.	0.17	1.78	85.	55.	15.	2.20	0.04	0.06	0.63
3.32	152.61	-148.	125.01	-154.	0.09	1.63	85.	95.	165.	3.94	0.13	0.09	0.82
2.64	196.61	-158.	135.59	-157.	0.06	2.58	85.	170.	160.	3.62	0.15	0.13	0.69
2.10	237.01	-152.	114.77	-161.	0.07	1.63	90.	0.	130.	1.17	0.19	0.09	0.48
1.66	152.98	-155.	117.17	-167.	0.06	1.56	90.	0.	105.	2.47	0.23	0.14	0.77
1.32	152.48	-164.	94.86	-168.	0.05	0.90	90.	160.	135.	2.60	0.20	0.14	0.62
1.05	113.54	-167.	79.84	-171.	0.03	0.47	90.	45.	35.	2.91	0.18	0.11	0.70
0.83	106.64	-174.	67.62	-172.	0.04	0.94	90.	0.	100.	2.03	0.16	0.08	0.63
0.66	80.05	-178.	47.97	-176.	0.02	0.34	90.	170.	130.	1.75	0.14	0.07	0.60
0.53	57.67	178.	40.59	178.	0.02	0.50	90.	25.	65.	2.09	0.17	0.06	0.70
0.42	41.14	174.	26.51	177.	0.01	0.34	90.	5.	45.	1.54	0.14	0.05	0.64
0.33	22.81	177.	10.47	180.	0.01	0.11	90.	145.	100.	0.90	0.11	0.04	0.46
0.26	13.32	-179.	7.71	-178.	0.02	0.22	95.	5.	80.	1.27	0.06	0.03	0.58
0.21	7.05	-165.	4.85	-160.	0.03	0.16	95.	150.	120.	1.68	0.07	0.04	0.69
0.17	6.46	-137.	4.80	-135.	0.02	0.14	95.	175.	100.	2.37	0.09	0.04	0.74
0.13	10.29	-124.	7.52	-117.	0.01	0.18	95.	165.	150.	1.60	0.04	0.03	0.73
0.11	14.76	-123.	11.32	-114.	0.01	0.33	95.	50.	45.	1.63	0.04	0.03	0.77
0.08	21.69	-120.	17.51	-112.	0.00	0.23	95.	150.	145.	1.50	0.06	0.02	0.81
0.07	18.60	-130.	17.00	-116.	0.01	1.88	95.	150.	35.	0.71	0.07	0.01	0.91

6 BELLE FOURCH-68 FILE-

PRD	R12	PH12	R21	PH21	RE1	PH1	ANG	ANGE	ANGH	SKW	BTA	RAN	AIS
1337.75	496.21	-109.	89.55	110.	50.64	15.10	85.	175.	85.	0.93	0.70	0.78	0.18
875.76	1068.60	-26.	611.64	83.	24.99	7.51	160.	170.	75.	1.02	0.18	0.70	0.57
668.87	293.94	21.	165.23	71.	24.43	11.32	170.	175.	80.	1.04	0.09	0.22	0.56
546.13	179.36	-120.	62.53	-145.	17.25	11.20	85.	5.	80.	0.73	0.11	0.05	0.35
463.41	180.49	-122.	44.18	-140.	14.46	6.45	85.	5.	95.	0.63	0.13	0.05	0.24
357.59	193.36	-125.	46.46	-151.	4.08	6.66	85.	15.	60.	0.75	0.19	0.11	0.24
291.92	182.06	-133.	47.66	-145.	6.74	4.74	85.	175.	65.	0.75	0.18	0.09	0.26
229.42	170.35	-137.	56.56	-148.	7.47	2.95	85.	170.	140.	0.46	0.08	0.02	0.33
189.19	168.52	-136.	47.19	-143.	5.85	6.35	85.	175.	95.	0.38	0.04	0.01	0.28
168.44	172.43	-135.	54.65	-143.	7.73	10.78	85.	175.	90.	0.52	0.07	0.02	0.32
133.80	184.48	-141.	51.41	-140.	2.76	2.59	85.	5.	70.	0.37	0.10	0.02	0.28
106.29	157.55	-139.	57.15	-138.	1.57	3.90	85.	170.	95.	0.64	0.09	0.03	0.36
84.43	154.52	-141.	64.74	-138.	0.31	0.43	85.	15.	55.	0.71	0.12	0.03	0.42
67.06	158.38	-140.	57.48	-139.	0.22	0.55	85.	170.	120.	0.49	0.11	0.03	0.36
53.27	160.90	-142.	60.25	-138.	0.19	0.68	85.	140.	145.	0.48	0.06	0.02	0.37
42.32	172.85	-143.	64.56	-138.	0.17	0.66	85.	155.	130.	0.62	0.06	0.02	0.37
33.61	154.96	-146.	62.76	-140.	0.16	0.48	85.	25.	25.	0.65	0.05	0.02	0.40
26.70	138.05	-148.	67.41	-141.	0.19	1.03	85.	90.	165.	0.85	0.05	0.03	0.49
21.21	141.91	-149.	66.11	-144.	0.21	1.24	85.	90.	160.	0.79	0.05	0.03	0.47
16.85	124.14	-151.	68.56	-147.	0.12	0.65	85.	150.	105.	1.14	0.06	0.03	0.55
13.38	122.74	-156.	57.25	-148.	0.26	0.88	85.	0.	100.	0.63	0.07	0.02	0.47
10.63	88.86	-160.	44.19	-153.	0.21	0.48	85.	30.	0.	1.28	0.02	0.05	0.50
8.44	67.06	-162.	39.75	-157.	0.27	1.62	85.	125.	120.	1.40	0.01	0.04	0.59
6.71	63.82	-169.	37.55	-159.	0.09	0.56	85.	80.	155.	1.18	0.04	0.03	0.59
5.33	59.92	-171.	33.92	-161.	0.15	1.13	85.	125.	145.	0.89	0.06	0.03	0.57
41.80	131.63	-152.	36.29	-139.	0.93	2.93	90.	45.	165.	0.28	0.09	0.02	0.28
27.37	100.34	-150.	23.92	-138.	1.11	2.32	90.	30.	175.	0.25	0.12	0.02	0.24
20.90	97.67	-153.	26.24	-147.	1.17	2.68	90.	25.	175.	0.46	0.14	0.04	0.27
17.07	98.58	-162.	26.67	-157.	1.33	2.75	85.	20.	175.	0.98	0.11	0.07	0.37
14.48	88.64	-166.	34.62	-155.	1.55	3.15	85.	20.	175.	1.22	0.09	0.10	0.39
11.17	99.75	-166.	25.31	-157.	0.49	3.37	85.	175.	145.	0.99	0.06	0.10	0.25
9.12	75.78	-165.	23.05	-155.	0.56	5.82	85.	145.	135.	1.31	0.06	0.15	0.30
7.17	60.86	-164.	17.87	-143.	0.62	5.00	80.	55.	145.	1.11	0.08	0.14	0.29
5.91	52.60	-168.	24.15	-154.	0.94	3.64	80.	15.	35.	1.29	0.09	0.09	0.46
5.26	50.86	-171.	27.20	-161.	0.41	3.00	85.	15.	100.	1.20	0.07	0.05	0.53
4.18	47.41	-169.	14.31	-172.	1.17	6.52	85.	165.	100.	0.70	0.08	0.04	0.30
3.32	38.05	-171.	13.44	-156.	0.86	3.54	85.	15.	55.	0.41	0.09	0.02	0.35
2.64	28.81	-174.	9.32	-169.	0.37	2.48	85.	85.	80.	0.92	0.02	0.06	0.32
2.10	22.77	-179.	9.57	-176.	0.50	3.21	85.	5.	85.	1.09	0.05	0.05	0.42
1.66	15.56	180.	6.79	-168.	0.48	2.36	85.	145.	165.	1.03	0.04	0.06	0.44
1.32	11.75	179.	7.09	-176.	0.56	2.43	85.	165.	15.	1.46	0.04	0.04	0.60
1.05	8.52	-172.	6.19	179.	0.26	1.82	85.	110.	0.	1.77	0.15	0.06	0.73
0.83	5.92	-176.	4.75	173.	0.20	1.15	90.	5.	100.	2.49	0.12	0.09	0.80
0.66	4.61	-170.	3.20	173.	0.23	1.29	85.	135.	140.	1.70	0.17	0.11	0.69
0.53	4.68	-172.	2.24	-178.	0.18	0.61	85.	0.	90.	1.22	0.09	0.06	0.48
0.42	2.34	-167.	1.59	-176.	0.15	0.46	85.	15.	175.	2.24	0.15	0.10	0.68
0.33	1.53	-167.	1.38	-161.	0.07	0.39	90.	65.	140.	2.53	0.06	0.02	0.90
0.26	1.04	-158.	0.76	-173.	0.11	0.10	90.	25.	65.	1.94	0.12	0.10	0.74
0.21	0.65	-138.	0.38	-146.	0.10	0.23	85.	30.	135.	1.95	0.09	0.09	0.59
0.17	0.63	-116.	0.51	-112.	0.12	0.21	90.	20.	160.	4.14	0.09	0.08	0.80
0.13	1.42	-100.	0.96	-91.	0.05	0.37	85.	120.	130.	1.63	0.09	0.05	0.68
0.11	2.68	-94.	1.78	-94.	0.05	0.54	85.	145.	150.	1.65	0.04	0.03	0.67
0.08	4.81	-94.	3.41	-94.	0.04	0.47	85.	130.	150.	1.62	0.05	0.02	0.71
0.07	5.64	-106.	3.55	-105.	0.12	1.83	90.	45.	25.	0.23	0.09	0.01	0.63

7 COLONY--76 FILE-

PRD	R12	PH12	R21	PH21	RE1	PH1	ANG	ANGE	ANGH	SKW	BTA	RAN	AIS
1337.75	124.64	-132.	119.72	-162.	2.26	0.22	85.	155.	100.	2.81	0.11	0.55	0.96
875.76	68.86	-142.	62.64	-168.	1.66	0.21	85.	155.	135.	2.88	0.06	0.43	0.91
668.87	64.49	-131.	38.54	-163.	1.40	0.23	85.	150.	65.	1.81	0.04	0.29	0.60
546.13	47.33	-122.	30.85	-171.	1.55	0.24	90.	145.	45.	1.17	0.09	0.26	0.65
463.41	43.44	-129.	24.92	-170.	1.37	0.32	90.	145.	35.	1.32	0.01	0.23	0.57
357.53	70.31	-134.	18.37	-162.	1.10	0.28	90.	145.	100.	0.91	0.03	0.12	0.26
291.92	64.85	-136.	17.29	-160.	0.96	0.30	90.	145.	115.	0.87	0.06	0.10	0.27
229.42	53.56	-141.	19.09	-150.	0.41	0.24	90.	165.	85.	1.03	0.07	0.07	0.36
189.19	53.54	-144.	23.46	-145.	0.25	0.18	95.	175.	90.	1.10	0.05	0.05	0.44
168.44	53.71	-145.	24.16	-144.	0.19	0.15	95.	175.	95.	0.99	0.05	0.04	0.45
133.80	46.83	-152.	22.27	-144.	0.24	0.21	95.	155.	115.	0.87	0.06	0.03	0.48
106.29	48.06	-152.	21.54	-143.	0.15	0.17	95.	155.	130.	0.70	0.07	0.03	0.45
84.43	38.10	-155.	18.39	-145.	0.08	0.10	95.	25.	65.	0.65	0.08	0.02	0.48
67.06	35.47	-156.	19.20	-148.	0.11	0.13	95.	0.	95.	0.57	0.10	0.02	0.54
53.27	32.46	-161.	18.63	-150.	0.11	0.17	95.	45.	45.	0.43	0.09	0.01	0.57
42.32	28.82	-165.	17.00	-151.	0.10	0.17	95.	35.	55.	0.36	0.12	0.02	0.59
33.61	22.30	-161.	16.48	-152.	0.06	0.10	90.	175.	100.	0.72	0.10	0.02	0.74
26.70	18.78	-162.	14.89	-155.	0.05	0.09	90.	170.	115.	0.66	0.06	0.01	0.79
21.21	16.15	-165.	13.19	-157.	0.05	0.11	90.	170.	110.	0.35	0.07	0.01	0.82
16.85	13.70	-166.	10.27	-157.	0.09	0.19	90.	175.	95.	0.22	0.08	0.01	0.75
13.38	10.47	-167.	8.75	-160.	0.06	0.12	90.	10.	75.	0.54	0.07	0.01	0.84
10.63	7.87	-166.	6.60	-161.	0.05	0.26	90.	35.	65.	0.65	0.07	0.01	0.84
8.44	6.64	-164.	5.52	-162.	0.06	0.17	90.	150.	75.	0.88	0.06	0.00	0.83
6.71	5.80	-161.	4.60	-156.	0.02	0.21	90.	175.	35.	0.44	0.04	0.00	0.79
5.33	5.70	-163.	5.29	-156.	0.01	0.17	90.	140.	75.	0.59	0.02	0.00	0.93
41.80	25.16	-159.	23.53	-150.	0.13	0.22	90.	150.	125.	1.67	0.06	0.02	0.94
27.37	16.14	31.	15.96	21.	0.13	0.22	0.	145.	125.	1.19	0.06	0.01	0.99
20.90	13.16	-158.	12.61	-152.	0.15	0.25	90.	150.	125.	1.58	0.06	0.01	0.96
17.07	13.60	-161.	9.49	-157.	0.18	0.29	95.	165.	115.	0.40	0.08	0.01	0.70
14.48	12.00	-164.	7.95	-158.	0.16	0.29	95.	140.	140.	0.40	0.09	0.01	0.66
11.17	9.56	-163.	6.21	-161.	0.15	0.31	95.	115.	170.	0.43	0.04	0.00	0.65
9.12	6.36	-159.	6.09	-161.	0.22	0.29	95.	170.	125.	2.26	0.07	0.01	0.96
7.17	5.90	17.	4.86	24.	0.19	0.48	0.	65.	40.	0.56	0.04	0.00	0.82
5.91	4.77	18.	4.09	20.	0.29	0.71	0.	20.	65.	1.58	0.04	0.01	0.86
5.26	4.21	22.	3.46	14.	0.25	0.62	0.	25.	85.	0.37	0.06	0.00	0.82
4.18	3.44	-154.	3.13	-150.	0.37	1.08	95.	85.	10.	1.88	0.06	0.01	0.91
3.32	3.26	-146.	3.22	-153.	0.13	0.60	90.	20.	55.	0.58	0.06	0.01	0.99
2.64	3.93	29.	2.74	37.	0.03	0.24	0.	70.	60.	0.55	0.09	0.01	0.70
2.10	2.67	-147.	2.67	-143.	0.06	0.14	90.	120.	155.	1.15	0.06	0.01	1.00
1.66	2.76	37.	2.69	33.	0.13	0.31	0.	150.	105.	2.01	0.07	0.01	0.97
1.32	3.04	36.	2.73	35.	0.04	0.12	0.	35.	95.	1.15	0.05	0.00	0.90
1.05	2.97	-140.	2.60	-142.	0.03	0.07	90.	145.	90.	0.51	0.04	0.00	0.88
0.83	3.13	36.	2.81	38.	0.02	0.13	0.	45.	55.	0.68	0.04	0.00	0.90
0.66	3.04	34.	2.76	34.	0.02	0.06	0.	105.	155.	1.65	0.04	0.00	0.91
0.53	3.03	33.	2.54	33.	0.01	0.03	0.	5.	30.	0.49	0.02	0.00	0.84
0.42	2.28	30.	2.17	29.	0.01	0.08	0.	25.	50.	1.10	0.03	0.00	0.95
0.33	1.47	-149.	1.07	-151.	0.01	0.04	90.	5.	50.	1.28	0.01	0.01	0.73
0.26	1.12	-148.	0.83	-150.	0.00	0.02	90.	5.	65.	0.25	0.02	0.00	0.74
0.21	0.75	-134.	0.63	-133.	0.01	0.03	90.	145.	115.	0.09	0.04	0.00	0.83
0.17	0.78	-108.	0.75	-103.	0.00	0.02	90.	145.	85.	0.38	0.04	0.00	0.96
0.13	1.40	89.	1.37	85.	0.00	0.02	0.	150.	90.	0.52	0.03	0.00	0.98
0.11	2.59	89.	2.36	87.	0.00	0.04	0.	130.	105.	1.18	0.05	0.00	0.91
0.08	4.20	87.	3.79	87.	0.01	0.08	0.	150.	75.	0.67	0.02	0.00	0.90
0.07	4.26	77.	3.46	85.	0.03	0.58	0.	100.	155.	0.53	0.06	0.01	0.81

PWD	R12	PH12	R21	PH21	RR1	RH1	ANG	ANGE	ANGH	SKW	SPA	RAN	AIS
1337.75	27.12	21.	18.06	1.	7.11	1.43	170.	150.	5.	4.10	0.67	1.07	0.67
875.76	14.14	170.	10.33	-163.	13.32	1.24	75.	130.	0.	2.94	0.70	0.99	0.73
668.87	40.62	165.	21.62	-165.	13.88	2.34	70.	130.	170.	2.62	0.55	0.88	0.53
546.13	55.69	160.	28.90	-169.	9.64	3.00	70.	120.	25.	2.62	0.50	0.87	0.52
463.41	77.79	46.	56.66	5.	10.32	4.06	175.	115.	10.	1.94	0.37	0.61	0.73
357.53	57.54	47.	30.22	32.	6.23	3.46	0.	105.	175.	1.63	0.01	0.11	0.53
291.92	69.44	40.	25.61	43.	3.34	2.66	0.	100.	20.	1.10	0.04	0.07	0.37
229.42	72.96	18.	22.91	40.	0.96	2.73	5.	165.	40.	0.51	0.17	0.05	0.31
189.19	104.56	17.	51.82	40.	1.02	0.73	0.	115.	130.	1.04	0.13	0.09	0.50
168.44	113.44	21.	63.26	38.	1.02	1.53	175.	120.	145.	1.51	0.09	0.10	0.56
133.80	101.51	19.	55.69	38.	0.54	0.71	175.	135.	115.	1.48	0.10	0.11	0.55
106.29	93.21	21.	61.26	34.	0.41	0.53	175.	135.	110.	2.01	0.03	0.10	0.66
84.43	81.12	19.	60.89	36.	0.51	0.68	175.	140.	110.	1.83	0.04	0.09	0.75
67.06	68.96	17.	44.35	29.	0.21	0.43	175.	135.	100.	1.88	0.08	0.08	0.64
53.27	65.27	18.	42.32	21.	0.17	0.34	0.	100.	145.	1.99	0.08	0.06	0.65
42.32	55.91	15.	38.34	25.	0.40	0.67	175.	130.	120.	1.67	0.06	0.05	0.69
33.61	45.49	17.	36.70	25.	0.13	0.22	175.	135.	175.	1.57	0.05	0.02	0.81
26.70	37.92	14.	36.91	22.	0.19	0.50	175.	120.	145.	2.75	0.03	0.03	0.97
21.21	36.66	16.	31.14	23.	0.10	0.25	175.	125.	145.	1.54	0.07	0.02	0.85
16.85	28.69	14.	26.32	22.	0.08	0.16	175.	120.	130.	1.98	0.09	0.03	0.92
13.38	26.81	12.	19.31	17.	0.09	0.10	175.	110.	170.	1.16	0.09	0.02	0.72
10.63	18.53	10.	13.30	19.	0.12	0.24	175.	120.	50.	0.52	0.05	0.01	0.72
8.44	18.75	11.	13.35	7.	0.12	0.25	175.	150.	55.	0.49	0.06	0.01	0.71
6.71	19.52	6.	12.85	14.	0.11	0.21	0.	90.	60.	1.20	0.05	0.03	0.66
5.33	25.12	8.	13.48	10.	0.04	0.31	0.	115.	15.	0.66	0.11	0.02	0.54
41.80	59.43	-160.	9.22	-172.	0.54	0.38	5.	110.	115.	0.88	0.15	0.14	0.16
27.37	39.91	-157.	5.44	-168.	0.28	0.61	0.	65.	65.	0.18	0.17	0.03	0.14
20.90	33.47	-155.	12.81	-162.	0.30	0.44	0.	95.	15.	0.73	0.10	0.03	0.47
17.07	32.93	-155.	24.51	-159.	0.42	0.47	0.	95.	25.	3.39	0.02	0.08	0.74
14.40	56.89	5.	45.15	28.	0.43	0.50	90.	100.	30.	1.81	0.25	0.20	0.79
11.17	22.01	-160.	15.33	-174.	0.33	0.48	170.	90.	150.	0.85	0.07	0.01	0.70
9.12	17.80	-160.	8.87	172.	0.16	0.31	175.	100.	10.	0.41	0.06	0.02	0.50
7.17	11.40	-170.	9.61	168.	0.64	0.96	0.	115.	175.	1.21	0.11	0.12	0.42
5.91	8.52	-178.	6.71	175.	0.62	1.53	0.	125.	5.	4.42	0.05	0.15	0.79
5.26	13.33	18.	8.37	3.	0.60	1.28	95.	140.	10.	2.01	0.10	0.13	0.63
4.18	6.31	-160.	5.65	-157.	0.30	0.55	0.	100.	160.	0.27	0.13	0.02	0.93
3.32	7.83	29.	6.14	9.	0.15	0.31	85.	115.	5.	0.36	0.09	0.01	0.78
2.64	5.80	-172.	5.35	-168.	0.07	0.50	0.	80.	5.	5.97	0.02	0.04	0.92
2.10	6.21	-170.	5.44	-171.	0.18	0.76	175.	105.	165.	0.77	0.09	0.01	0.88
1.66	6.22	-163.	5.95	-164.	0.05	0.29	175.	65.	45.	0.58	0.08	0.01	0.64
1.32	5.31	-164.	4.73	-167.	0.04	0.18	0.	45.	40.	1.58	0.07	0.01	0.89
1.05	4.16	10.	3.88	25.	0.02	0.05	85.	90.	25.	0.39	0.08	0.01	0.93
0.83	4.58	17.	4.34	25.	0.02	0.15	85.	110.	95.	0.53	0.07	0.01	0.94
0.66	4.95	21.	4.35	20.	0.02	0.17	85.	55.	10.	1.80	0.04	0.01	0.88
0.53	5.16	-158.	5.05	-163.	0.03	0.12	175.	110.	85.	0.24	0.04	0.00	0.98
0.42	4.42	-160.	4.37	-166.	0.02	0.08	175.	115.	125.	1.27	0.02	0.01	0.99
0.33	4.19	11.	3.88	12.	0.01	0.04	85.	75.	5.	1.34	0.02	0.00	0.87
0.26	3.35	4.	2.46	9.	0.01	0.07	85.	100.	5.	1.07	0.08	0.02	0.73
0.21	2.62	-1.	2.49	-8.	0.00	0.02	85.	150.	95.	1.46	0.07	0.01	0.87
0.17	1.57	-4.	1.35	-6.	0.00	0.03	85.	130.	105.	0.96	0.07	0.01	0.96
0.13	0.89	-4.	0.81	-6.	0.00	0.03	90.	0.	50.	0.25	0.09	0.01	0.86
0.11	0.36	0.	0.66	7.	0.01	0.02	85.	115.	145.	0.32	0.08	0.01	0.83
0.08	0.14	-141.	0.14	-142.	0.01	0.04	175.	110.	155.	1.81	0.05	0.00	0.97
0.07	0.16	66.	0.69	78.	0.35	1.56	85.	90.	60.	0.80	0.07	0.02	0.60

9 WALL--86

FILE-

PHD	R12	PH12	R21	PH21	PE1	PH1	ANG	ANGE	ANGH	SKW	BTA	BAN	BIS
1337.75	34.72	23.	6.81	28.	1.26	0.15	175.	65.	100.	1.26	0.10	0.22	0.20
875.76	42.56	17.	9.62	15.	0.70	0.20	175.	55.	105.	1.63	0.07	0.30	0.23
668.87	49.59	22.	11.06	13.	0.53	0.12	175.	55.	105.	1.69	0.02	0.34	0.22
546.13	49.81	-8.	20.08	6.	0.57	0.08	0.	50.	75.	3.00	0.27	0.55	0.40
463.41	1887.81	-31.	2.95	173.	0.56	0.18	130.	40.	65.	0.08	0.15	0.01	0.00
357.53	471.85	-56.	21.60	-91.	0.61	0.21	110.	35.	70.	1.00	0.21	0.36	0.05
291.92	38.31	12.	8.06	114.	0.76	0.25	155.	40.	65.	0.48	1.02	0.58	0.21
229.42	30.34	-112.	23.56	-123.	0.63	0.21	90.	45.	75.	3.60	0.16	0.20	0.78
189.19	21.77	-61.	19.92	83.	0.31	0.15	175.	40.	120.	2.68	0.12	0.27	0.91
168.44	18.70	64.	13.52	93.	0.31	0.15	175.	55.	130.	1.84	0.18	0.26	0.72
133.80	71.95	33.	20.89	58.	0.41	0.25	170.	40.	5.	1.44	0.09	0.26	0.29
106.29	394.71	-15.	44.77	27.	0.31	0.24	165.	75.	85.	1.13	0.21	0.38	0.11
88.43	204.66	46.	37.65	66.	0.21	0.20	170.	35.	145.	1.42	0.14	0.34	0.18
67.06	35.94	27.	10.29	41.	0.18	0.12	175.	45.	5.	0.98	0.08	0.10	0.29
53.27	27.63	40.	7.61	48.	0.19	0.17	175.	70.	150.	0.85	0.04	0.07	0.28
42.32	25.46	35.	7.55	55.	0.18	0.17	0.	55.	135.	0.53	0.09	0.04	0.30
33.61	22.34	28.	10.24	53.	0.12	0.14	0.	60.	30.	0.68	0.08	0.04	0.46
26.70	20.60	30.	6.53	49.	0.05	0.11	0.	155.	115.	0.34	0.01	0.01	0.32
21.21	20.61	25.	8.08	45.	0.07	0.14	0.	160.	110.	0.42	0.08	0.02	0.39
16.85	18.32	25.	7.66	42.	0.04	0.10	0.	140.	130.	0.42	0.03	0.01	0.42
13.38	17.02	18.	8.22	47.	0.03	0.12	0.	100.	105.	0.63	0.12	0.05	0.48
10.63	88.71	21.	15.81	40.	0.02	0.12	170.	95.	100.	1.38	0.11	0.32	0.18
8.44	599.84	31.	392.03	50.	0.05	0.22	175.	45.	120.	4.54	0.17	0.81	0.65
6.71	1398.46	-11.	269.38	36.	0.08	0.15	165.	55.	155.	1.50	0.38	0.67	0.19
5.33	759.54	-12.	292.18	41.	0.09	0.20	170.	40.	165.	1.64	0.45	0.77	0.38
41.80	36.91	-14.	45.46	-118.	0.15	0.14	0.	115.	110.	1.37	0.10	0.10	0.69
27.37	27.52	-13.	14.43	-123.	0.11	0.26	5.	155.	175.	1.54	0.10	0.08	0.52
20.90	26.65	-13.	13.81	-121.	0.14	0.26	5.	70.	110.	1.61	0.03	0.08	0.51
17.07	22.71	-13.	10.71	-127.	0.15	0.28	0.	95.	130.	1.14	0.06	0.06	0.47
14.48	28.01	-14.	9.32	-136.	0.08	0.09	0.	120.	135.	0.88	0.10	0.07	0.33
11.17	116.61	-12.	48.68	-135.	0.10	0.15	0.	105.	140.	3.05	0.17	0.47	0.42
9.12	349.67	-13.	211.91	-129.	0.09	0.28	0.	10.	85.	6.37	0.06	0.71	0.61
7.17	512.25	-25.	430.99	-66.	0.21	0.44	175.	40.	70.	2.33	0.42	0.95	0.86
5.91	1167.34	20.	1.84	-45.	0.36	0.66	150.	45.	25.	0.58	0.04	0.14	0.007
5.26	658.46	25.	0.83	-92.	0.22	0.80	145.	45.	20.	0.40	0.14	0.09	0.00
4.18	1879.82	-8.	4.49	-106.	0.20	0.76	130.	30.	65.	0.40	0.25	0.11	0.00
3.32	877.37	7.	1.42	-110.	0.29	1.55	135.	35.	45.	0.05	0.05	0.00	0.00
2.64	2015.10	22.	85.10	-37.	0.23	1.00	120.	40.	40.	0.81	0.48	0.40	0.04
2.10	5555.18	-130.	33.48	-133.	0.12	0.86	155.	40.	55.	0.65	0.05	0.17	0.01
1.66	296.46	-137.	34.37	-103.	0.04	0.26	165.	70.	70.	1.19	0.20	0.38	0.12
1.32	48.04	176.	18.63	-140.	0.04	0.19	165.	65.	25.	1.18	0.40	0.40	0.33
1.05	58.12	-159.	14.88	-147.	0.05	0.18	170.	15.	15.	1.68	0.09	0.31	0.25
0.83	34.63	-174.	10.47	-156.	0.05	0.10	170.	40.	50.	1.60	0.14	0.27	0.30
0.66	32.09	-166.	9.04	-162.	0.03	0.04	170.	0.	35.	1.35	0.16	0.22	0.28
0.53	9.43	-175.	5.00	-157.	0.01	0.14	175.	25.	145.	1.10	0.20	0.09	0.59
0.42	10.25	-169.	4.04	-169.	0.01	0.04	175.	70.	175.	0.82	0.09	0.04	0.43
0.33	5.08	-166.	3.72	-170.	0.02	0.05	0.	25.	100.	1.78	0.08	0.02	0.73
0.26	2.95	180.	4.60	179.	0.01	0.04	0.	105.	60.	3.22	0.02	0.05	0.90
0.21	1.65	-5.	1.04	-13.	0.01	0.06	90.	140.	75.	2.57	0.07	0.04	0.87
0.17	0.74	-14.	0.80	-12.	0.02	0.03	90.	25.	145.	10.80	0.06	0.10	0.89
0.13	0.46	-8.	0.45	-7.	0.02	0.05	90.	80.	175.	9.48	0.05	0.02	0.97
0.11	0.24	-176.	0.19	-172.	0.02	0.07	175.	5.	105.	1.70	0.08	0.02	0.79
0.08	0.09	37.	0.08	38.	0.05	0.11	90.	100.	175.	0.98	0.04	0.00	0.96
0.07	0.05	71.	0.03	119.	0.11	0.21	85.	25.	80.	1.39	0.01	0.33	0.65

/0 CHEYENNE R.---02

FILE-

PRD	P12	PH12	P21	PH21	BET	PH1	ANG	ANGE	ANGH	SKW	BTA	RAN	AIS
1337.75	20.37	57.	6.64	-8.	8.88	2.01	5.	80.	90.	0.31	0.38	0.11	0.33
875.76	22.86	46.	6.47	-15.	6.66	1.88	10.	95.	85.	0.23	0.28	0.07	0.28
668.87	27.19	36.	8.16	-35.	5.16	1.57	5.	95.	90.	0.21	0.15	0.03	0.30
546.13	23.27	30.	6.70	-50.	4.31	1.47	5.	85.	100.	0.22	0.20	0.04	0.29
463.41	28.56	36.	6.62	-47.	4.85	1.07	5.	100.	95.	0.31	0.18	0.06	0.23
357.53	41.51	37.	15.71	-66.	1.49	0.72	175.	5.	90.	0.18	0.02	0.02	0.38
291.92	53.24	171.	39.68	-137.	2.38	1.06	85.	160.	100.	0.45	0.10	0.05	0.75
229.42	126.20	-136.	43.98	-142.	1.97	0.88	85.	120.	120.	0.79	0.39	0.18	0.35
189.19	45.28	36.	9.73	37.	0.73	0.56	0.	0.	55.	0.30	0.08	0.02	0.21
168.44	48.26	32.	7.32	31.	0.85	0.95	0.	155.	80.	0.38	0.09	0.03	0.15
133.80	41.50	33.	6.69	62.	1.39	0.70	5.	85.	65.	0.17	0.21	0.04	0.16
106.29	40.85	35.	10.10	53.	0.96	0.63	5.	90.	35.	0.36	0.11	0.03	0.25
84.43	39.74	30.	13.00	48.	0.44	0.36	5.	90.	85.	0.38	0.16	0.03	0.33
67.06	35.24	30.	13.65	46.	0.20	0.30	0.	55.	65.	0.50	0.09	0.03	0.39
53.27	38.32	26.	12.31	45.	0.18	0.24	5.	70.	45.	0.29	0.09	0.01	0.32
42.32	31.48	24.	12.31	42.	0.14	0.23	5.	60.	50.	0.28	0.11	0.02	0.39
33.61	28.98	22.	12.80	41.	0.17	0.33	0.	80.	25.	0.38	0.10	0.02	0.44
26.70	23.09	19.	13.05	38.	0.11	0.23	0.	25.	65.	0.30	0.08	0.01	0.57
21.21	20.25	17.	9.49	35.	0.08	0.19	0.	5.	100.	0.51	0.10	0.02	0.47
16.85	17.48	17.	8.58	30.	0.08	0.25	0.	15.	50.	0.73	0.08	0.03	0.49
13.38	14.03	13.	8.23	31.	0.06	0.20	0.	40.	50.	0.40	0.11	0.02	0.59
10.63	11.97	11.	7.50	27.	0.06	0.29	0.	175.	50.	0.27	0.08	0.01	0.63
8.44	10.55	11.	5.97	23.	0.07	0.33	0.	70.	40.	0.54	0.06	0.01	0.57
6.71	9.59	12.	6.86	20.	0.05	0.35	0.	75.	55.	0.98	0.05	0.01	0.72
5.33	10.69	10.	6.87	11.	0.13	0.96	0.	5.	60.	1.96	0.02	0.05	0.68
41.80	23.59	-147.	3.92	-106.	0.34	0.13	5.	85.	25.	0.60	0.18	0.11	0.17
27.37	19.19	-147.	3.23	-119.	0.25	0.16	0.	90.	30.	0.48	0.04	0.04	0.17
20.90	17.34	-142.	4.00	-112.	0.22	0.40	175.	55.	75.	0.53	0.16	0.07	0.23
17.07	20.20	-147.	2.49	-113.	0.27	0.20	0.	110.	150.	0.58	0.15	0.09	0.12
14.48	26.64	-160.	3.97	-41.	0.14	0.33	5.	30.	110.	0.26	0.13	0.05	0.15
11.17	27.06	-175.	3.60	-50.	0.25	0.14	10.	15.	65.	0.12	0.15	0.02	0.14
9.12	29.23	168.	1.33	-23.	0.21	0.83	15.	0.	95.	0.45	0.66	0.27	0.05
7.17	51.68	174.	0.89	-1.	0.33	2.15	25.	20.	95.	0.48	0.11	0.13	0.02
5.91	26.69	-155.	3.80	-3.	0.34	1.15	30.	15.	95.	0.22	0.15	0.04	0.14
5.26	23.88	33.	19.05	14.	0.20	0.61	70.	20.	95.	3.45	0.15	0.39	0.80
4.18	10.31	173.	4.45	-121.	0.30	1.94	170.	105.	105.	1.10	0.52	0.56	0.43
3.32	14.57	60.	7.14	9.	0.15	0.44	60.	135.	105.	1.45	0.61	0.60	0.49
2.64	12.64	60.	6.44	8.	0.16	0.40	80.	175.	70.	0.31	0.08	0.02	0.65
2.10	15.13	65.	6.81	22.	0.29	0.72	80.	25.	75.	0.65	0.15	0.08	0.67
1.66	20.88	79.	4.31	22.	0.06	0.77	80.	170.	120.	0.25	0.04	0.02	0.21
1.32	5.14	-153.	4.56	-142.	0.07	0.18	0.	120.	30.	1.02	0.12	0.05	0.50
1.05	4.43	-147.	3.51	-139.	0.07	0.37	0.	20.	40.	1.88	0.15	0.05	0.79
0.83	6.40	48.	4.75	30.	0.03	0.14	90.	160.	5.	0.71	0.24	0.07	0.74
0.66	5.06	-157.	4.70	-152.	0.03	0.20	0.	175.	75.	2.91	0.09	0.03	0.93
0.53	7.44	29.	5.35	26.	0.04	0.14	90.	45.	10.	0.56	0.09	0.01	0.72
0.42	6.19	20.	5.09	19.	0.01	0.14	85.	105.	125.	7.29	0.08	0.03	0.92
0.33	5.10	-166.	3.57	-170.	0.01	0.10	175.	65.	25.	2.32	0.03	0.03	0.78
0.26	3.14	0.	4.11	8.	0.01	0.05	80.	125.	0.	0.79	0.09	0.02	0.67
0.21	2.58	-3.	1.81	-0.	0.01	0.06	90.	80.	170.	0.52	0.10	0.01	0.70
0.17	2.01	-4.	1.11	-5.	0.01	0.06	90.	140.	100.	0.38	0.08	0.00	0.55
0.13	0.83	-8.	0.75	-3.	0.01	0.08	90.	0.	75.	0.95	0.07	0.00	0.91
0.11	0.39	14.	0.33	5.	0.01	0.06	90.	95.	25.	0.42	0.12	0.01	0.89
0.08	0.13	-140.	0.13	-144.	0.02	0.07	175.	10.	70.	1.46	0.11	0.01	0.97
0.07	0.25	123.	0.19	116.	0.15	0.69	95.	30.	50.	9.01	0.29	0.75	0.76

// WALKER--36 FILE-

PRD	R12	PH12	R21	PH21	RE1	RH1	ANG	ANGE	ANGH	SKW	BTA	RAN	AIS
1337.75	35.00	31.	34.83	40.	2.75	0.34	5.	55.	105.	10.28	0.09	0.64	1.00
875.76	36.13	-145.	28.53	-155.	2.42	0.23	95.	55.	90.	7.26	0.09	0.64	0.79
668.87	40.40	-141.	28.45	-148.	3.26	0.76	95.	55.	140.	7.11	0.12	0.62	0.70
546.13	38.06	-137.	29.61	-147.	2.93	0.53	95.	55.	145.	7.48	0.10	0.62	0.78
463.81	39.29	-135.	24.70	-149.	3.00	0.48	95.	55.	75.	4.71	0.13	0.62	0.63
357.53	37.41	-137.	20.91	-139.	2.05	0.43	100.	50.	75.	4.72	0.20	0.50	0.56
291.92	31.11	-133.	20.67	-139.	0.75	0.39	95.	40.	65.	5.84	0.15	0.47	0.66
229.42	30.01	-141.	19.15	-143.	0.21	0.53	95.	105.	5.	5.19	0.08	0.35	0.64
189.19	45.03	-149.	17.88	-142.	0.72	0.38	100.	45.	115.	2.23	0.10	0.27	0.40
168.44	47.86	-150.	18.22	-141.	0.70	0.36	95.	45.	100.	2.14	0.10	0.27	0.38
133.80	35.03	-149.	17.22	-139.	0.70	0.40	95.	55.	25.	2.29	0.09	0.20	0.49
106.29	35.63	-148.	18.17	-136.	0.27	0.19	95.	65.	15.	2.12	0.10	0.18	0.51
84.43	34.75	-147.	19.49	-139.	0.32	0.31	95.	50.	50.	2.64	0.10	0.19	0.56
67.06	32.20	-146.	23.88	-140.	0.18	0.22	95.	60.	35.	4.01	0.10	0.14	0.74
53.27	33.86	-146.	24.67	-137.	0.17	0.23	95.	50.	50.	2.87	0.10	0.11	0.73
42.32	32.34	-146.	20.99	-143.	0.09	0.19	95.	75.	30.	2.47	0.12	0.09	0.65
33.61	31.13	-149.	16.88	-141.	0.13	0.26	95.	110.	175.	1.56	0.13	0.09	0.54
26.70	30.16	-151.	15.98	-141.	0.05	0.18	95.	55.	55.	1.12	0.11	0.05	0.53
21.21	26.44	-151.	17.08	-142.	0.05	0.25	95.	80.	60.	1.19	0.13	0.04	0.65
16.85	25.33	-155.	13.96	-141.	0.10	0.32	95.	95.	30.	0.73	0.15	0.04	0.55
13.38	22.09	-156.	11.31	-144.	0.10	0.50	95.	75.	45.	0.73	0.18	0.05	0.51
10.63	19.21	-155.	11.93	-146.	0.08	0.33	90.	95.	25.	0.76	0.18	0.04	0.62
8.44	18.96	-157.	8.35	-148.	0.09	0.46	90.	160.	85.	0.56	0.24	0.07	0.44
6.71	15.06	-163.	6.00	-158.	0.15	0.60	95.	105.	55.	0.80	0.18	0.05	0.40
5.33	12.87	-163.	5.66	-165.	0.10	0.62	95.	90.	115.	0.86	0.17	0.06	0.48
41.80	31.93	2e.	41.17	29.	0.30	0.59	105.	60.	125.	4.04	0.09	0.18	0.66
27.37	25.26	3e.	12.72	50.	0.34	0.70	95.	65.	155.	1.51	0.05	0.05	0.62
20.90	20.92	47.	9.75	44.	0.22	0.56	95.	75.	25.	1.72	0.13	0.12	0.47
17.07	17.25	45.	8.31	43.	0.31	0.96	95.	85.	5.	1.76	0.10	0.11	0.48
14.48	20.60	2e.	7.09	40.	0.89	1.84	90.	110.	170.	0.29	0.11	0.02	0.34
11.17	11.25	39.	7.41	50.	0.61	0.52	90.	120.	0.	0.89	0.13	0.03	0.66
9.12	12.53	-13e.	1e.2e	-146.	1.34	2.16	5.	145.	105.	2.16	0.11	0.11	0.81
7.17	23.93	-15e.	5.75	-160.	1.61	4.80	5.	145.	90.	0.23	0.07	0.01	0.24
5.91	167.10	-14e.	14.51	-128.	1.0e	6.16	170.	45.	100.	1.19	0.59	0.62	0.07
5.26	43.10	-10e.	5.4e	-147.	2.35	11.32	165.	175.	90.	0.86	0.51	0.40	0.13
4.18	25.81	-16e.	11.2e	-159.	0.60	4.08	5.	35.	75.	0.99	0.31	0.13	0.44
3.32	17.54	-14e.	8.0e	-154.	0.33	3.22	175.	85.	45.	0.37	0.05	0.01	0.51
2.64	24.33	-16e.	1e.9e	-15e.	0.33	3.63	175.	5.	90.	0.33	0.07	0.01	0.45
2.10	23.91	-16e.	8.0e	-159.	0.22	1.37	175.	15e.	14e.	0.17	0.07	0.01	0.28
1.66	20.33	-161.	6.1e	-163.	0.12	1.41	0.	75.	6e.	0.31	0.11	0.02	0.30
1.32	19.68	-16e.	6.3e	-16e.	0.31	1.87	175.	2e.	6e.	0.21	0.14	0.02	0.32
1.05	20.17	-17e.	4.0e	-161.	0.21	1.37	175.	2e.	75.	0.18	0.11	0.01	0.24
0.83	21.71	-17..	4.ve	-163.	0.16	1.52	175.	17e.	10e.	0.17	0.13	0.02	0.19
0.66	17.03	-17e.	4.1e	-159.	0.14	1.10	0.	13e.	95.	0.10	0.12	0.01	0.24
0.53	14.53	171.	3.5e	-166.	0.12	1.31	175.	175.	85.	0.0e	0.13	0.01	0.24
0.42	11.77	167.	3.4e	-168.	0.12	1.35	175.	1e.	8e.	0.1e	0.13	0.02	0.29
0.33	7.90	164.	4.7e	-172.	0.10	0.93	0.	0.	9e.	0.0e	0.09	0.01	0.35
0.26	3.53	157.	1.3e	-177.	0.09	0.44	0.	25.	11e.	0.37	0.04	0.01	0.55
0.21	2.52	15e.	1.0i	-179.	0.09	0.56	0.	5.	14e.	0.45	0.03	0.02	0.40
0.17	1.86	154.	0.7i	177.	0.07	0.38	0.	5.	6e.	0.14	0.07	0.01	0.63
0.13	0.74	16e.	0.5i	179.	0.06	0.31	0.	175.	9e.	0.1e	0.07	0.01	0.69
0.11	0.29	17e.	0.4e	-170.	0.09	0.33	0.	0.	8e.	0.11	0.0e	0.00	0.78
0.08	0.14	-15e.	0.1i	-139.	0.07	0.21	0.	1e.	7e.	0.17	0.07	0.00	0.77
0.07	0.10	-11e.	0.ve	-102.	0.12	0.52	175.	35.	4e.	0.0e	0.03	0.05	0.42

/2 ABEMORE--26

-FILE-

PRD	R12	PR12	R21	PR21	RE1	RR1	ANG	ANG2	ANGH	SKW	RTA	RAN	AIS
1337.75	50.92	-129.	26.15	-162.	7.20	1.66	85.	30.	90.	2.18	0.40	0.65	0.88
875.76	49.99	-136.	22.98	-162.	5.15	1.34	85.	25.	85.	2.45	0.37	0.62	0.86
668.87	46.63	-138.	20.38	-158.	3.99	1.18	85.	25.	80.	2.61	0.30	0.55	0.84
546.13	45.74	-143.	20.20	-150.	2.52	0.95	85.	25.	80.	3.16	0.18	0.45	0.88
463.41	41.37	-144.	18.91	-147.	2.67	0.78	85.	20.	80.	3.33	0.15	0.43	0.86
357.53	40.23	-146.	17.69	-147.	2.63	0.72	85.	20.	75.	2.93	0.13	0.35	0.84
291.92	37.63	-147.	18.10	-148.	2.05	0.70	85.	20.	75.	3.24	0.14	0.35	0.88
229.42	36.15	-150.	18.67	-148.	1.51	0.57	85.	20.	75.	3.57	0.13	0.35	0.52
189.19	35.71	-151.	17.56	-148.	1.16	0.46	85.	20.	75.	3.20	0.11	0.33	0.49
168.44	35.10	-150.	16.88	-151.	0.93	0.38	85.	20.	75.	3.09	0.15	0.32	0.48
133.80	30.40	-154.	15.85	-154.	0.77	0.38	85.	15.	105.	3.33	0.13	0.30	0.52
106.29	25.88	-154.	14.22	-152.	0.52	0.25	85.	15.	75.	3.48	0.14	0.28	0.55
84.43	21.56	-154.	10.66	-150.	0.45	0.27	90.	15.	155.	2.57	0.14	0.22	0.49
67.06	21.79	-156.	9.46	-149.	0.34	0.24	90.	10.	150.	1.72	0.05	0.13	0.43
53.27	18.65	-158.	9.68	-151.	0.25	0.21	90.	10.	0.	2.07	0.05	0.13	0.52
42.32	16.61	-158.	8.42	-152.	0.20	0.23	90.	0.	155.	1.98	0.06	0.12	0.51
33.61	13.33	-160.	7.84	-153.	0.17	0.22	90.	165.	160.	2.13	0.04	0.10	0.59
26.70	11.51	-161.	6.20	-150.	0.11	0.19	90.	145.	0.	1.50	0.01	0.07	0.56
21.21	11.45	-160.	5.60	-151.	0.09	0.16	90.	130.	165.	1.33	0.02	0.06	0.49
16.85	8.73	-160.	5.66	-153.	0.09	0.17	90.	130.	165.	1.95	0.05	0.06	0.65
13.38	6.98	-160.	4.67	-150.	0.10	0.18	90.	120.	165.	1.59	0.05	0.05	0.67
10.63	5.49	-156.	4.49	-148.	0.08	0.15	85.	85.	0.	1.90	0.09	0.04	0.82
8.44	4.76	-151.	4.10	-148.	0.07	0.12	85.	110.	160.	3.53	0.09	0.04	0.86
6.71	4.69	-149.	3.47	-142.	0.06	0.12	90.	100.	165.	1.70	0.07	0.03	0.74
5.33	4.56	-148.	3.16	-141.	0.05	0.13	85.	100.	150.	1.10	0.08	0.02	0.69
41.80	14.97	31.	14.10	32.	0.32	0.34	85.	30.	35.	19.33	0.05	0.10	0.94
27.37	13.37	2..	7.7.	39.	0.27	0.29	90.	10.	30.	1.25	0.07	0.06	0.58
20.90	10.90	2..	6.61	36.	0.21	0.23	90.	5.	10.	1.83	0.11	0.07	0.61
17.07	9.90	20.	6.1.	35.	0.17	0.21	90.	170.	140.	1.18	0.10	0.05	0.62
14.48	9.05	19.	5.84	35.	0.15	0.21	90.	165.	135.	0.98	0.10	0.04	0.60
11.17	7.26	23.	5.10	35.	0.09	0.17	90.	135.	150.	1.20	0.10	0.04	0.70
9.12	6.26	2e.	4.45	36.	0.08	0.15	90.	130.	155.	1.22	0.08	0.03	0.68
7.17	5.26	34.	3.91	40.	0.08	0.15	90.	130.	155.	2.29	0.04	0.04	0.74
5.91	5.75	41.	4.41	47.	0.14	0.26	90.	20.	70.	2.88	0.12	0.07	0.77
5.26	4.57	4..	4.23	46.	0.10	0.22	90.	35.	50.	4.34	0.07	0.03	0.93
4.18	8.90	-139.	4.50	-132.	0.20	0.75	5.	140.	105.	8.57	0.04	0.03	0.29
3.32	10.33	-150.	4.22	-108.	0.10	0.80	10.	175.	100.	0.31	0.41	0.15	0.21
2.64	57.28	-135.	18.43	-139.	0.13	0.41	10.	165.	100.	2.71	0.03	0.54	0.32
2.10	32.36	54.	47.56	58.	0.09	0.56	90.	175.	140.	10.49	0.02	0.34	0.85
1.66	24.36	-12e.	7.71	-125.	0.10	0.50	0.	75.	145.	1.46	0.06	0.16	0.32
1.32	33.79	-114.	19.84	-129.	0.07	0.55	0.	115.	70.	2.88	0.13	0.29	0.58
1.05	14.63	-130.	10.87	-134.	0.03	0.12	0.	50.	85.	2.80	0.03	0.06	0.73
0.83	10.57	4e.	1.66	44.	0.04	0.39	85.	170.	75.	4.28	0.05	0.03	0.90
0.66	15.15	3..	1.79	39.	0.02	0.21	90.	95.	85.	3.63	0.12	0.07	0.94
0.53	12.46	34.	11.69	34.	0.03	0.15	85.	25.	80.	1.72	0.03	0.00	0.89
0.42	11.87	2e.	10.98	27.	0.02	0.15	85.	25.	80.	2.91	0.09	0.01	0.93
0.33	11.86	19.	9.64	20.	0.01	0.10	85.	20.	165.	1.19	0.06	0.01	0.81
0.26	9.56	11.	7.31	12.	0.01	0.06	90.	40.	0.	0.85	0.08	0.01	0.76
0.21	7.31	2.	3.34	-0.	0.02	0.11	90.	60.	5.	0.23	0.07	0.01	0.54
0.17	4.23	-3.	4.70	-6.	0.02	0.14	90.	75.	5.	0.55	0.06	0.01	0.64
0.13	1.82	-6.	1.34	-5.	0.01	0.07	90.	70.	15.	0.46	0.05	0.00	0.74
0.11	0.92	7.	0.59	4.	0.02	0.10	90.	75.	30.	0.61	0.06	0.01	0.64
0.08	0.38	39.	0.17	35.	0.02	0.06	85.	60.	20.	0.45	0.07	0.01	0.77
0.07	0.21	71.	0.15	39.	0.23	1.71	85.	20.	105.	1.22	0.07	0.12	0.73

/3 CLARETON--14

FILE-

PHD	R12	PH12	R21	PH21	RE1	RH1	ANG	ANGE	ANGH	SKW	BTA	BAN	AIS
1337.75	120.43	-141.	11.89	-124.	1.36	0.46	170.	35.	85.	1.36	0.11	0.43	0.10
875.76	115.13	-148.	15.06	-146.	0.46	0.48	170.	0.	95.	1.44	0.06	0.38	0.13
668.87	101.03	-150.	15.19	-147.	0.56	0.43	170.	15.	110.	1.50	0.08	0.37	0.15
546.13	89.51	-147.	24.06	-149.	0.32	0.35	175.	110.	105.	1.96	0.06	0.35	0.23
463.41	84.96	-147.	23.18	-158.	0.34	0.40	170.	145.	110.	2.05	0.08	0.41	0.27
357.53	83.21	-146.	24.05	-158.	0.39	0.49	170.	175.	110.	2.04	0.10	0.39	0.29
291.92	77.13	-146.	31.49	-156.	0.52	0.59	175.	5.	100.	2.51	0.12	0.34	0.41
229.42	70.15	-149.	30.24	-148.	0.50	0.56	175.	10.	105.	2.57	0.03	0.29	0.43
189.19	65.92	-154.	27.81	-142.	0.43	0.58	175.	10.	100.	2.13	0.01	0.28	0.42
168.44	65.33	-151.	26.19	-145.	0.37	0.53	175.	0.	105.	2.34	0.06	0.28	0.40
133.80	45.84	-157.	19.08	-138.	0.49	0.53	0.	15.	115.	2.21	0.12	0.35	0.42
106.29	47.85	-158.	17.25	-152.	0.30	0.51	175.	175.	115.	2.32	0.04	0.33	0.36
84.43	41.01	-158.	15.10	-151.	0.44	0.53	175.	20.	105.	2.39	0.05	0.34	0.37
67.06	38.97	-156.	14.03	-155.	0.30	0.52	175.	5.	105.	2.31	0.04	0.32	0.36
53.27	33.38	-160.	11.95	-148.	0.30	0.51	175.	5.	105.	2.05	0.08	0.30	0.36
42.32	29.63	-161.	11.15	-148.	0.25	0.54	175.	170.	110.	2.06	0.07	0.28	0.38
33.61	24.71	-162.	10.30	-146.	0.23	0.52	175.	160.	115.	2.05	0.09	0.27	0.42
26.70	20.88	-163.	10.80	-150.	0.20	0.47	0.	165.	115.	2.68	0.08	0.28	0.52
21.21	18.78	-163.	9.59	-152.	0.17	0.45	0.	155.	115.	2.59	0.09	0.25	0.51
16.85	16.68	-164.	9.65	-150.	0.16	0.41	0.	160.	120.	2.33	0.07	0.19	0.58
13.38	14.02	-164.	8.53	-153.	0.15	0.38	0.	165.	120.	2.58	0.05	0.16	0.61
10.63	10.99	-163.	6.60	-153.	0.14	0.35	0.	145.	130.	2.29	0.05	0.13	0.60
8.44	10.64	-163.	9.54	-149.	0.09	0.23	175.	145.	155.	2.51	0.03	0.12	0.90
6.71	27.69	24.	20.68	19.	0.10	0.26	90.	140.	170.	4.78	0.13	0.17	0.75
5.33	33.00	34.	14.52	33.	0.08	0.19	85.	160.	100.	2.07	0.21	0.21	0.44
41.80	49.01	18.	16.04	23.	0.22	0.61	0.	135.	125.	1.62	0.09	0.19	0.33
27.37	30.27	23.	11.48	30.	0.21	0.57	0.	145.	130.	1.65	0.08	0.16	0.38
20.90	21.91	24.	9.25	29.	0.19	0.50	0.	145.	125.	2.06	0.10	0.21	0.42
17.07	20.12	24.	8.16	35.	0.18	0.50	0.	150.	130.	1.83	0.05	0.20	0.41
14.48	17.72	24.	8.84	30.	0.19	0.51	0.	165.	125.	2.30	0.05	0.17	0.50
11.17	10.13	23.	8.37	34.	0.15	0.31	175.	100.	170.	1.50	0.06	0.16	0.35
9.12	14.54	20.	14.80	49.	0.23	0.40	175.	165.	140.	0.76	0.14	0.05	0.88
7.17	45.37	-7.	18.52	-25.	0.28	0.49	20.	140.	125.	1.93	0.09	0.27	0.41
5.91	6.11	31.	4.64	-80.	0.35	0.35	170.	110.	75.	0.66	0.25	0.19	0.79
5.26	4.82	34.	1.60	-35.	0.41	0.45	170.	155.	85.	0.73	0.23	0.22	0.33
4.18	5.42	33.	4.88	13.	0.20	0.49	175.	80.	90.	0.78	0.09	0.04	0.53
3.32	10.00	15.	4.77	11.	0.12	0.42	175.	155.	75.	0.69	0.07	0.05	0.28
2.64	4.46	23.	4.56	35.	0.09	0.18	175.	120.	135.	2.28	0.06	0.15	0.57
2.10	2.51	18.	2.08	36.	0.15	0.14	0.	95.	155.	1.62	0.14	0.09	0.83
1.66	3.69	32.	2.08	42.	0.09	0.35	0.	120.	70.	1.71	0.17	0.11	0.56
1.32	2.71	34.	2.04	44.	0.07	0.28	0.	90.	85.	1.58	0.07	0.04	0.75
1.05	2.59	-135.	2.45	-147.	0.04	0.21	90.	115.	90.	0.84	0.07	0.01	0.95
0.83	3.16	30.	3.13	43.	0.05	0.27	0.	135.	90.	0.73	0.10	0.02	0.99
0.66	3.69	34.	3.46	27.	0.05	0.35	0.	150.	95.	1.91	0.05	0.02	0.94
0.53	3.77	20.	3.65	21.	0.04	0.16	0.	40.	45.	8.28	0.02	0.02	0.97
0.42	3.75	19.	3.33	20.	0.02	0.17	0.	15.	90.	1.83	0.02	0.00	0.89
0.33	3.31	10.	4.64	6.	0.02	0.07	0.	0.	35.	1.93	0.04	0.01	0.85
0.26	2.58	0.	4.31	1.	0.01	0.08	0.	150.	70.	1.35	0.04	0.01	0.90
0.21	1.77	174.	1.65	170.	0.02	0.16	90.	20.	85.	1.85	0.01	0.01	0.92
0.17	1.03	175.	4.95	169.	0.01	0.08	90.	25.	65.	0.56	0.04	0.00	0.93
0.13	0.50	170.	0.50	172.	0.01	0.04	90.	120.	130.	0.75	0.03	0.00	0.99
0.11	0.22	-174.	0.41	-177.	0.01	0.04	90.	135.	85.	1.05	0.02	0.00	0.92
0.08	0.11	-140.	0.09	-147.	0.01	0.04	90.	150.	110.	0.43	0.01	0.00	0.85
0.07	0.11	-100.	0.07	-122.	0.14	0.49	100.	35.	150.	2.18	0.04	0.14	0.66

/4 ROBECRAFT--8

FILE-